HEAT TRANSFER AND BOUNDARY-LAYER TRANSITION IN SHOCK-TUBE FLOWS WITH SHOCK-INDUCED EXOTHERMIC REACTIONS

by

Jerry Lee Hall

A Dissertation Submitted to the

Graduate Faculty in Partial Fulfillment of

The Requirements for the Degree of

DOCTOR OF PHILOSOPHY

Major Subject: Mechanical Engineering
Aerospace Engineering

Approved:

Signature was redacted for privacy.

In Charge of Major Work

Signature was redacted for privacy.

Heads of Major Departments

Signature was redacted for privacy.

Dean of Graduate College

Iowa State University
Of Science and Technology
Ames, Iowa

1967

TABLE OF CONTENTS

NOMENCLATURE

Symbol	Units	Description
A	--	Voltage response ratio for thin-film gages
a	mm/μsec	Acoustic velocity, $\sqrt{\gamma g_c RT}$; also a dimensionless constant defined in Equation 82
b	--	Constant defined in Equation 82
C	--	Ratio of density-viscosity product, $\frac{\rho\mu}{(\rho\mu)_w}$
c	cal/gm°C	Thermal-energy capacity of thin-film gage backing material
c_p	cal/gm°C	Specific heat at constant pressure
c_v	cal/gm°C	Specific heat at constant volume
E	volts	Voltage drop across a thin-film gage
H	--	Dimensionless enthalpy, $\frac{h\rho}{p}$; also stagnation enthalpy in Equation 17
h	cal/gm	Enthalpy
I	amperes	Current through thin-film gage
K	cm^2/sec	Thermal diffusivity
k	cal/sec cm^2°C/cm	Thermal conductivity
M	gm/mole	Molecular weight; also dimensionless Mach number, $\frac{u}{a}$
m	--	Slope of line defined in Equation 80
Nu	--	Nusselt number, $\frac{\lambda x}{k}$
P	--	Dimensionless pressure ratio
Pr	--	Prandtl number, $\frac{c_p \mu}{k}$
p	Torr	Pressure

Q	cal/cm^2 sec	Thermal-energy flux
q	cal/cm^2 sec	Thermal-energy flux (same as Q)
R	cal/gm°K	Gas constant, R_u/M; also resistance of thin-film gage in ohms
Re	--	Reynolds number, $\frac{\rho u x}{\mu}$
R_u	cal/mole°K	Universal gas constant, 1.9873
r	--	Recovery factor, $\sqrt{Pr}$ for laminar flow
St	--	Stanton number, $\frac{q}{\rho u(h_{aw}-h_w)} = \frac{\lambda}{\rho u}$
s	--	Laplace variable
T	°K	Temperature; also dimensionless temperature ratio
t	microseconds(μsec)	Time
U	--	Dimensionless velocity, $u\sqrt{\frac{\rho}{p}}$; also velocity ratio
u	mm/μsec	Velocity for x direction in the shock-wave attached coordinate system
V	mm/μsec	Velocity for x direction in the laboratory fixed coordinate system
v	mm/μsec	Velocity for y direction in the shock-wave attached coordinate system
$\frac{W_x}{x}$	--	Uncertainty interval of any variable denoted by x, $\pm$ %
X	--	Dimensionless independent variable in mathematical model for regression analysis
x	mm	Coordinate direction; distance from shock-wave in the shock-wave attached coordinate system
Y	--	Dimensionless dependent variable in mathematical model for regression analysis

y	mm	Coordinate direction normal to the shock-tube wall
Z	--	Compressibility factor $\frac{p}{\rho RT}$
α	$1/^{\circ}C$	Temperature coefficient of resistance, $\frac{\Delta T}{R_o \Delta R}$
β	$cal/cm^2 {}^{\circ}C \sqrt{sec}$	Thermal product, $\sqrt{\rho kc}$
γ	--	Specific heat ratio, $\frac{c_p}{c_v}$
Δ	mm	Thermal boundary layer thickness
δ	mm	Velocity boundary layer thickness
ε	--	Correlation coefficient defined by Equation 83
η	mm	Transformation variable defined in Equation 13
λ	gm/cm^2 sec	Heat-transfer coefficient (surface conductance) defined in Equation 68
μ	gm/cm sec	Coefficient of viscosity (absolute viscosity)
ν	cm^2/sec	Kinematic viscosity, $\frac{\mu}{\rho}$
ξ	mm	Transformation variable defined in Equation 12
ρ	gm/cm^3	Density
τ	$dyne/cm^2$	Shearing stress, $\mu \frac{\partial u}{\partial y}$; also a dummy time variable or an exponential time constant in microseconds
ϕ	$^{\circ}C$	Temperature change from an initial value, $T - T_o = \Delta T$
χ	--	Dimensionless enthalpy difference, $H - H_1$
ψ		Stream function defined by Equation 14

Subscripts	Description
o	Variables at time zero; subscript for stagnation properties; and subscript for shock-tube driver section properties
1	Variable in the driven section of the shock tube before passing through the shock wave
2	Variable in the driven section of the shock tube after passing through the shock wave
∞	Denotes a reference condition which is usually taken to be the free-stream condition above a boundary layer
aw	Adiabatic wall condition
b	Pertains to the thin-film gage backing material
c	Pertains to the combustible mixtures
e	Free-stream condition; same as 2
f	Pertains to the thin-film gage; also represents a calibration fluid
i	Pertains to any variable evaluated in Region i where i may be either 1 or 2; also represents inert mixtures
ij	Used in dimensionless parameters formed by ratios of like quantities, for example, $U_{ij} = U_i/U_j$, $P_{ij} = p_i/p_j$ and $T_{ij} = T_i/T_j$
ℓ	Pertains to laboratory time
p	Pertains to particle time
q	Pertains to heat-transfer technique of obtaining transition times
r	Quantities associated with recovery factor
s	Pertains to the shock wave
T	Pertains to temperature technique of obtaining transition times
t	Pertains to any quantity evaluated at transition
u	Represents a universal quantity

w	Wall condition; same as 1

Superscript	Description
*	Quantities evaluated at Eckert's reference temperature; also dimensionless variables defined in Equation 68

INTRODUCTION

Object of the Investigation

In shock-wave studies it is well known that any boundary layer behind the shock wave will cause some attenuation of the shock-wave. Before an estimation of shock-wave attenuation can be made it is necessary to know if the boundary layer is laminar, turbulent or both. Thus, one must know whether or not boundary layer transition has occurred.

When using optical instrumentation in shock tubes, where measurements depend on changes in fluid density, refractive index, absorption or emittance, the interpretation of data often depends on the assumption that changes in the measured variable occur in the main stream and that boundary layer effects are negligible. In these cases, it is necessary to predict the extent of the validity of this approximation. This prediction will naturally depend on the type of boundary layer, hence, on whether or not boundary-layer transition has occurred.

In detonation-wave studies, the effect of the boundary layer on the formation process of the detonation wave may be required. In this process the flame-front velocity depends on fluid turbulence as well as viscous effects in the boundary layer. The extent of the boundary-layer effect will depend on the type of boundary layer in addition to duct size. Therefore, in certain instances, boundary-layer transition could be a contributing factor in transition from a flame front to a detonation wave.

If the shock tube is to be used as a short duration aerodynamic wind tunnel, the testing time available may depend on the time for boundary-layer closure to occur. The closure time will depend on the type of

boundary layer and, consequently, on whether or not boundary layer transition has occurred.

A concept of major importance is the boundary-layer development behind a shock wave moving along a solid surface. When a moving shock wave passes through a gas at rest, that gas is instantaneously compressed, heated, and set into motion. If this resulting flow of gas particles is constrained to move along a solid surface, such as a shock-tube wall, a boundary layer will be formed on that surface. Such a shock-induced boundary layer is normally laminar for a short distance behind the shock wave then goes through a transition regime to a turbulent boundary layer. When the test gas is inert, boundary-layer transition is known to be affected by surface roughness, pressure gradient, free-stream turbulence level and thermal-energy flux passing through the boundary layer (1). For the case of an inert gas and a laminar boundary layer, the thermal-energy transfer at the wall and the wall temperature rise have been determined analytically (2) and experimentally (3), using rapid-response thin-film resistance thermometers developed especially for studying shock-tube flows. The thin-film resistance thermometer can also be used to discriminate between laminar and turbulent boundary layers.

If the test gas is not inert, but combustible, the shock wave may induce an exothermic chemical reaction and a new flow situation occurs that has until recently been neglected experimentally and discussed theoretically only in qualitative terms. Some features of this new flow situation follow (4).

First, there is a region immediately behind the shock wave called the

induction zone, in which temperature, pressure, and composition remain nearly constant. The duration of this zone can be calculated if the chemical reactions and corresponding reaction rates are known. Second, the exothermic reaction occurs causing a temperature rise and density gradient in the gas. Under some circumstances a pressure gradient is also generated. Finally, if the reaction proceeds fast enough, an irregular flow structure with considerable turbulence is generated.

It is not clear what effects these new features in the flow will have on the stability of the shock-induced laminar boundary layer and on the thermal-energy transfer to the wall of the shock tube. For example, one would believe that the disturbances in the main flow caused by combustion would promote early transition from laminar to turbulent flow in the boundary layer. However, theory (5) indicates thermal-energy release above the boundary layer will stabilize it so that transition will not occur as it normally would without the thermal-energy release. In addition, some investigators (6) have observed a so called "transition reversal" effect where the boundary layer is first stabilized by heat-energy release and then destabilized when the heat-energy release becomes large enough.

Boundary-layer transition and, thus, heat-transfer rates to the shock-tube wall will be governed by the effect which dominates. Accordingly, this investigation was initiated in order to obtain data that would help in defining and understanding this new problem.

The primary objective of the investigation was to study, experimentally, the effect of free-stream thermal-energy release, as obtained from

shock-wave induced exothermic reactions, on boundary-layer transition and to measure the corresponding surface heat-transfer rates at transition in shock-tube flows. The results should serve as a guide for future analysis of the effect of incident thermal energy on boundary-layer transition.

The experimental results should assist in the estimation of heat-transfer rates to the wall of combustion chambers and nozzles in rocket engines or in any other equipment that might have burning gases flowing adjacent to solid surfaces. These applications are, of course, in addition to those involving shock-tube studies in which it is necessary to know how the boundary layer and other flow characteristics develop so that the shock tube may be used effectively and intelligently as an experimental testing facility.

General Considerations in Planning

Use of the shock tube

During the last decade the shock tube has become prominent as a device for producing and studying high-temperature short-duration gas flows and it is an especially convenient vehicle for this investigation because the boundary layers and exothermic reactions can be produced simultaneously with relative ease.

In its simplest form the shock tube consists of two closed chambers separated by a diaphragm. Gases such as hydrogen, helium or air are introduced at a relatively high pressure into one of the closed chambers while a test gas of desired composition is introduced at a relatively low pressure into the other closed chamber. The high pressure chamber is called the driven or expansion section. .

When the desired pressures are obtained in the driver (compression) and driven (expansion) sections, the flow is generated by rupturing the diaphragm separating the two sections. This allows the driver gas to expand into the driven section causing compression waves to propagate ahead of the driver gas into the test gas. At the same time rarefaction (expansion) waves propagate back into the high pressure driver gas. As the compression waves move into the test gas they coalesce to form a shock wave. Passage of this shock wave through the stationary test gas causes a compression, heating and acceleration of test gas particles.

The velocity of compressed gas depends on the strength of the shock wave inducing the motion as well as the molecular weight of the test gas. For a given test gas, it is possible to achieve various shock strengths, yielding a wide range of flow temperatures, pressures and velocity, by merely adjusting the pressure ratio across the diaphragm before the bursting operation. The details of controlling shock-wave strength as used in this investigation are discussed later.

The expanding driver gas, behaving much like a piston in a cylinder, forms a contact surface (that is, a surface which separates driver gas from test gas) as it moves into the driven section. The region between the contact surface and the shock wave was used as the testing region in this investigation. Ideally, this region has uniform properties of pressure and temperature. Actually, there may be deviations from the ideal case depending on shock-wave strength and nature of the test gas. Figure 1 illustrates the initial and operating conditions of a typical shock tube. The testing region is denoted as Region 2 in Figure 1-b. The

Figure 1. Ideal shock tube flow

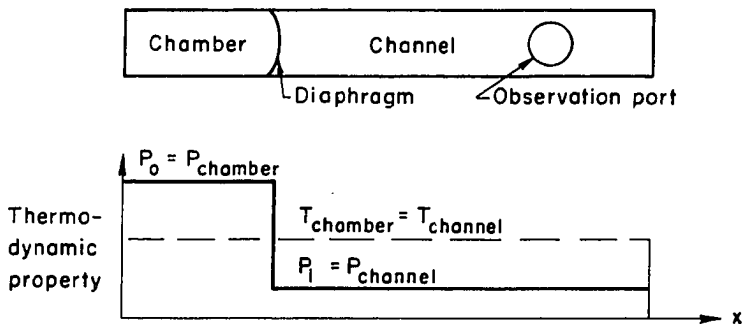

a) Initial conditions

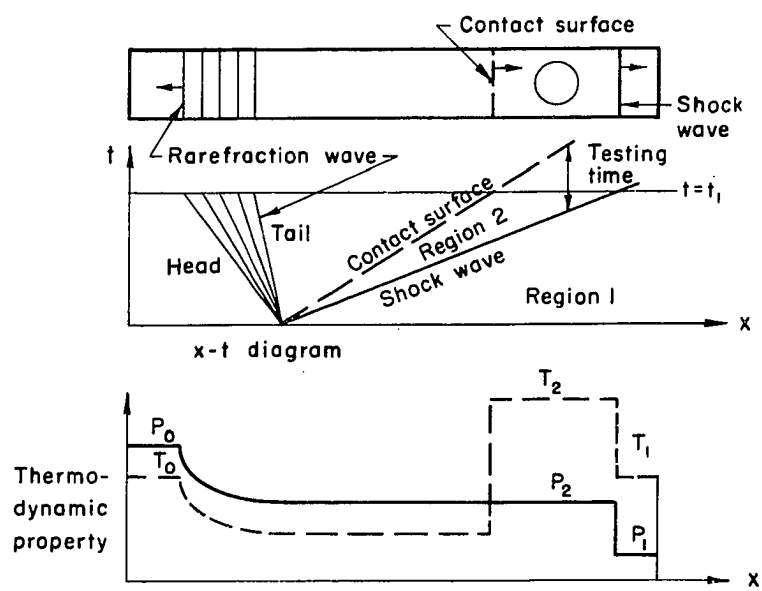

b) Operating conditions

theoretical testing time in Region 2 is shown on the x-t diagram in Figure 1-b. Actual testing times are about 50% of this value because of non-ideal conditions which occur (such as particle diffusion across the contact surface) and boundary-layer formation behind the shock wave.

Flow model

The flow model presented schematically in Figure 2 is that of a boundary layer developing in two-dimensional unsteady flow over a flat surface. The following regions are illustrated.

Region 1: In a laboratory fixed coordinate system the test gas in Figure 2-a is at rest with pressure p_1 and temperature T_1 respectively. A normal (plane) shock wave is moving from right to left with velocity V_1 into the stationary test gas.

Region 2: The moving shock wave compresses, heats, and accelerates the test gas to a new pressure, temperature and velocity denoted by p_2, T_2 and V_2 respectively. Boundary-layer development occurs in Region 2 as illustrated in Figure 2-a and is unsteady in this coordinate system.

If, instead of the laboratory fixed coordinate system, one fixes a coordinate system to the moving shock wave the flow is reduced to steady state. This coordinate transformation is illustrated in Figure 2-b.

In the shock-fixed coordinate system the shock wave is stationary while both the test gas in Region 1 and the shock-tube wall approach the shock wave with velocity u_1. The shock wave reduces the test gas velocity to u_2 while the wall velocity is unaffected. This results in a boundary layer along the wall behind the shock wave in Region 2 since the "no-slip" condition applies at the wall surface.

Figure 2. Flow model

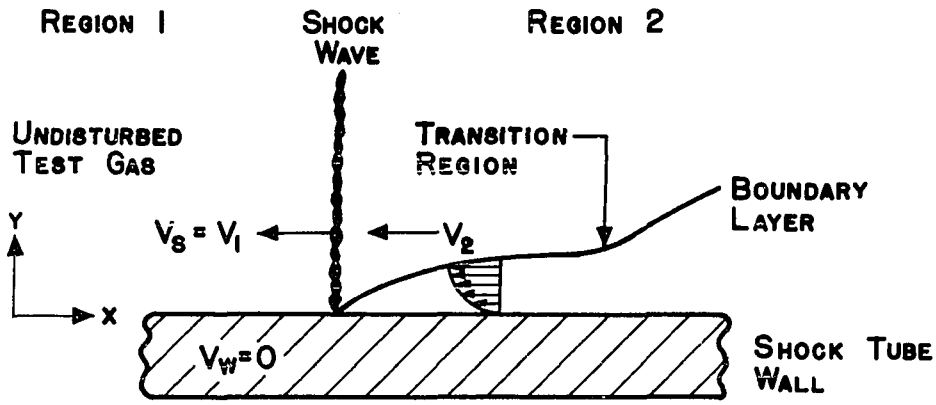

A) LABORATORY COORDINATES

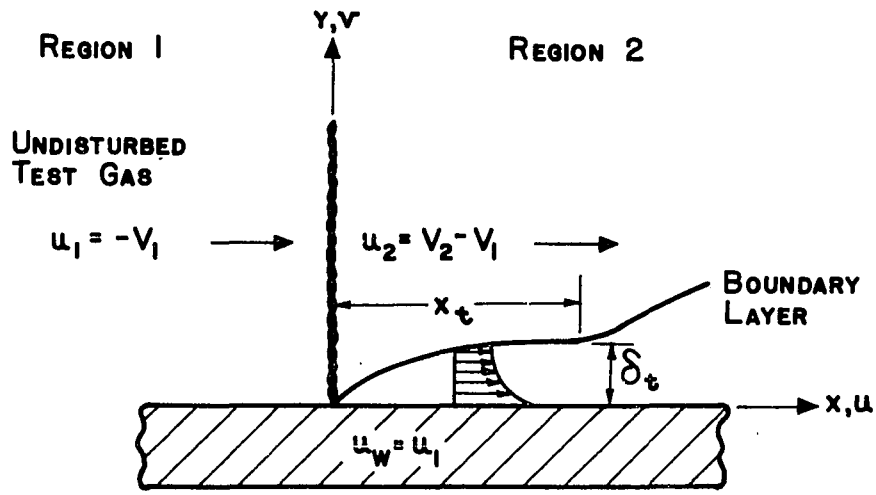

B) SHOCK WAVE COORDINATES

For this case of a two-dimensional laminar boundary layer in steady flow, the following equations are given by Mirels (2) to make up the mathematical model of the flow.

Mass conservation (continuity): $$\frac{\partial(\rho u)}{\partial x} + \frac{\partial(\rho v)}{\partial y} = 0 \tag{1}$$

Momentum conservation: $$u\frac{\partial u}{\partial x} + v\frac{\partial u}{\partial y} = \nu\frac{\partial^2 u}{\partial y^2} \tag{2}$$

Energy conservation: $$\rho u\frac{\partial h}{\partial x} + \rho v\frac{\partial h}{\partial y} = \frac{\partial}{\partial y}\left(\frac{\mu}{Pr}\frac{\partial h}{\partial y}\right) + \mu\left(\frac{\partial u}{\partial y}\right)^2 \tag{3}$$

Equation of state: $$p = Z\rho RT \tag{4}$$

The boundary conditions needed for solution of these equations are:

$$\begin{aligned} &\text{(i)} && u(x,0) = u_w = u_1 \\ &\text{(ii)} && v(x,0) = 0 \\ &\text{(iii)} && h(x,0) = h_w \\ &\text{(iv)} && u(x,\infty) = u_e = u_2 \\ &\text{(v)} && h(x,\infty) = h_e = h_2 \end{aligned} \tag{5}$$

Equations 1 through 4 are those that apply to the laminar flow of a gas over a semi-infinite flat plate. It should be noted, however, that boundary condition (i) differs from those for semi-infinite flat-plate flow. Thus, the solutions to Equations 1 through 4 differ from solutions for semi-infinite flat-plate flow.

In addition to Equations 1 through 4 the following relations are used at the surface of the shock-tube wall.

Wall shear stress: $$\tau_w = \mu\left(\frac{\partial u}{\partial y}\right)_w \tag{6}$$

Heat flux into wall: $q_w = k(\frac{\partial T}{\partial y})_w = \frac{\mu}{Pr}(\frac{\partial h}{\partial y})_w = \lambda(h_{aw} - h_w)$ (7)

Equations 1 through 7 are solved by Mirels for the case of an inert gas with both Prandtl number and heat capacity constant. His solutions are indicated in the Literature Review section. Equations 1 through 7 are also used in the Dimensional Analysis section to indicate the set of dimensionless variables relevant for data correlation.

Test gas mixtures

It was deemed necessary for this study to obtain experimental data from matched sets of combustible and inert-gas mixtures over a range of shock-wave strengths. Proper selection of shock-wave strength would insure that the flow temperature in the test region would be above the ignition temperature of the combustible mixture and within a temperature range where the appropriate chemical kinetics were known. Thus, one would be certain to obtain both ignition after a suitable ignition-delay time (induction time) and the induction time from the known chemical kinetics and reaction rates.

Combustible and inert mixtures were made up by matching molecular weights between hydrogen-oxygen-nitrogen combustible combinations and hydrogen-nitrogen inert combinations. Thus, both combustible and inert diatomic mixtures would have the same sound speed and virtually the same transport properties. In this way, any peculiar results arising from uncontrolled factors in the experiment would be detected and separated from effects attributable only to the combustion reactions.

Combustible mixtures consisting only of diatomic molecules of hydrogen, oxygen and nitrogen (an inert diluent) were used. The volume percentage of

hydrogen in the mixture was kept below that for which detonation would occur and above the lower flammability limit. This limitation was used as a safety precaution and also because the boundary layer normally becomes turbulent directly behind a detonation wave (7).

Concept of laboratory and particle time

At this point it is necessary to introduce some definitions and important concepts associated with shock-tube flows. Reference to Figure 3 is necessary for their understanding.

Laboratory time, t_ℓ, is defined, for a given position on the shock-tube wall, as the time interval between arrival of the shock wave and arrival of the so called "transition point" of the boundary layer. This time is that which would be detected by a transducer placed in the side wall of the shock tube. Particle time, t_p, is defined as the interval between passage of a fluid particle in the free stream through the shock wave and the time at which the moving transition point reaches this fluid particle. Thus, as illustrated in Figure 3, $t_\ell = t_3 - t_2$ and $t_p = t_3 - t_1$. The length x_t is the distance measured from the shock wave to the transition point and is equal to $V_1 t_\ell$. The length x_p is the distance a fluid particle moves relative to the wall from the time it passes through the shock wave until overtaken by the moving transition point. This distance is equal to $V_2 t_p$. Consideration of similar triangles in Figure 3 yield important results given below for relating both laboratory to particle time and x_p to x_t. From Figure 3

$$\frac{x_p + x_t}{t_p} = \frac{x_t}{t_\ell} \quad \text{or} \quad \frac{t_\ell}{t_p} = 1 - \frac{x_p t_\ell}{x_t t_p} \tag{8}$$

Figure 3. Illustration of laboratory and particle time

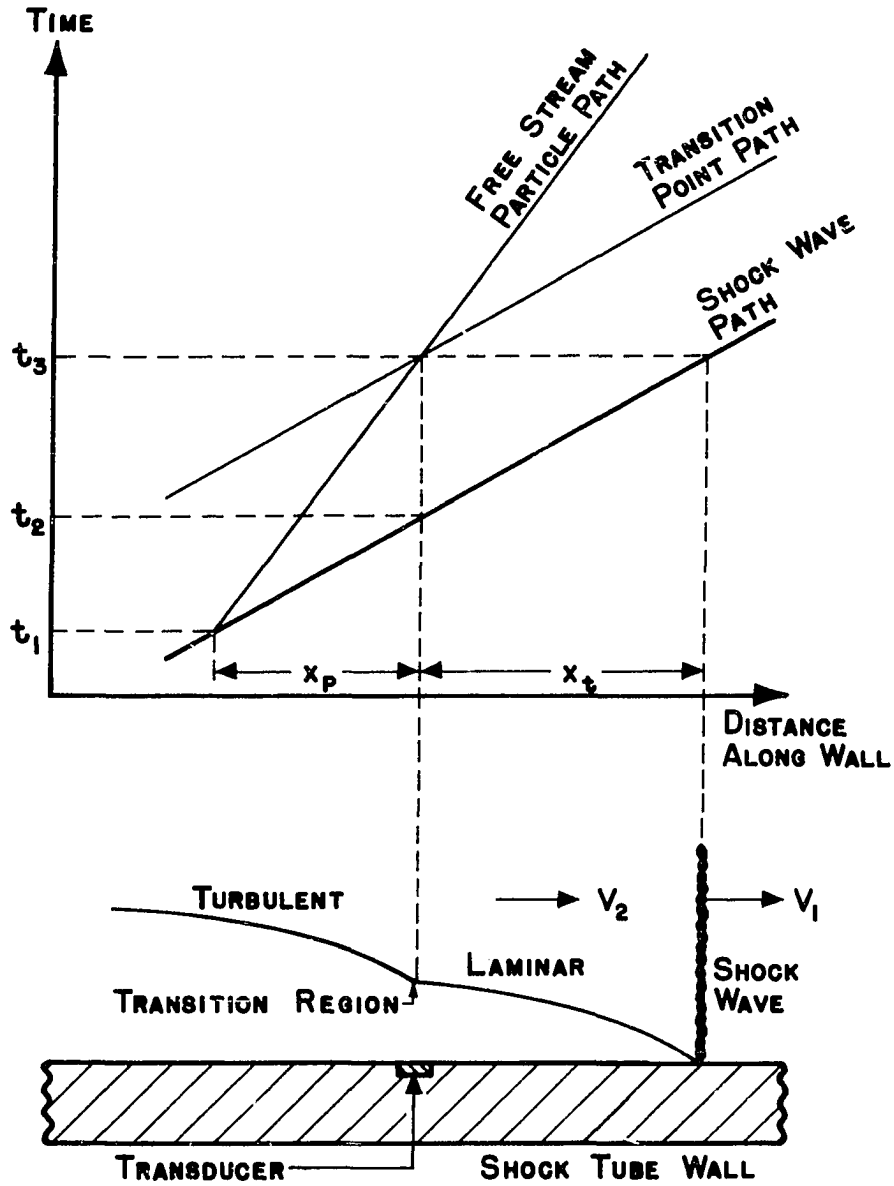
TIME
FREE STREAM PARTICLE PATH
TRANSITION POINT PATH
SHOCK WAVE PATH
t_3
t_2
t_1
x_p
x_t
DISTANCE ALONG WALL
TURBULENT
V_2
V_1
LAMINAR
SHOCK WAVE
TRANSITION REGION
TRANSDUCER
SHOCK TUBE WALL

Using $x_t = V_1 t_\ell$ and $x_p = V_2 t_p$ along with the velocities u_w and u_e in the coordinate system fixed to the moving shock wave and mass conservation across the shock wave, this relation becomes

$$1 - \frac{V_2}{V_1} = \frac{t_\ell}{t_p} = \frac{V_1 - V_2}{V_1} = \frac{u_e}{u_w} = \frac{1}{U} = \frac{\rho_1}{\rho_2}$$

or

$$t_p = U t_\ell = \frac{\rho_2}{\rho_1} t_\ell \tag{9}$$

Substitution of Equation 9 into Equation 8 yields the relation between x_t and x_p as follows

$$x_p = x_t(U-1) \tag{10}$$

LITERATURE REVIEW

Historically, the initial reason for studying shock-tube boundary layers was to determine their role in departures from ideal shock-tube flow. In particular, emphasis was placed on determining the influence of a boundary layer behind a shock wave on shock-wave attenuation. Additionally, estimates of decreased testing time were desired.

More recently, the reason for studying shock-tube boundary layers has been to examine effects of high-temperature phenomena such as dissociation and ionization on boundary-layer behavior. This is because such high temperature phenomena can be produced with relative ease in shock tubes as compared to conventional steady-flow facilities.

In current investigations, knowledge of the shock-tube boundary layer is necessary in order to correctly interpret experimental data. This is especially true with optical measurements as was indicated in the Introduction section.

General References

Glass and Hall (8) have presented an excellent review of shock-tube investigations made before 1960, and Bernstein (9) has evaluated attenuation studies prior to 1961. In an experimental investigation, Bernstein (10) not only extended previous attenuation studies to shock tubes of arbitrary cross section, but included effects of converging or diverging passages.

Shock-Tube Boundary-Layer Solutions and Pertinent Experimental Observations

Constant $\rho\mu$ across the boundary layer

Hollyer (11) was the first to employ the appropriate differential equations and correct boundary conditions to investigate shock tube boundary layers. His analysis, based on the Karman-Pohlhausen integral technique, yielded laminar skin-friction and heat-transfer coefficients. Later (12), he used a numerical procedure to solve the boundary layer equations for the same coefficients and, after a correction in Reference 11, found the integral results to agree reasonably well with his numerical results as well as with other numerical work by Mirels (13).

Since that time Mirels (13,14,15,2) has completely solved the case of a laminar boundary layer in a non-reacting gas with zero-pressure gradient and a uniform-surface temperature. Under these conditions, and others to be mentioned later, Mirels obtained velocity and temperature profiles along with skin-friction and heat-transfer coefficients, and recovery factors. A brief summary of Mirels' analysis based on Equations 1 through 7 of the Introduction section is presented below because his results are applicable to the inert gas experiments in this investigation. Understanding of items in later references to be mentioned will also depend on this analysis.

Mirels uses a stream function ψ such that

$$\frac{\partial \psi}{\partial y} = \frac{\rho u}{\rho_w} \qquad \text{and} \qquad \frac{\partial \psi}{\partial x} = -\frac{\rho v}{\rho_w} \tag{11}$$

in order to satisfy the continuity relation (Equation 1). To transform the partial differential equations of energy and momentum for the boundary

layer to ordinary differential equations Mirels uses a similarity parameter η. This similarity parameter is of the Dorodnitsyn-Howarth type such that density ρ and coordinate variable y are replaced by η in the partial differential equations. The transformation equations are

$$\xi = x \tag{12}$$

$$\eta = \left(\frac{u_e}{2x\nu_w}\right)^{1/2} \int_0^y \frac{\rho}{\rho_w}\, dy \tag{13}$$

In terms of the new independent variables ξ and η Mirels takes the stream function ψ to have the form

$$\psi = (2u_e\, \xi\, \nu_w)^{1/2} f(\eta) \tag{14}$$

and the following definitions are used.

$$C \equiv \frac{\rho\mu}{(\rho\mu)_w} \tag{15}$$

$$U \equiv \frac{u_w}{u_e} \tag{16}$$

$$g \equiv \frac{H}{H_e} \equiv \frac{h + u^2/2}{H_e} = \frac{h}{H_e} + \frac{u_e^2}{2H_e}(f')^2 \tag{17}$$

The relations above allow the following ordinary differential equation for momentum and energy, respectively, to be obtained.

$$[Cf'']' + ff'' = 0 \tag{18}$$

$$\left[\frac{C}{Pr}\, g'\right]' + fg' + \frac{u_e^2}{2H_e}[2C(1 - 1/Pr)f'f'']' = 0 \tag{19}$$

The boundary conditions for Equations 18 and 19 become

(i) $f(0) = 0$

(ii) $f'(0) = U$ (no-slip condition) (20)

(iii) $f'(\infty) = 1$

(iv) $g(0) = \frac{h_w}{H_e} + \frac{u_e^2 U}{2H_e}$

(v) $g(\infty) = 1$

It should be noted that the value of $f'(0)$ in boundary condition (ii) is the difference between semi-infinite flat plate boundary layers and shock tube boundary layers.

The shearing-stress and heat-energy transfer at the wall, in terms of the transformation variables, become

$$\tau_w = \left(\mu \frac{\partial u}{\partial y}\right)_w = \mu_w u_e (u_e/2\xi\nu_w)^{1/2} f''(0) \tag{21}$$

$$q_w = \left(k \frac{\partial T}{\partial y}\right)_w = \left(\frac{\mu}{Pr}\right)_w (u_e/2\xi\nu_w)^{1/2} h'(0) \tag{22}$$

By assuming $\rho\mu$ is constant (C=1) across the boundary layer Equation 18 reduces to the familiar Blasius form $f''' + f'' = 0$. If, in addition, Pr = 1 Equation 19 reduces to $g'' + fg' = 0$. When $(U-1) \ll 1$, the problem reduces to that of an infinite plate impulsed suddenly to velocity U-1. This special case is called "Stokes first problem" although, as indicated in Reference 16, it is commonly called (without justification) the "Rayleigh problem".

Mirels (13) "re-solves" this special case analytically and also solves Equations 18 and 19 numerically for C = Pr = 1 with U values of 1.5, 2, 3, 4, 5 and 6; and for C = 1, Pr = 0.72, with U values of 2, 4 and 6. The numerical procedure used is presented by Albers in Appendix B of Reference 17. Even though Mirels solves the flow governing equations from a steady

flow viewpoint, he defines dimensionless Reynolds and Nusselt numbers based on the unsteady flow coordinate system by using the flow velocity relative to the wall. He also uses a characteristic length $(u_w - u_e)t$ which is the distance a particle in the free stream moves relative to the wall in time t. These dimensionless correlation parameters are given as

$$Re = \frac{(u_w - u_e)^2 t}{\nu_w} \tag{23}$$

$$Nu = s'(0)(2Re/U)^{1/2} \tag{24}$$

where s satisfies $s'' + (Pr)fs' = 0$, and when Pr = 1 becomes

$$s = (f'-1)/(U-1) \tag{25}$$

For transition, t becomes t_p and the transition Reynolds number becomes

$$Re_t = \frac{(u_w - u_e)^2 t_p}{\nu_w} = \frac{(U-1)^2 u_e x_t}{\nu_w} \tag{26}$$

in view of definitions presented in the Introduction section.

In Reference 14, Mirels extends this work for C = 1 to include boundary layers behind expansion waves of zero thickness (so called "negative shocks"), turbulent boundary layers and wall temperature. Because values of U and Pr have to be specified for each numerical solution Mirels also obtained integral solutions of the Karman-Pohlhausen type to provide a guide for obtaining expressions which would accurately represent the numerical data. The expressions presented for evaluation of wall-surface heat transfer and wall-surface shearing stress (via Equations 21 and 22) for Pr = 1 with laminar flow are

$$\frac{-f''(0)}{U-1} = \frac{h'(0)}{h_r - h_w} = 0.489(1 + 1.665U)^{0.5} \tag{27}$$

where

$$\frac{h_r}{h_e} = 1 + [U-1]^2[u_e^2/2h_e]Pr^{0.39-0.023U} \tag{28}$$

when $Pr \neq 1$, $h'(0)$ is multiplied by the factor

$$Pr^{-(0.48+0.022U)} \tag{29}$$

These formulas allowed agreement within 1% of the numerical data for $Pr = 0.72$ and U between 1 and 6. Other expressions for turbulent boundary layers were obtained by assuming a 1/7 power profile in velocity relative to the wall. For data correlation the Reynolds number as given in Equation 23 was used.

Mirels also found the wall-surface temperature to be constant with distance behind the shock wave for laminar boundary layers and to vary non-linearly with distance behind the shock wave for turbulent boundary layers.

Bromberg (3), in a study independent of Reference 14, used a Crocco type transformation where u and x are used as independent variables in the momentum and energy equations. The dependent variables become viscous stress τ and enthalpy h. This transformation allowed a separation of variables type solution for viscous stress of the form $\tau = \chi(x)U(u)$ when $C = Pr = 1$.

By assuming the shock-tube wall behaves as a semi-infinite body to heat-energy flux, and that no relaxation processes occur in the shock-tube flow, Bromberg found the wall-surface temperature to remain constant behind the shock wave in laminar flow. This was in agreement with Mirels' result as previously presented. More significantly, Bromberg was one of the first

(if not the first) to recognize the importance of this result whereupon he suggested using wall-temperature measurements to study shock-tube boundary-layer characteristics. In recent years this has become a common technique with thin-film resistance thermometers used to discriminate between laminar and turbulent boundary layers, and to obtain "transition points". A modification of this technique has been used in this experimental investigation.

Bershader and Allport (18) present a treatment of the shock-tube boundary-layer problem under the same assumptions as Bromberg. In addition, they obtain laminar-flow measurements of density profiles with an interferometer and wall-surface temperatures with a thin-film resistance thermometer. The wall-surface temperature variation was in agreement with the theoretical predictions of Bromberg and Mirels.

Trimpi and Cohen (19), using the Karman-Pohlhausen integral approach for C = 1 and Prandtl numbers of 0.72 and 1 respectively, present results for the entire shock tube problem. In particular, they solve the complete shock-tube flow for driver-chamber to driven-chamber gases of air-air, hydrogen-air and helium-air with Pr = 0.72; and air-air with Pr = 1. Skin-friction and heat-transfer coefficients for the region behind the shock wave agree with those predicted by Mirels in Reference 14.

Duff (20), using Mirels' theoretical development, solved the boundary layer equations on an analog computer for argon with values of U of 1.5, 2.0, 2.5, 3.0 and 3.5. Agreement with the previous work of Hollyer and Mirels was good.

Variable $\rho\mu$ across the boundary layer

An assumption common to the investigations previously mentioned has been constant $\rho\mu$ (C=1) across the boundary layer. This was a convenient assumption since it allowed simplification of Equations 18 and 19. However, Mirels (15) in extending the results of References 13 and 14 to stronger shock waves estimated the effects of variable $\rho\mu$ on both laminar and turbulent shock-tube boundary layers in air. Real gas properties were used and the boundary layer was assumed to be in thermodynamic equilibrium with Pr = 1. Later, Mirels (2) extends this work for Pr = 0.72. Numerical results for shear-stress and heat-transfer coefficients are extended up to U = 11.33 (M_s = 14). The resulting interpolation formula for Pr = 1, T_1 = 522°R and p_1 = 0.001 atmospheres agreed within 3% of the numerical results and is a modification of Equation 27 by the factor $C_e^{0.29}$, thus,

$$\frac{-f''(0)}{U-1} = \frac{h'(0)}{h_r-h_w} = 0.489(1 + 1.665U)^{0.5} \left(\frac{(\rho\mu)_e}{(\rho\mu)_w}\right)^{0.29} \qquad (30)$$

The effect of a constant Prandtl number other than one can be estimated in the same way as given previously by Equation 29. Mirels obtained comparisons with numerical results within 4% for Pr = 0.72 with this modification and within 2.5% if, in addition, the exponent on C_e is changed from 0.29 to 0.265.

Theoretical wall-surface temperatures were also determined in more detail than before with the following result. Wall-surface temperature rises discontinuously across the shock wave, remains uniform behind the shock wave until boundary layer transition occurs, then increases non-

linearly with distance from the effective origin of the turbulent boundary layer raised to the 0.3 power. Experimental measurements of References 18 and 21 agree approximately with this prediction especially for the laminar case.

Mirels defines a transition Reynolds number for correlation of experimental transition data. As in Reference 13, the characteristic velocity is taken to be the velocity of the free stream relative to the wall ($u_w - u_e$) and the characteristic distance is taken as x_p (that is, the distance a particle in the free stream would move relative to the wall before being overtaken by the transition point). However, the kinematic viscosity is evaluated at the free-stream temperature rather than the wall temperature. Recall from the Introduction section that $x_p = x_t\,(U-1)$ so that

$$Re_t = \frac{(u_w - u_e)}{\nu_e}\, x_p = \frac{u_e (U-1)^2 x_t}{\nu_e} \tag{31}$$

Mirels apparent justification for selecting this particular form of Reynolds number is that it reduces to a result commonly used in flat-plate steady-flow analysis when $u_w = U = 0$.

Glass and Hall (8) define a similar transition Reynolds number except for kinematic viscosity evaluated at the wall temperature. This is equivalent to Equation 26.

Mirels expresses the need for experimental data in all of his references and specifically, in Reference 15, points out the need for boundary-layer transition data.

Several experimental investigations have been carried out to verify

assumed velocity profiles as well as to determine transition Reynolds numbers for the shock tube boundary layer. In addition to the previously mentioned work of Bershader and Allport, Martin (22) and Gooderum (23) have made interferometer studies of turbulent boundary layers. Results of both Martin and Gooderum have indicated power profiles in velocities relative to the wall from 1/5 to 1/7 depending on free-stream velocity and wall roughness. Thus, Mirels assumption of a 1/7 power profile was approximately verified. Martin also obtained transition Reynolds numbers by Schlieren and shadowgraph measurements to compare with simultaneously obtained thin-film resistance thermometer data. Using the transition Reynolds number defined in Equation 31 Martin found considerable differences between the optical technique and the thin-film technique. Typically, the thin-film technique gave larger transition Reynolds numbers than the optical technique and in some cases, was more than 100% larger. No explanation for this difference was given.

Becker (24) presents a survey of studies before 1959 for non-steady compressible boundary layers behind both shock and expansion waves. He also includes experimental interferometric data for turbulent flow velocity profiles with values of U from 2.0 to 3.3. His experimental results are between 1/5 and 1/7 power profiles. Becker defines a Reynolds number, different than that generally used by Mirels and others, which is equivalent to the following equation at transition.

$$Re_t = \frac{V_2^2 V_1 x_t}{\nu_w} = \frac{(U-1)^2 u_w x_t}{\nu_w U^2} \qquad (32)$$

Instead of using this Reynolds number to correlate data Becker uses $Re_t(U)$

which is equivalent to using Equation 23 as defined by Mirels. At transition $Re_t(U)$ was approximately 7×10^5 for the range of U given above.

Daiber (25) developed a Schlieren-photomultiplier combination to obtain transition Reynolds numbers as well as local density within the boundary layer. His transition Reynolds numbers are slightly less than those obtained optically by Martin.

More recently, particle tracer techniques used to measure velocity profiles by Chen and Emrich (26), and Gion (27) gave reasonable agreement with Mirels' assumption for turbulent flow. However, Chen and Emrich show appreciable differences for laminar flow. The "zero slip" condition is questioned by Chen and Emrich on the basis of their experimental observations and they suggest that finite slip at the wall may be the reason for poor comparison of velocity profiles in laminar flow. Gion obtains good comparison of laminar velocity profiles except when his measurements are made very close to the shock wave. His observations also support the notion of finite slip at the wall at least during the initial formation of the boundary layer behind the shock wave.

Variable free-stream properties

The most recent references attempt to account for non-uniform free-stream properties in the flow direction. Such variable properties may occur behind shock waves that are either attenuating due to viscous action or accelerating due to detonation phenomena. Mirels and Hamman (28) have extended the previous references of Mirels by a theoretical analysis of the shock-induced laminar boundary layer behind shock waves moving at non-uniform velocity. The shock wave velocity is represented by the power

law $u_1 = cmt^{m-1}$ where c and m are constants. Plane, cylindrical and spherical shock waves are studied with particular emphasis on shock waves generated by explosions, electrical discharges or conventional shock tubes.

Bertin (29) solves the flow field behind a moving shock wave with a laminar boundary layer considering variations in thermodynamic properties as well as velocity. The momentum and energy equations are solved subject to a gross continuity equation where the mass flow across any given cross section of the shock tube is equal to the mass flow across the shock wave. Bertin uses the so called Levy-Lees transformation equations in the following form:

$$\xi = \int_0^x \rho_w \mu_w u_w \, dx \tag{33}$$

$$\eta = \frac{\rho_w \mu_w}{(2\xi)^{1/2}} \int_0^y \frac{\rho}{\rho_w} \, dy \tag{34}$$

The momentum equation has one additional term because of the pressure gradient dp/dx. Equation 18 is then replaced by the following transformed momentum equation while the energy equation (Equation 19) remains the same.

$$[Cf']' + ff'' + 2\xi \frac{\rho_e u_e}{\rho u_w^2} \frac{du_e}{d\xi} = 0 \tag{35}$$

Bertin determines testing times from solutions of the momentum, energy and continuity to compare with measured testing times and finds good agreement with testing times measured by hot-wire anemometers in investigation by Roshko (30) and Sandborn (31). Additionally, theoretical calculations of the heat-transfer correlation parameter $St\sqrt{Re}$ yielded an approximately

constant value of 1.13 over a range in M_s from 4.5 to 9.5. This is nearly 100% larger than experimental results of Hartunian et al. (32) to be discussed later.

Exact numerical solutions of the non-steady compressible Navier-Stokes equations have been carried out by Kurzrock and Mates (33). They assume an ideal, non-reacting gas with both Prandtl number and specific heat constant. In applying their solutions to shock-tube flow they find their results to be in qualitative agreement with existing experimental and theoretical results.

Breeze and Ferriso (34) have recently measured, with thin-film resistance thermometers, transition Reynolds numbers in argon and carbon dioxide. They have found good comparison with previous results reported for air. Average values of their transition Reynolds numbers are about 8×10^5 as determined by Equation 31.

Effect of Thermal-Energy Transfer on Shock-Tube Boundary-Layer Transition

The effects of heat transfer on boundary-layer transition on a flat plate in steady flow have been studied theoretically by Low (5) and experimentally by Van Driest and Boison (35). Their investigations indicate that a boundary layer can be stabilized by heat addition near the outer edge of the boundary layer or by cooling the plate surface. For example, energy release by combustion in the free stream, condensation of a vapor in the free stream or evaporation of liquid on the plate surface would result in a heat-energy flux in a direction from the free stream to the plate surface and possibly delay boundary layer transition. The experimental results of Jack et al. (6) , Higgens and Pappas (36), and Kline

and Shapiro (37) have indicated this possibility of delaying boundary layer transition as long as an extreme heat-energy flux is avoided. When the heat-energy flux becomes too high the boundary layer is destabilized and boundary layer transition occurs sooner than expected. This is the so called "transition reversal" effect.

In shock tubes, Stetson (38) has observed for flow over blunt bodies that transition Reynolds numbers did not change appreciably with surface cooling. Thus, some uncertainty exists concerning the effects of heat-energy flux on boundary layer transition.

Hartunian, et al. (32), performed an experimental investigation to obtain, for air, systematic boundary-layer transition data as well as laminar and turbulent heat-transfer rates on the shock-tube wall. The data was obtained by means of thin-film resistance thermometers placed on a glass sidewall of the shock tube. Values of the shock wave Mach number ranged from 1.5 to 10 while values of the wall-to-stream temperature ratio T_w/T_e ranged from 0.8 to 0.07. Available transition data from other prior investigations were included in this work for comparison purposes.

The effect of heat-transfer rate on boundary-layer transition was shown indirectly by a plot of wall-to-stream temperature ratio T_w/T_e as a function of transition Reynolds number as given in Equation 31. The transition Reynolds number increased as the stream temperature increased for a given wall temperature indicating an increase in boundary-layer stability with increased temperature difference (and thus, heat flux) across the boundary layer. Some additional data taken in this investigation with argon, where an increase in heat-transfer rate over convection

occurred because of radiation, for a range of T_w/T_e between 0.37 and 0.15 gave considerable increases in transition Reynolds numbers over those of the air data for the same range of T_w/T_e. Thus, the effect of an increase in heat-transfer rate from the free stream to the wall was to stabilize the boundary layer and increase the transition Reynolds number. Of the results presented, none indicate any "transition reversal" phenomena. It should be noted that more explicit results could have been obtained if actual heat-transfer rate had been used rather than a temperature ratio.

Considerable scatter existed in the data mentioned above for which there are at least two possible explanations. Cross-sectional dimensions and surface finishes of the shock tube varied widely, and some of the data was obtained by optical means while other data was obtained by transient surface-temperature measurements using thin-film resistance thermometers. Also, there was some uncertainty as to what length should be used in the transition Reynolds number. Using boundary-layer thickness for this characteristic length yielded a poorer correlation while a displacement thickness yielded slightly better results compared to x_t.

Heat transfer rates measured on the shock-tube wall where correlated in terms of a plot of $St(Re)^{1/n}$ as a function of the shock wave Mach number M_s. The value of n was 2 for a laminar boundary layer and 5 for a turbulent boundary layer. Even though considerable scatter characterizes this data, general trends have been established. For the laminar case $St(Re)^{1/2}$ was approximately 0.7 at an M_s of 3 and did not change significantly with M_s within the scatter of their data. This was in reasonable agreement with theoretical calculations of Mirels. Agreement was not so

good in the turbulent case as $St(Re)^{1/5}$ remained approximately constant at 0.037 as M_s was varied while Mirels' theory predicts a decrease in $St(Re)^{1/5}$ as M_s is increased. However, at an M_s of 3 good agreement for the turbulent case existed.

Sichel and David (7) have calculated expected heat-transfer rates behind detonation waves in hydrogen-oxygen mixtures. By assuming a turbulent boundary layer and using turbulent relations presented by Mirels in Reference 15 they obtain a value 0.0446 for the correlation parameter $St(Re)^{1/5}$. This value is applicable over a wide range of pressures and temperatures for Chapman-Jouguet detonations when U is between 1.71 and 1.79. Presumably, the value of $St(Re)^{1/5}$ is higher than the experimental result of Hartunian et al. for air because of the increase in heat transfer to the wall due to combustion.

Ostrach and Thornton (39) have presented a theoretical analysis of the stability of shock-tube boundary layers with particular emphasis on determining the effects of surface cooling on boundary-layer transition. They determine minimum critical transition Reynolds numbers to compare with the experimental data of Hartunian et al. and others. The comparison is very poor as there are large differences in magnitudes and the general trends of the data are in complete opposition to the theory. Ostrach and Thornton conclude that the theoretical model studied and the phenomena observed in the shock tube do not appear to be closely related. Thus, as they indicate, one should not conclude that either the theory or the experiments are incorrect, however, more applicable transition data as well as new theoretical approaches are necessary.

Recent investigations by Sheetz (40), and Rumsey and Lee (41) have verified that boundary-layer transition is delayed with surface cooling over various geometric shapes while investigations of Brinich (42), and Deem and Murphy (43) show virtually no effect of surface cooling on boundary-layer transition.

The data of Richards and Stollery (44) is of particular interest because they obtained a "double reversal" effect on flat plates in a gun tunnel. The boundary layer was first stabilized with wall cooling, then destabilized with further wall cooling and finally stabilized again with even more wall cooling. This "double reversal" effect had been predicted earlier by Wisniewski and Jack (45) experimentally, and then analytically by Reshotko (46) in a boundary-layer stability analysis. The result of Richard and Stollery for a Reynolds number per unit length of 7.1×10^5 and a flow Mach number of 8.2 show that as the ratio of wall-to-recovery temperatures decreases between 0.3 and 0.2 the entire "double transition" phenomena occurs. Transition lengths were obtained optically with a shadowgraph technique and also with wall mounted thin-film resistance thermometers. It was found that the optical measurements corresponded to the end of transition as measured by the thin-film detectors. Maximum transition Reynolds numbers could not be established as in some cases the boundary layer was still laminar at the end of the flat plate.

Most of the investigations mentioned above have verified that wall cooling will stabilize the boundary layer and that a "transition reversal" effect occurs. However, there has been no satisfactory explanation of the reversal phenomena. Furthermore, the maximum transition Reynolds number

which can be reached by wall cooling has not yet been established.

EXPERIMENTAL INVESTIGATION

Experimental Facilities and Instrumentation

The apparatus used in this investigation consisted of a shock tube[1], its associated instrumentation and gas mixtures. Figure 4 shows a schematic diagram of the installation. Figures 5, 6 and 7 are actual photographs of the apparatus. Extensive description of typical shock tube apparatus and performance exist in the literature (8) while description of the specific apparatus and procedure used in this investigation is given below.

Shock tube

The shock tube used in this investigation has been partially described by Belles and Lauver (47) and further description follows. The compression (driver) section was a stainless steel cylinder with an internal diameter of 78 mm and a length of 1177 mm. The expansion section consisted of four smaller sections bolted and sealed together. Adjacent to the compression section was a diaphragm section 78 mm in internal diameter designed to hold and seal the diaphragm. Next, there was a transition section designed to couple the 78 mm diameter circular cross section to a 37 by 74 mm rectangular cross section. The third part of the driven section was made of waveguide tubing (37 by 74 mm rectangular cross section). The walls of the waveguide tubing were reinforced

---

[1]These facilities were located at the Lewis Research Center of the National Aeronautics and Space Administration in Cleveland, Ohio and provided by the Kinetics Section of the Chemistry and Energy Conversion Division.

Figure 4. Schematic diagram of experimental facility

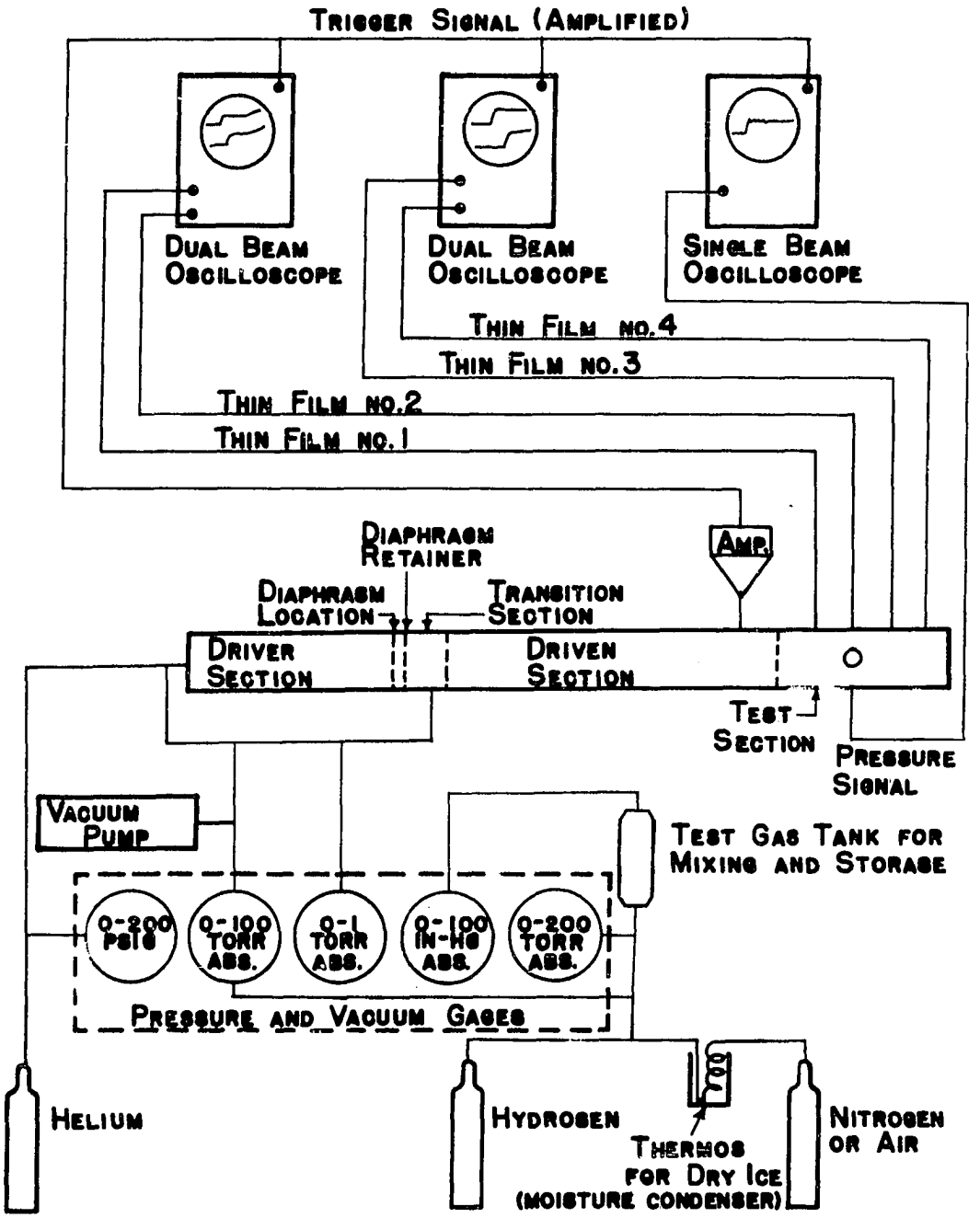
TRIGGER SIGNAL (AMPLIFIED)
DUAL BEAM OSCILLOSCOPE
DUAL BEAM OSCILLOSCOPE
SINGLE BEAM OSCILLOSCOPE
THIN FILM NO.4
THIN FILM NO.3
THIN FILM NO.2
THIN FILM NO.1
AMP.
DIAPHRAGM RETAINER
DIAPHRAGM LOCATION
TRANSITION SECTION
DRIVER SECTION
DRIVEN SECTION
TEST SECTION
PRESSURE SIGNAL
VACUUM PUMP
TEST GAS TANK FOR MIXING AND STORAGE
0-200 PSIG
0-100 TORR ABS.
0-1 TORR ABS.
0-100 IN-HG ABS.
0-200 TORR ABS.
PRESSURE AND VACUUM GAGES
HELIUM
HYDROGEN
THERMOS FOR DRY ICE (MOISTURE CONDENSER)
NITROGEN OR AIR

Figure 5. View of shock tube from driver section

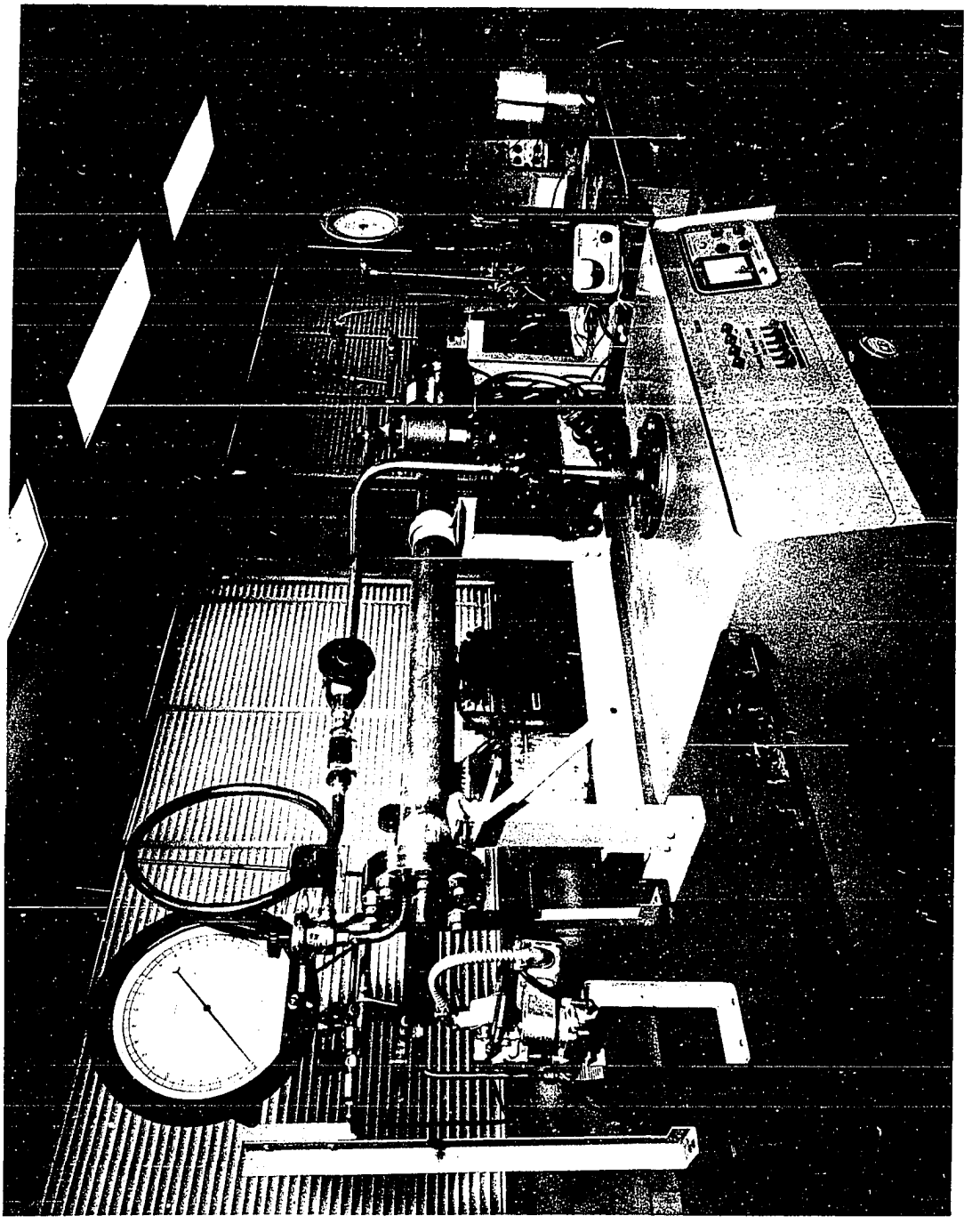

Figure 6. View of shock tube from test section

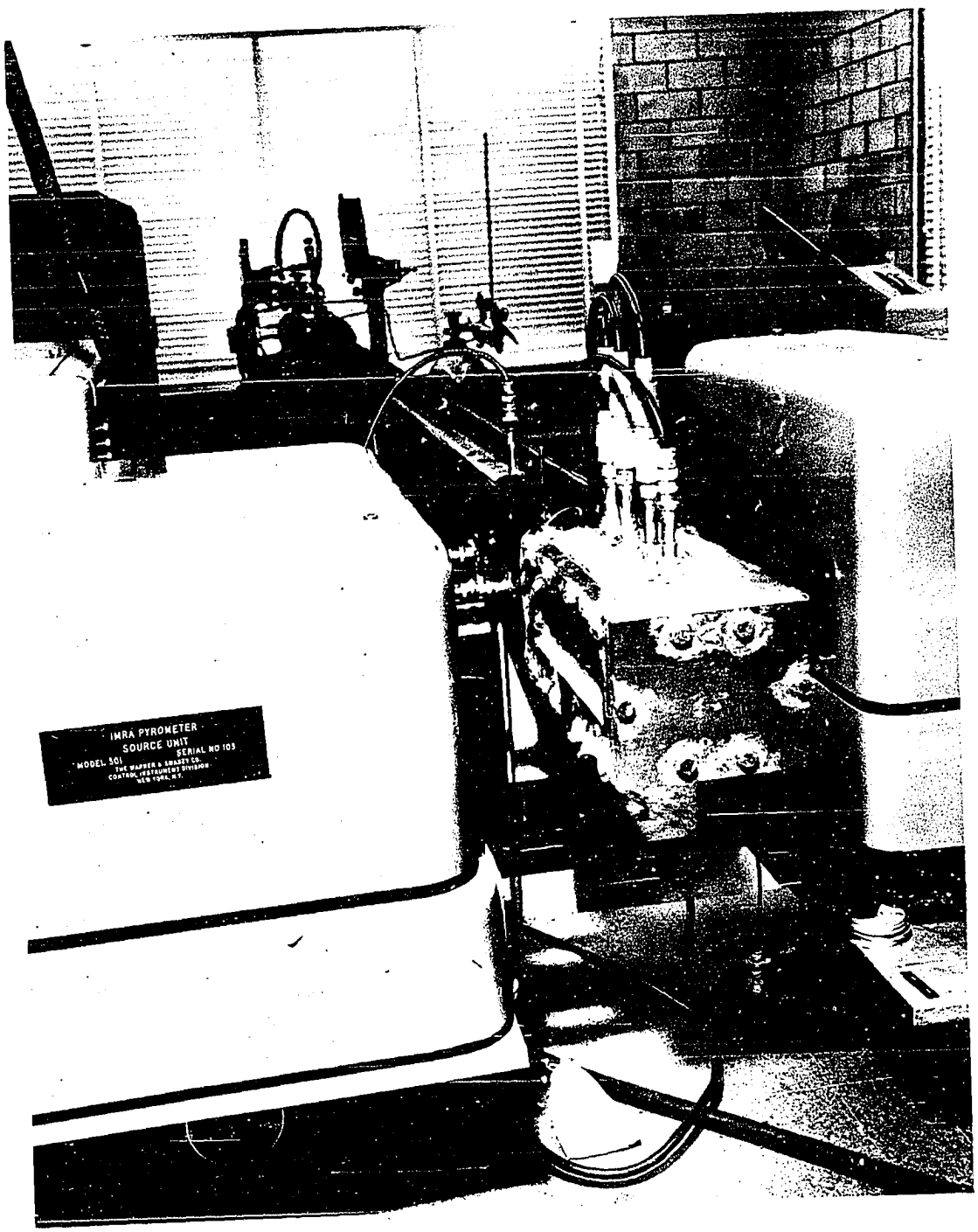
IMRA PYROMETER
SOURCE UNIT
MODEL 501
SERIAL NO 103
THE BAILEY & ANSLEY CO.
CONTROL INSTRUMENT DIVISION
NEW YORK, N.Y.

Figure 7. View of shock tube instrumentation

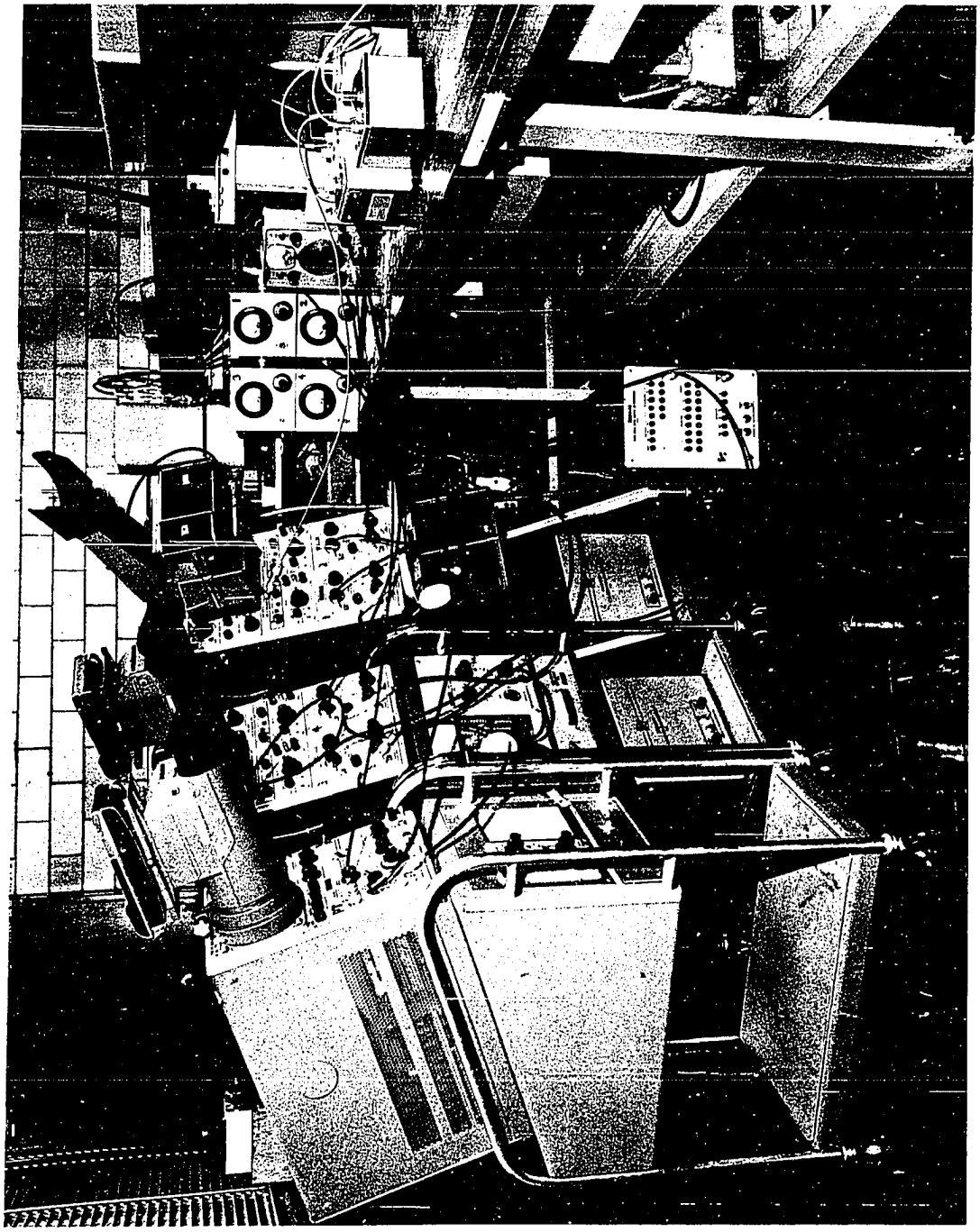

with steel backing plates. The last part of the driven tube was made of stainless steel plates bolted together. All of the flow measurements were made by instrumentation placed in this section, hence, it will be referred to hereafter as the test section. The lengths of the diaphragm, transition, waveguide and test section were 45, 155, 3660 and 260 mm respectively yielding a total length of 4120 mm for the expansion section. All of the sections indicated above are illustrated in Figure 4.

Instrumentation

Instantaneous heat-transfer rates can be obtained in shock tubes by means of thin-film resistance thermometers. A thin-film resistance thermometer is a thin metallic film of negligible heat capacity and very rapid response. The proper operation of this type of gage depends on the film having a negligible thermal capacity so that any incident heat flux is completely absorbed by the film backing material. Under these conditions the film will function to give instantaneous surface temperatures of the backing material.

In use, a thin-film resistance thermometer is supplied with a nearly constant electrical current by means of a ballast circuit as shown in Figure 8. A change in gage resistance with temperature will then yield a voltage change across the film by virtue of Ohm's law. This voltage change can be directly measured by a cathode-ray oscilloscope as shown in Figure 8. A typical sensor of this type made of platinum deposited on a pyrex substrate has a thickness less than 1 micron and a response time (risetime) less than 1 microsecond (48). Detailed description of the construction and use of such thin-film resistance thermometers is contained in existing literature (49,50).

Figure 8. Heat-transfer gage operating circuit

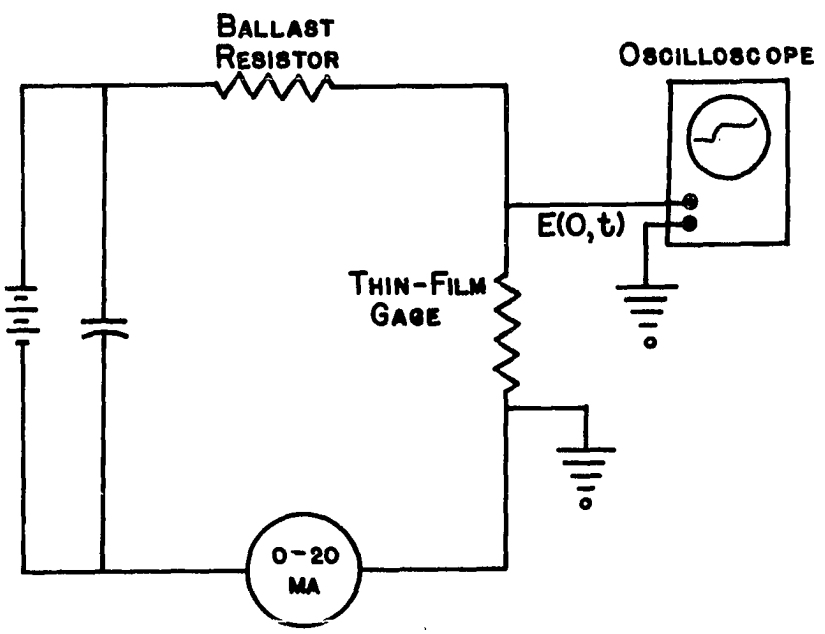
BALLAST
RESISTOR
OSCILLOSCOPE
E(0,t)
THIN-FILM
GAGE
0-20
MA

To obtain quantitative heat-transfer data, knowledge of the thermal properties of the backing material in the form of the "thermal product", $\beta = \sqrt{\rho\ k\ c}$, as well as the temperature coefficient of resistance, α, of the gage is required. Descriptions of the techniques required and used to obtain α and β are presented in Appendix B along with a tabulation of the calibration results for gages used in this investigation. The technique for calculating heat-transfer rates from surface-temperature histories is discussed in a later section.

For all shock-tube testing times of interest, the backing material behaves as a semi-infinite body even though its actual thickness may be only a few hundredths of a centimeter. For example, a pyrex backing material and shock-tube testing time of 10 milliseconds requires a substrate thickness of only 0.022 cm (48). In practice, the backing material is made an integral part of the surface on which temperature and heat-transfer rate is desired. In this case, the surface is the shock-tube wall.

Five thin-film resistance thermometers were flush mounted in the upper wall of the shock tube. One of these sensors was used to trigger the readout instruments so outputs from all other detector-transducers in the test section could be recorded. The thin film used for the trigger signal was located upstream of the test section while the other four thin films used for measuring surface-temperature history were located 226.5, 182.0, 108.5, and 75.5 mm respectively from the downstream end of the shock tube. The relative location of these gages is illustrated in Figure 4.

All of the thin-film detectors were placed in ballast circuits and except for the thin-film used as a trigger, their voltage outputs were recorded on Tektronix Type 555 dual-beam oscilloscopes. The voltage output from the thin-film used as trigger was amplified 60 db (a factor of 1000) before it was fed into the external trigger circuit of the recording oscilloscopes. Outputs from each of two adjacent thin-film gages were recorded by Polaroid type 46L film in Dumont type 2620 cameras attached to each dual-beam oscilloscope. Both 10- and 100-microsecond timing marks from a Tektronix Type 180A secondary standard time-mark generator were superimposed on these recordings. Typical recordings are shown in Figures 9-a and 9-b.

Instantaneous flow pressures were measured by means of a Kistler type 601 piezoelectric pressure transducer flush mounted in the lower wall of the shock tube. The position of this transducer was directly below the thin-film resistance thermometer located 182.0 mm from the end wall of the shock tube. In this way both instantatneous pressure and surface temperature are sensed at the same axial potition in the shock tube. The detected pressure level was transduced to an analogous voltage signal, amplified by a Kistler type 655 amplifier-calibrator, then displayed on a Tektronix type 541 oscilloscope. This signal, along with superimposed 10- and 100-microsecond timing marks from a Tektronix Type 180A secondary standard time-mark generator, and a 50 psi calibration trace were recorded from the oscilloscope by means of Polaroid type 47 film in a Tektronix type C-12 camera. A typical recording is shown in Figure 9-c.

Gas Mixtures

The mixtures of test gas were prepared from commercially obtained compressed gases by the method of partial pressures. This technique consisted of first evacuating and outgassing a closed container or mixing tank. Hydrogen was then admitted very slowly and carefully to the mixing tank to a pressure level (relative to the final pressure desired in the mixing tank) corresponding to the volume percentage of hydrogen desired. For example, if the final pressure in the mixing tank was to be 100 psia and the desired volume percentage of hydrogen was 12 percent, then enough hydrogen was admitted to the mixing tank so that its pressure was 12 psia. After the hydrogen was placed in the mixing tank, either dry air or nitrogen was admitted very slowly to yield the final pressure desired.

The air and nitrogen were passed through a "dry ice" condenser as shown in Figure 4 to insure that no water vapor would enter the test mixture from the commercially obtained compressed gases. This was necessary because spectroscopic analysis of the air and nitrogen in their compressed gas containers indicated slight amounts of water vapor present. For all mixtures the component gases were admitted slowly enough so that the gas temperature remained virtually constant at room temperature. This precaution was necessary to insure the validity of the method of partial pressures for making up the test gas mixture. After each mixture was made up steam was passed externally over the mixture tank. This promoted molecular activity and mixing of the component gases to insure obtaining a homogeneous test-gas mixture. Approximately 3 hours was required to make up a test mixture and an additional 3 hours of steam promoted mixing

was used. The mixture was then allowed to cool to room temperature before use in the shock tube.

To insure the validity of the mixture proportions, two of the eight test mixtures made up were checked spectroscopically. Both of these mixtures were correctly proportioned, as desired, within a precision of $\pm$ 1% of the pressure measurements used to make up the mixtures by the partial-pressure technique.

A total of eight mixtures were used in this investigation. For each combustible hydrogen-air mixture there was a matched inert hydrogen-nitrogen mixture. Molecular weight was used to match inert and combustible mixtures since this would yield identical sound speeds and virtually identical transport properties between the matched mixtures. The following equation was used to perform the matching where x is the percent hydrogen with air and y is the percent hydrogen with nitrogen.

$$x\, M_{H_2} + (1-x)(0.209\, M_{O_2} + 0.791\, M_{N_2}) = y\, M_{H_2} + (1-y)\, M_{N_2} = M_{mix}$$

$$\therefore\ y = 1.032(x) - 0.032 \qquad (36)$$

Equation 36 represents a molecular weight balance with air assumed to consist of 20.9 percent oxygen and 79.1 percent nitrogen.

Since the amount of hydrogen in air to yield detonation is near 16 percent (51,52), the maximum portion of hydrogen used in these test mixtures was 15 percent. The minimum portion of hydrogen with air was 3.1 percent since this conveniently allowed pure nitrogen to be used as one of the inert matching mixture. Listings of the proportions of the gas mixtures used, in this investigation, are given below in Table 1.

Table 1. Mixture proportions for combustible and inert test gases

Combustible Test Gas	Mixture Molecular Weights	Inert Matching Gas
3.1% H_2 in air	28.0	100% N_2
7.0% H_2 in air	27.0	4.0% H_2 in N_2
11.0% H_2 in air	25.9	8.2% H_2 in N_2
15.0% H_2 in air	24.8	12.3% H_2 in N_2

Operating Procedure

The driver gas used in this investigation was helium as supplied commercially from compressed-gas cylinders. The test gas was either combustible hydrogen-oxygen-nitrogen or inert hydrogen-nitrogen mixtures prepared as previously described.

Diaphragms initially separating the driver and test gas were made of Mylar polyester film. Shock-wave strength was varied by using different thicknesses of Mylar since the driver pressure required for bursting is directly related to diaphragm thickness. Mylar diaphragm thicknesses used were 10.0, 7.5, 5.0 and 3.0 thousands of an inch which required bursting pressures of approximately 150, 120, 90 and 50 psia respectively. For a given diaphragm thickness, shock-wave strength (and therefore flow properties) were further controlled by selection of the test gas pressure (p_1) before the bursting operation. Initial test gas pressures of 5, 10, 20, 35 and 50 Torr were used for each diaphragm thickness selected. These values of diaphragm thickness and initial test gas pressure were selected because, with few exceptions, they yielded test gas flow temperatures (T_2)

between 900°K and 2100°K. The intent here was to keep the temperature of the flowing test gas above the ignition temperature of hydrogen in air but within a temperature range where the chemical kinetics of the combustion reactions are known. Lewis and von Elbe (53, Figure 1) show temperatures above 853°K would provide ignition of stoichiometric hydrogen-oxygen mixtures for pressures between 1 and 10,000 Torr. For leaner mixtures using air instead of oxygen the expected ignition temperature would be higher than 853°K. Belles and Lauver (47) use temperatures above 1000°K in their investigation to insure ignition of 5% H_2 in air mixtures. They have also presented the appropriate chemical kinetics which apply to this investigation (54).

The procedure followed to obtain a given experimental run was:

(1) select the desired diaphragm thickness and place the diaphragm in the shock tube

(2) evacuate and outgas, by means of a vacuum pump, both the driver and driven sections until the absolute pressure in the shock tube was below 1 micron

(3) adjust and ready the instrumentation for recording

(4) introduce helium in the driver section to a pressure slightly below the diaphragm bursting pressure

(5) introduce test gas into the driven section to the desired pressure

(6) raise the pressure of helium in the driver section until the diaphragm bursts thus generating the shock tube flow.

Since there were five initial test gas pressures used for each of

four diaphragm thicknesses, at least twenty experimental runs were required for each of eight test gas mixture. In order to duplicate each of the experimental runs, forty runs on each of eight test mixtures were obtained yielding a total of 320 runs. Some of these runs were not useful because of the flow-temperature limitation previously described, because boundary-layer transition occurred too soon behind the shock wave, or because of mistakes made in taking the data. Any run in which boundary-layer transition occurred within 10 microseconds after passage of the shock wave was not used. It was felt this data would be unreliable because of lack of desired precision of recorded and calculated data this near the shock wave where the boundary layer was being initiated. A total of 239 runs were eventually used in this investigation. Measurements, calculations and reduction-of-data for each run are described in the next section.

Measurements, Calculations and Data Reduction

Surface-temperature measurements

Instantaneous surface-temperature changes are determined from voltage-time measurements of thin-film resistance thermometers by combining Ohm's law with the temperature coefficient of resistance for the film as follows below.

Ohm's Law (constant current): $\Delta E = I(\Delta R)$

temperature coefficient of resistance: $\alpha = \Delta R/(R_o \Delta T)$

combination: $\phi = \Delta T = \Delta E/(IR_o\alpha)$ (37)

Equation 37 shows that gage current I, gage initial resistance R_o, and α are required to relate gage-voltage change to surface-temperature change.

Heat-transfer calculations

Basic equations Surface heat-transfer rates are calculated from surface-temperature histories by means of the one-dimensional non-steady heat-conduction equation. The solution of this equation for an arbitrary surface-temperature variation is given in detail by Hall (48) and summarized below.

For the physical model, consider a semi-infinite solid bounded by a surface at y = 0 and extending to infinity in the positive y direction. It is assumed that the energy transfer and temperature distribution through the body are governed respectively by the one-dimensional non-steady, Fourier conduction equation and the Fourier temperature field equation. These equations are given below for an isotropic homogeneous solid.

$$q = \frac{-k\partial T}{\partial y} = \frac{-k\partial \phi}{\partial y} \tag{38}$$

$$\frac{\partial^2 \phi}{\partial y^2} = K \frac{\partial \phi}{\partial t} \tag{39}$$

In these equations $\phi = T-T_o$ represents the temperature change from some initial temperature while k and K represent thermal conductivity and thermal diffusivity respectively. The boundary and initial conditions are listed as follows.

$$\begin{array}{lll} \text{(i)} & \phi(y,0) = 0 & y \geq 0 \\ \text{(ii)} & \lim_{y\to\infty} \phi(y,t) = 0 & t \geq 0 \\ \text{(iii)} & \phi(0,t) = \phi(t) & t > 0 \end{array} \tag{40}$$

Using Laplace transforms, Equation 39 can be changed to an ordinary differential equation in the transform plane (i.e., the y-s plane), where

it can be solved by conventional methods. Then, if desired, the solution to Equation 39 in the actual physical plane (i.e., the y-t plane) can be obtained by taking the inverse transform of the y-s plane solution. One can proceed as shown in Reference 48 to obtain the equations of interest here.

The transform plane solution of Equation 39 is given as

$$q(o,s) = \beta \sqrt{s} \quad \bar{\phi}(0,s) \tag{41}$$

where β is the thermal product of the backing material and $\bar{\phi}(o,s)$ is the Laplace transform of $\phi(o,t)$. The physical plane solution of Equation 39 is obtained by using the convolution theorem on Equation 41 to yield

$$q(o,t) = \frac{\beta}{\sqrt{\pi}} \int_o^t \left(\frac{1}{\sqrt{t - \tau}}\right) \frac{\partial \phi(o,t)}{\partial \tau} \, d\tau \tag{42}$$

where τ is a dummy time variable. When the surface-temperature variation with time, as obtained by thin-film resistance thermometer, is known and can be expressed mathematically, Equation 42 can usually be used to obtain heat-transfer rates at the substrate surface. When the surface temperature variation is arbitrary and cannot be explicitely expressed in mathematical form it is more convenient to integrate Equation 42 by parts. This result can be manipulated to give the following expression

$$q(o,t) = \frac{\beta}{\sqrt{\pi}} \left[\frac{\phi(o,t)}{\sqrt{t}} + \frac{1}{2} \int_o^t \frac{\phi(o,t) - \phi(o,\tau)}{(t - \tau)^{3/2}} \, d\tau\right] \tag{43}$$

Equation 43 is the basic equation used to obtain heat-transfer rates from arbitrary surface-temperature changes. The form of Equation 43 is desirable because the integral term can be integrated, numerically, on a digital computer. Hence, the surface heat flux may be any arbitrary

function of time and still be determined as long as the thermal product, β, is known and the arbitrary temperature history is recorded (e.g., in the form of voltage-time oscilloscope recordings from outputs of thin-film resistance thermometers). Before proceeding to illustrate the numerical integration procedure, it is of interest to note some special cases, thus, simplifying Equations 42 and 43.

When the surface heat-transfer rate is a constant value, q_o, the surface temperature (hence, gage voltage) will vary parabolically with time (i.e., $\phi(o,t) = \text{constant}\sqrt{t}$) according to the following relation

$$\frac{\phi(o,t)}{\sqrt{t}} = \frac{2\, q_o}{\beta \sqrt{\pi}} = \text{constant} \tag{44}$$

Conversely, if $\phi(o,t)$ varies parabolically with time, q_o will be constant. This important result is used to determine β as shown in Appendix B.

When the surface experiences a step change in temperature, ϕ_o, the surface heat-transfer rate is given by the following relation

$$q(o,t) = \beta \frac{\phi_o}{\sqrt{t}} \tag{45}$$

From Equation 45 it is evident that $q(o,t)$ varies inversely with $\sqrt{t}$. This important result is used to discriminate between laminar and turbulent boundary layers as described later.

Combination of Equation 37, expressing the relation between surface temperature and voltage output of a thin-film resistance thermometer, and Equation 43 yields the following expression relating surface-heat transfer rate to the thin-film voltage recording.

$$q(o,t) = q(t) = \frac{\beta}{\sqrt{\pi}\,\alpha I R_o}\left[\frac{E(t)}{\sqrt{t}} + \frac{1}{2}\int_o^t \frac{E(t) - E(\tau)}{(t-\tau)^{3/2}}\,d\tau\right] \qquad (46)$$

If the voltage-time oscilloscope recording from the resistance thermometer is approximated by a piecewise linear function using arbitrary time increments Equation 46 can be changed to a form whereby numerical integration can be used for its solution. This procedure has been used by Cook and Felderman (55) for the special case of equal time increments and their result is presented as Equation 4 in Reference 55. For unequal time increments the following equation may be derived as shown in Appendix D.

$$q(t) = q(t_n) = \frac{2\beta}{\sqrt{\pi}\,\alpha I R_o}\left[\sum_{i=1}^{n} \frac{E(t_i) - E(t_{i-1})}{\sqrt{t_n - t_i} + \sqrt{t_n - t_{i-1}}}\right] \qquad (47)$$

For the special case of equal time increments Δt, where $t_i = i(\Delta t)$ and i is an integer ranging from 1 to n, Equation 47 reduces to the following result.

$$q(t_n) = \frac{2\beta}{\sqrt{\pi}\sqrt{\Delta t}\;\alpha I R_o}\left[\sum_{i=1}^{n} \frac{E(t_i) - E(t_{i-1})}{\sqrt{n-i} + \sqrt{1+n-i}}\right] \qquad (48)$$

Equation 48 can also be obtained from the result of Cook and Felderman by expansion of their summation terms followed by appropriate cancellation and recombination, and, in addition, realizing that $E(t_o)$ and t_o are actually zero in their equation. Equation 48 is slightly more efficient than the result of Cook and Felderman and therefore saves digital computer time when a large amount of data must be reduced.

Calculation procedure Voltage-time traces from thin-film gages were recorded from oscilloscopes by means of Polaroid type 46L film as

previously mentioned. Each recording was a positive transparency which was later enlarged by a Thermofax enlarger-printer so that a grid could be superimposed on the enlarged voltage-time trace to determine the voltage amplitude for any desired time. Typically 75, but in no case less than 40, values of voltage amplitude and time were read from each enlargement of each thin-film output. These discrete values of voltage-time data were used in Equation 47 to calculate heat-transfer rates for each discrete time value by means of an IBM 360/50 digital computer. The flow chart for this digital computer program and a copy of the actual program are included in Appendix E as Figures 33 and 34, respectively.

In a test case, where Equation 44 is valid (i.e., $\phi(o,t) = \sqrt{t}$), Cook and Felderman (55) have shown that three equal time intervals are required, using their equation for the calculated heat-transfer rate, to be within 2.8% of the true heat-transfer rate as determined from Equation 44. In the same manner 10 intervals yield heat-transfer rates within 0.4%. Therefore, in this investigation, the minimum time used to calculate a corresponding heat-transfer rate was the time at the end of the third interval. Actually, calculated heat-transfer rates using less than 10 intervals in Equation 47 were not presented in this investigation. In all cases 10 intervals corresponded to a time slightly less than 10 microseconds, thus, if transition time occurred within the first 10 microseconds the run was discarded.

Figures 9-a and 9-b show actual recordings of thin-film outputs while Table 2 tabulates voltage, time and calculated heat-transfer rates for a given thin-film recording. Figure 10 is a plot of the heat-transfer rate

Figure 9. Typical oscilloscope recordings

NOTE: Traces a and b should be read from right-to-left. Vertical sensitivity is 2 millivolts per major graticule division. Trace c should be read from left-to-right. Vertical sensitivity is 100 millivolts per major graticule division with 50 psi calibration lines shown.

All traces have a horizontal sensitivity of 50 microseconds per major graticule division. Timing marks are superimposed on all traces at intervals of 10 and 100 microseconds.

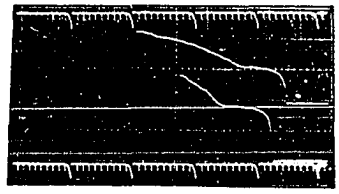

b) gage 3 and 4

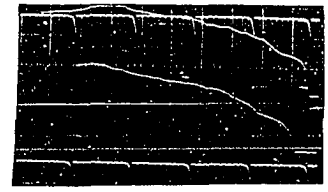

a) gage 1 and 2

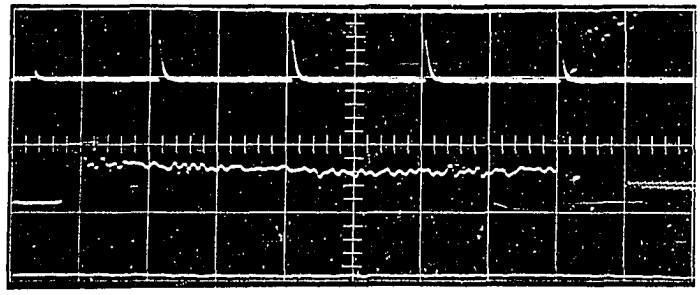

c) Pressure Trace

Table 2. Typical heat-transfer data obtained from thin-film resistance thermometer

t^a, grid lines	E^a, grid lines	t, μsec	E, mv	q(t), cal/cm^2 sec	t^a, grid lines	E^a, grid lines	t, μsec	E mv	q(t) cal/cm^2 sec
200.0	102.5	212.7	4.22	27.7	32.0	32.8	34.0	1.35	19.4
190.0	101.7	202.1	4.19	31.7	30.0	32.3	31.9	1.33	19.7
180.0	98.1	191.4	4.04	32.1	28.0	31.8	29.7	1.31	20.0
170.0	93.3	180.8	3.84	28.1	26.0	31.3	27.6	1.29	20.4
160.0	91.0	170.2	3.75	28.2	24.0	30.8	25.5	1.27	21.1
150.0	89.0	159.5	3.67	30.7	22.0	30.2	23.4	1.24	21.2
140.0	84.7	148.9	3.49	27.1	20.0	29.8	21.2	1.22	23.3
130.0	83.2	138.2	3.43	29.8	19.0	29.3	20.2	1.20	22.7
120.0	80.0	127.6	3.29	30.3	18.0	29.0	19.1	1.19	23.2
110.0	76.3	117.0	3.14	30.4	17.0	28.7	18.0	1.18	23.8
100.0	72.1	106.3	2.97	28.4	16.0	28.4	17.0	1.17	25.4
95.0	70.8	101.0	2.91	28.8	15.0	27.8	15.9	1.14	25.3
90.0	69.7	95.7	2.87	31.1	14.0	27.3	14.8	1.12	26.2
85.0	67.6	90.4	2.78	31.4	13.0	26.6	13.8	1.09	25.0
80.0	65.3	85.1	2.69	32.2	12.0	26.4	12.7	1.08	28.0
75.0	62.3	79.7	2.56	30.5	11.0	25.7	11.7	1.05	29.3
70.0	60.0	74.4	2.47	30.9	10.0	24.7	10.6	1.01	28.4
65.0	57.3	69.1	2.36	30.1	9.0	24.0	9.5	0.98	29.7
60.0	55.0	63.8	2.26	31.3	8.0	23.2	8.5	0.95	32.6
55.0	52.0	58.5	2.14	31.3	7.0	21.7	7.4	0.89	31.2
50.0	48.7	53.1	2.00	30.9	6.0	20.5	6.3	0.84	31.9
45.0	45.3	47.8	1.86	32.3	5.0	19.3	5.3	0.79	35.2
40.0	40.2	42.5	1.65	29.1	4.0	17.3	4.2	0.71	35.4
35.0	35.2	37.2	1.45	24.8	3.0	15.1	3.1	0.62	36.9
33.0	33.2	35.1	1.36	20.1					

[a]This data is from RUN 1005 of 8.2% H_2 in N_2, gage #2. Voltage scale factor is 24.3 grid lines/millivolt and time scale factor is 0.940 grid lines/microsecond.

Figure 10. Heat-transfer rate history

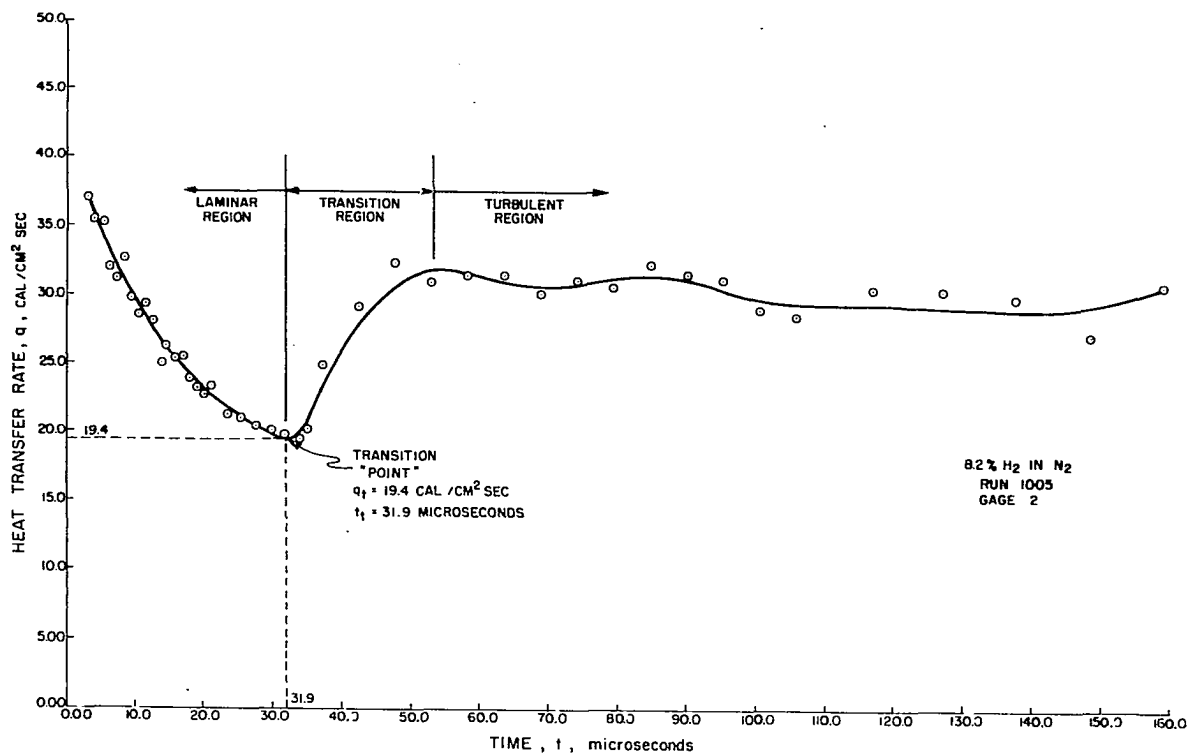
LAMINAR REGION
TRANSITION REGION
TURBULENT REGION
TRANSITION "POINT"
q_t = 19.4 CAL /CM^2 SEC
t_t = 31.9 MICROSECONDS
8.2% H_2 IN N_2
RUN 1005
GAGE 2
19.4
31.9
HEAT TRANSFER RATE, q , CAL /CM^2 SEC
TIME , t , microseconds
50.0
45.0
40.0
35.0
30.0
25.0
20.0
15.0
10.0
5.00
0.00
0.0
10.0
20.0
30.0
40.0
50.0
60.0
70.0
80.0
90.0
100.0
110.0
120.0
130.0
140.0
150.0
160.0

as a function of time for a given run as obtained from Equation 47 and thin-film data. The drop in heat-transfer rate is nearly inversely parabolic (i.e., $q(o,t) \sim 1/\sqrt{t}$) for short periods of time. This is characteristic of laminar flow because Bromberg (3) has shown $\phi(o,t)$ will be constant in laminar flow for $\rho\mu$ constant through the boundary layer. If $\phi(o,t)$ is then constant for laminar flow Equation 44 shows $q(o,t)$ will vary as $(t)^{-\frac{1}{2}}$. This is an extremely important result because it provides a technique of using outputs from thin-film resistance thermometers for discriminating between laminar and turbulent boundary layers. In turbulent flow $\phi(o,t)$ is not constant, thus, $q(o,t)$ will not vary as $(t)^{-\frac{1}{2}}$. This concept is used to obtain boundary-layer transition points as illustrated in the following section.

Transition times

In this investigation $\phi(o,t)$ was not quite constant for laminar flow but increased slightly with time as can be seen from Figures 9-a and 9-b. This variation from ideal may be a result of additional heat-transfer from the hot test gas by a radiation mode as well as an indication of variable $\rho\mu$ through the boundary layer. Thus, $q(o,t)$ does not quite vary as $(t)^{-\frac{1}{2}}$ but instead varies as $(t)^{-1/p}$ where p was found by a least-squares curve fit to be nearly 3 in many cases and close to 2 in other cases.

The beginning of transition is characterized by increased diffusion and mixing of particles in the boundary layer. Hence, the heat-energy flux to the shock-tube wall increases and continues to do so until the boundary layer is fully turbulent. This transition process can be readily seen from the time variation of heat-transfer rate shown in Figure 10.

Typical transition periods for these experimental runs were in the order of 10 to 20 microseconds.

Even though the transition process does not occur instantaneously a transition point or time must be selected to characterize the end of the laminar boundary layer. Correspondingly, this point was selected as that point where the heat-transfer rate ceased to decrease as $(t)^{-1/p}$ and started to increase, thus, indicating an increased mixing or diffusion of particles as is physically characteristic of turbulence. This technique is different from that of others (e.g., 18,32,34) who have used thin-film resistance thermometers, in that heat-transfer rate history is used to determine transition rather than surface-temperature history. The advantage of using heat-transfer rate is that it depends on temperature gradient at the surface and is therefore more sensitive than temperature level. This is extremely important when the thin-film output does not indicate a sudden temperature change at transition but instead indicates a slightly smoother temperature change. With this condition, using temperature level to determine transition may not be sensitive enough to give accurate transition points compared to the heat-transfer technique. A comparison of values obtained by both techniques for the data of this investigation may be observed in the tabulated comparisons of Tables 15 through 22 in Appendix A.

To obtain transition times using heat-transfer rate history an IBM 360/50 computer program subroutine was used to plot the heat-transfer rates as they were calculated by means of a California Computer Products Model 1627 digital incremental plotter. This subroutine is a portion of Figure

34 in Appendix E. This routine was also used to draw a smooth curve through the data points. The transition time, as well as heat-transfer rate at this time, were then taken from the smooth curves as illustrated in Figure 10. These values of transition time correspond to laboratory time and not the actual time it takes the particle (gas time or particle time) to go from the shock wave to the transition point. Multiplication of the laboratory time by the density ratio across the shock wave yields the particle time as shown in the Introduction section.

The particle transition times and the heat-transfer rates at transition were then combined with appropriate flow properties to calculate dimensionless Reynolds and Stanton numbers respectively. Flow-property calculations and dimensionless variables for data correlation are presented in following sections.

Flow properties

Application of the one-dimensional conservation and state relations across the normal shock wave yields free-stream flow properties in the test region directly behind the shock wave. These relations are listed below for steady flow in a constant area duct with the coordinate system affixed to the moving shock wave.

$$\rho_1 u_1 = \rho_2 u_2 = \rho_i u_i = \text{constant} \tag{49}$$

$$h_1 + \frac{u_1^2}{2} = h_2 + \frac{u_2^2}{2} = h_i + \frac{u_i^2}{2} = \text{constant} \tag{50}$$

$$p_1 + \rho_1 u_1^2 = p_2 + \rho_2 u_2^2 = p_i + \rho_i u_i^2 = \text{constant} \tag{51}$$

$$\frac{p_1}{\rho_1 T_1} = \frac{p_2}{\rho_2 T_2} = \frac{p_i}{\rho_i T_i} = \text{constant} \tag{52}$$

The following dimensionless quantities are convenient to use in the above relations to facilitate their solution.

$$U_{ij} = U_i/U_j = u_i/u_j \qquad \chi_i = H_i - H_1$$

$$U_i = (\rho_1/p_1)^{\frac{1}{2}} u_i \qquad T_{ij} = T_i/T_j$$

$$H_i = (\rho_1/p_1)\, h_i \qquad P_{ij} = p_i/p_j$$

Substitution of these dimensionless quantities into the conservation and state relations yield the following set of dimensionless equations.

$$\rho_1/\rho_2 = U_{21} \tag{53}$$

$$\chi_2 = \frac{1}{2}(U_1^2 - U_2^2) \tag{54}$$

$$P_{21} = 1 + U_1^2 - (U_{12})U_2^2 \tag{55}$$

$$P_{21} = U_{12}\, T_{21}$$

Solution of Equations 53 to 56 can be accomplished for any arbitrary composition of a gaseous mixture provided the test gas composition and corresponding temperature-enthalpy ($\chi = \chi(T)$) data are specified. Tables of thermodynamic data, for the 8 mixtures listed in Table 1, were provided by Roger A. Svehla (at Lewis Research Center of NASA) according to techniques outlined in References 56 and 57. Markstein (58) has presented a graphical method that avoids iteration procedures in solution of the conservation relations across shock or detonation waves. However, in this investigation, an iterative method was developed in order to use the capacilities of a digital computer. This was necessary because of the large amount of data and resulted in considerably less calculation time than the graphical technique would have required.

The iterative scheme requires known values of U_1, p_1, T_1 and temperature-enthalpy data for a given composition. The dimensionless shock-wave velocity U_1 is determined by calculating the shock-wave velocity u_1 from values of measured time it takes the shock wave to travel measured distances between thin-film detectors. With p_1 and T_1 measured before the shock wave was generated, one can combine u_1, p_1 and T_1 to obtain U_1. The iteration process can then be initiated by combining U_1 with an assumed U_{12}. For all experimental runs in this investigation the minimum density ratio across the shock wave was 4.5 and, by virtue of Equation 53, the minimum value of U_{12} was 4.5. This value of U_{12} was found to be convenient as an initial assumption. The iterative process is itemized below.

(1) With U_1 known and U_{12} assumed calculate U_2 from the relation $U_2 = U_1/U_{12}$.

(2) Calculate χ_2, P_{21} and T_{21} respectively from Equations 54, 55 and 56.

(3) Use T_{21} to interpolate in the temperature-enthalpy data to find $\bar{\chi}_2$.

(4) Compare χ_2 and $\bar{\chi}_2$. If they do not agree within a specified amount change U_{12} and repeat steps 1 through 4.

In step 3, Sterling's interpolation formula was used in a computer program to find $\bar{\chi}_2$ from temperature-enthalpy data stored in the computer memory.

After several different correction methods were tried, a convenient and efficient technique was found by forming the ratio of χ_2 and $\bar{\chi}_2$. This χ_2 ratio was then multiplied by U_{12} to give a new U_{12} for another iteration.

This procedure was continued until the χ_2 ratio was within 1.0000 ± 0.0005. This value was found to be appropriate since differences in T_2 and $\overline{T}_2$ (corresponding to χ_2 and $\overline{\chi}_2$ respectively) were not significant. Furthermore, comparison of these calculations for the case of pure nitrogen with the more exact partition function calculations of Bernstein (59) show good agreement. This agreement substantiates the use of one for the value of compressibility factor Z in this investigation. Typically, on the order of 10 iterations were required before the χ_2 ratio converged to the desired value.

A flow chart illustrating the flow-property calculations as well as a copy of the IBM 360/50 computer program are included in Appendix E as Figures 35 and 36 respectively.

Induction-zone kinetics

If a combustible mixture containing hydrogen, oxygen and an inert diluent is suddenly heated and compressed by means of a shock wave to a temperature greater than its ignition temperature (for the prevailing pressure), its ignition is preceded by a short delay or induction period. During the initial part of this induction period an unknown chemical reaction initiates the production of either H, O or OH radical (47). The rest of the induction period allows concentration of H, O, and OH to increase with time by means of chain-branching reactions. However, at the end of the induction period the resulting concentrations of free radicals of H, O, and OH are not appreciable with less than 10^{-4} mole/liter being typical (47). In fact, the end of the induction period is identified, after Schott and Kinsey (60), to be the time when 10^{-6} mole/

liter of OH radical is produced. Recombination reactions then occur which result in the formation of H_2O vapor and an appreciable amount of heat-energy release. Induction times range from a few to a few hundred micro-seconds for the pressures and temperatures used in this investigation.

Belles and Lauver (54) have shown that only four reactions are needed to describe the build up of atoms and free radicals during the induction period. First, the initiation reaction for the range of temperatures of this experiment (900°K - 2100°K) is uncertain but has been postulated (47) to be:

$$\text{(i)} \qquad H_2 + O_2 \rightarrow 2OH \tag{57}$$

After a short initiation period which is only a small part of the total induction period, the following reactions branch the chain.

$$\text{(I)} \qquad OH + H_2 \rightarrow H_2O + H \tag{58}$$

$$\text{(II)} \qquad H + O_2 \rightarrow OH + O \tag{59}$$

$$\text{(III)} \qquad O + H_2 \rightarrow OH + H \tag{60}$$

Reaction rates k_i, k_I, k_{II}, k_{III} are available for all of these reactions and are of the form $k = A \exp(-E/RT)$. Table 3 is a listing of these reaction rates as well as their source.

Using heats of formation from Reference 61, it can be shown that Reaction (I) is exothermic by 15.0 kcal/mole OH at 1500°K (the midrange temperature of these experiments) while Reactions (II) and (III) are endothermic by 15.9 and 1.9 kcal/mole OH respectively. Thus, the set of chain branching reactions is endothermic by 2.8 kcal/mole OH. However, since the production of OH radical is so small (10^{-6} mole OH/liter) the net energy required for the induction period reactions is 2.8×10^{-3}

Table 3. Reaction rates

Reaction	Collision Factor, A (liter/mole-sec)	Activation Energy, E (cal/mole)	Reference
(i)	2.5×10^{9}	3.90×10^{4}	54[1]
I	6.3×10^{10}	5.90×10^{3}	62
II	4.0×10^{11}	1.70×10^{4}	54
III	1.2×10^{10}	8.95×10^{3}	54

[1]Belles, F. E., Cleveland, Ohio. Suggested reaction rate replacement. Private communication. 1965.

cal/liter. Hence, except for the possibility of vibrational relaxation effects concerning diatomic molecules, isothermal conditions prevail during the induction period.

As concerns vibrational relaxation in mixtures of diatomic molecules, White and Millikan (63) have presented a general correlation relation that permits the relaxation time of O_2 in any mixture of O_2, H_2, Ar and N_2 to be estimated. Subsequently, they discovered (64) that H_2 is extremely effective in collisionally exciting the vibrational degree of freedom of O_2, thus, the vibrational relaxation time of O_2 with H_2 present is much faster than their correlation relation indicates. Asaba et al. (65) in a shock-tube study of H_2 - O_2 reactions, show that the greatest contribution to O_2 relaxation comes from collisions with H_2, even when H_2 is in concentrations lower than 1%. Calculations by Belles and Lauver (54) of the vibrational relaxation times for O_2 in H_2-air mixtures gave much faster relaxation times than induction times because of the presence of H_2. For example, at 1500°K, their observed induction times were 6 and 10 times

longer than calculated O_2 relaxation times for 5% H_2-95% air-and 20% H_2-80% air respectively. They also point out that the N_2 relaxation times are much faster than induction times because of the exchange of vibrational energy from the easily excited O_2. The vibrational relaxation time of H_2 in H_2-air mixtures has not been measured, has not been reliably calculated (54), and is, therefore, unknown. White and Moore (66) have found this relaxation process so fast that it could not be resolved interferometrically in their experiments. Thus, it is believed the effect of H_2 vibrational relaxation on induction time is very small if not negligible.

Since the induction period comes before the heat-energy release reactions, and because vibrational relaxation times of all species present in the combustible mixture are very much shorter than the induction time (65), the temperature of the induction zone during most of its history will be the thermal-equilibrium value. Furthermore, since the resulting concentrations of atoms and free radicals are so small, the chemical composition of the mixture (hence, mixture molecular weight) remains virtually constant throughout the induction period. The induction period is thus characterized by thermal equilibrium with slight chemical non-equilibrium where pressure, temperature, and reactant concentrations remain nearly constant. The induction zone temperature, pressure and composition are taken as those calculated through the shock wave for a fixed chemical composition. These calculations have been previously explained in the Flow-properties section. Calculated equilibrium temperatures in the induction zone behind the shock wave ranged from 900°K to 2100°K while the corresponding pressures ranged from 100 to 1100 Torr. Calculation of induction

times depend on these thermodynamic properties as well as the reaction rates given in Table 3 and are obtained by solution of the chemical kinetics of the induction zone as explained below.

In order to calculate the time variable concentrations of H, O, and OH during the induction period it is necessary to integrate the following set of differential-rate equations based on reactions (i) through (III).

$$\frac{d[OH]}{dt} = -k_I[H_2][OH] + k_{II}[O_2][H] + k_{III}[H_2][O] + i_{OH} \tag{61}$$

$$\frac{d[H]}{dt} = k_I[H_2][OH] - k_{II}[O_2][H] + k_{III}[H_2][O] + i_H \tag{62}$$

$$\frac{d[O]}{dt} = k_{II}[O_2][H] - k_{III}[H_2][O] + i_O \tag{63}$$

In these equations, k's are the reaction rate constant, [ ] represent concentrations, and i's represent rates at which the atoms or radicals are generated spontaneously. Belles and Lauver (47) have numerically integrated these rate equations for a 5% H_2 - 95% air mixture and they were used to explain the chemiluminescence of hydroxyl radical during the induction period in their investigation. Their calculations show that during the induction period the time dependence of free radical concentration is exponential and is given as

$$\frac{[H]}{[H]_o} = \frac{[O]}{[O]_o} = \frac{[OH]}{[OH]_o} = \exp\left(\frac{t}{\tau_c}\right) \tag{64}$$

where t is the time, τ_c is the exponential time constant, and concentrations with subscript zero are obtained by extrapolation of the calculated time-variable concentrations to zero time.

Brokaw (52) has presented an approximate technique for obtaining an analytic solution to Equations 61 through 63 that gives excellent agreement

with the results of numerical integrations by Belles and Lauver.

Induction times

The results obtained by Brokaw (52) are used herein. He has obtained the following relations which are applicable to this investigation.

$$\frac{1}{\tau_c} = [H_2] \left\{ \frac{2k_I k_{III} [\{1+(8k_{II}[O_2]/k_{III}[H_2])\}^{1/2} - 1]}{2 + [1+(k_I[H_2]/k_{II}[O_2])][\{1+(8k_{II}[O_2]/k_{III}[H_2])\}^{1/2} + 1]} \right\}^{1/2} \quad (65)$$

$$[OH]_o = 2\, k_i [O_2]/k_I \quad (66)$$

Combination of Equations 64, 65 and 66 yield the following relation for induction time t_i where $[OH] = 10^{-6}$ mole/liter.

$$t_i = \frac{1}{[H_2]} \left\{ \frac{2+[1+(k_I[H_2]/k_{II}[O_2])][\{1+(8k_{II}[O_2]/k_{III}[H_2])\} + 1]}{2k_I k_{III}[\{1+(8k_{II}[O_2]/k_{III}[H_2])\}^{1/2} + 1]} \right\}^{1/2} \ell n \left[\frac{k_I(10^{-6})}{2k_i[O_2]}\right] \quad (67)$$

Belles and Lauver (54) point out that large errors can be made in $[OH]_o$ without appreciably affecting the result calculated from Equation 67. This is extremely important because they stress that there is no independent evidence as to the rate constant or even the occurrence of Reaction (i).

Excellent agreement between experimental data and Equation 67 has been obtained. The data covers a range of $[H_2]/[O_2]$ ratio from 0.0075 to 24, a temperature range from 1000°K to 2000°K, and include observations in H_2-air, H_2-O_2-Ar, and H_2-O_2 mixtures. Comparisons and discussions of these experiments are made in Reference 54.

In this investigation Equation 67 is solved for induction time by an IBM 360/50 computer in a subroutine of the Flow-Property Calculation

program previously described and is presented as a portion of Figure 36 in Appendix E.

Dimensional analysis

In order to predict a basic set of suitable dimensionless variables for data correlation, a dimensional analysis must be performed on the flow model. The differential-equation method is used here instead of either the Buckingham or Rayleigh methods. The advantages of this approach are that the dimensionless groups are obtained directly in the logical form for use and this method possibly conveys more clearly the meaning of the derived dimensionless groups (67). Thus, the differential equation technique is more efficient to use than the other methods. However, it does require more knowledge of the nature of the problem since the appropriate differential equations must be known. For the case of an inert gas, Equations 1 through 7 in the Flow Model section apply. Equations 1 through 7 are non-dimensionalized by defining an appropriate set of dimensionless variables, such as those given below, to replace the dimensional variables in these differential equations:

$$
\begin{aligned}
u^* &= u/u_\infty & v^* &= v/u_\infty \\
h^* &= h/u_\infty^2 & p^* &= p/p_\infty \\
T^* &= T/T_\infty & U_\infty &= u_\infty(\rho_\infty/p_\infty)^{1/2} \\
\rho^* &= \rho/\rho_\infty & \nu^* &= \nu/\nu_\infty = \nu\,\rho_\infty/\mu_\infty \\
\mu^* &= \mu/\mu_\infty & c_p^* &= c_p/c_{p\infty} \\
x^* &= x/x_\infty & y^* &= y/x_\infty \\
\tau^* &= \tau/p_\infty & k^* &= k/k_\infty \\
q^* &= q/q_\infty = \lambda^*(h_r-h_w)^* = \lambda(h_r-h_w)/\lambda_\infty u_\infty^2
\end{aligned}
\qquad (68)
$$

Substitution of the above definitions into Equations 1 through 7 yield the following dimensionless relations:

(a) continuity

$$\frac{\partial(\rho^* u^*)}{\partial x^*} + \frac{\partial(\rho^* v^*)}{\partial y^*} = 0 \tag{69}$$

(b) momentum

$$u^* \frac{\partial u^*}{\partial x^*} + v^* \frac{\partial u^*}{\partial y^*} = \left[\frac{\mu_\infty}{\rho_\infty u_\infty x_\infty}\right] \nu^* \frac{\partial^2 u^*}{\partial y^{*2}} \tag{70}$$

(c) energy

$$\rho^* u^* \frac{\partial h^*}{\partial x^*} + \rho^* v^* \frac{\partial h^*}{\partial y^*} = \left[\left(\frac{k_\infty}{c_{p_\infty} \mu_\infty}\right)\left(\frac{\mu_\infty}{\rho_\infty u_\infty x_\infty}\right)\right] \frac{\partial}{\partial y^*}\left(\frac{\mu^*}{Pr^*} \frac{\partial h^*}{\partial y^*}\right)$$

$$+\left[\frac{\mu_\infty}{\rho_\infty u_\infty x_\infty}\right] \mu^* \left(\frac{\partial u^*}{\partial y^*}\right)^2 \tag{71}$$

(d) state

$$p^* = \rho^* R^* T^* \tag{72}$$

(e) wall shear stress

$$\tau^* = \left[\left(\frac{\rho_\infty u_\infty^2}{p_\infty}\right)\left(\frac{\mu_\infty}{\rho_\infty u_\infty x_\infty}\right)\right] \mu^* \frac{\partial u^*}{\partial y^*} \tag{73}$$

and (f) wall heat flux

$$q^* = \left[\left(\frac{1}{Pr_\infty}\right)\left(\frac{\mu_\infty}{\rho_\infty u_\infty x_\infty}\right)\left(\frac{\rho_\infty u_\infty}{\lambda_\infty}\right)\right] \frac{\mu^*}{Pr^*} \frac{\partial h^*}{\partial y^*} \tag{74}$$

In Equations 70 through 74 the reference variables are specially grouped within brackets. Each group is dimensionless and will be recognized by the following names.

Reynolds number: $Re = \frac{\rho u x}{\mu}$

Stanton number: $St = \frac{\lambda}{\rho u} = \frac{q}{\rho u(h_r - h_w)}$

Prandtl number: $Pr = \frac{\mu c_p}{k}$

Dimensionless velocity: $U = u(\frac{\rho}{p})^{1/2}$

(Note: Mach number = $M = \frac{U}{\sqrt{\gamma}}$)

The set of dimensionless differential equations will apply to a two-dimensional, steady flow, laminar boundary layer of an inert gas with zero pressure gradient. For two given flow situations governed by Equations 69 through 74, flow similarity will exist when the dimensionless parameters in brackets (i.e., Reynolds number, Prandtl number, Stanton number and Mach number) are equal in the two cases. Hence, some appropriate combination of these dimensionless parameters should come very close to correlating the data in this investigation.

An appropriate reference length x_∞ must be selected in this investigation to characterize boundary-layer transition. All other reference quantities are taken, for convenience, to be free-stream equilibrium values above the boundary layer. The exact form of the dimensionless parameters and characteristic transition length found to correlate data of this investigation are presented in the Results and Discussion section.

RESULTS AND DISCUSSION

Range of the Experiments

For a given mixture of test gas at room temperature free-stream flow properties were varied by selection of initial test gas pressure and control of the shock-wave strength by selection of different Mylar diaphragm thicknesses to yield free-stream temperatures before combustion from 900 to 2100°K, free-stream pressures from 100 to 1100 Torr, and shock-wave Mach numbers from 3.5 to 5.5. Tabulations of flow properties are presented in Appendix A in Tables 7 through 14.

Heat-transter rates, transition times and induction times are tabulated in Tables 15 through 22 of Appendix A.

Ideal flow duration times were calculated and then decreased by 50% to obtain a "rule-of-thumb" (8) estimate of actual flow duration. A plot of estimated flow duration as a function of velocity factor $u_1(U-1)$ is included as Figure 25 in Appendix A.

Transition times presented in Tables 15 through 22 include those obtained from both surface-temperature histories and surface heat-transfer rate histories. There is some disagreement between the two methods in several cases, therefore, the values from the more sensitive heat-transfer rate history have been used in this investigation. Values of these transition times are nearly always much larger than induction times and well within estimated flow duration times. This precludes boundary-layer transition caused by either contact surface arrival or initial heat-energy release portion of the combustion process. This allows the measured and calculated data of this investigation as presented in Appendix A to be

used for studying effects of heat-energy flux on boundary layer transition.

Correlation of Data

Dimensional considerations

To accomplish the stated objectives of this investigation correlation of experimental data must be made in such a fashion to show the effect of incident heat-energy flux on boundary-layer transition. As indicated in the Dimensional Analysis section the dimensionless Stanton number, Reynolds number, Mach number, and Prandtl number should combine in an appropriate way to permit such a correlation.

The Prandtl numbers for the gas mixtures of this investigation are between 0.57 and 0.70 and do not vary appreciably within a given mixture for the range of pressures and temperatures used herein. This may be observed in Tables 7 through 14 of Appendix A. Thus, Prandtl number should not have a significant effect on the data correlation of this investigation. With this idea in mind correlation was attempted using Stanton number, Reynolds number and Mach number.

The Mach number selected was that of the moving shock wave since it is unique in that it characterizes both the flow Mach number and the strength of the shock wave that induces the flow. The shock-wave Mach number, M_s, was determined by the following relation.

$$M_s = \frac{u_1}{a_1} = \frac{u_1 \sqrt{M}}{\sqrt{\gamma\, g_c\, R_u\, T_1}} \tag{75}$$

Stanton numbers were used to represent heat-energy flux measured at transition and was calculated by the following equation.

$$St_t = \frac{q_t}{\rho_2 u_2 (h_r - h_w)} \tag{76}$$

A transition Reynolds number based on an appropriate transition distance was used to represent boundary-layer transition. The relation to calculate this Reynolds number is

$$Re_t = \frac{\rho_2 u_2 x_\infty}{\mu_2} \tag{77}$$

where x_∞ represents a characteristic transition length which will be discussed in a later paragraph. The flow properties in Stanton and Reynolds numbers were evaluated at the free-stream temperature for convenience. The effect of using a different temperature for property evaluation is small and is illustrated in a later paragraph. The free-stream velocity is used because it is the velocity above the boundary layer in the steady-flow coordinate system. This is the coordinate system for which flow model and boundary-layer equations, as given in the Introduction section, apply. However, Mirels (15) and Hartunian et al. (32) use the free-stream velocity $(u_2 - u_1)$ based on the unsteady-flow coordinate system even though their flow models are based on a steady-flow coordinate system. Their velocity is that of the flow relative to the wall. Their reasoning for using this velocity is that their Reynolds number will reduce to the conventional flat-plate value when u_1 is zero. It should be noted, however, that the Reynolds number used herein is already in the form applicable to conventional flat plate flow. Another feature of using the flow velocity relative to the wall is that the velocity profile through the boundary layer is the same shape as those of conventional flat-plate

boundary layers. The relative merits of this feature may be questionable.

Before proceeding to determine a correlation equation from a dimensional analysis viewpoint alone, it was felt desirable to analyze the data from a statistical viewpoint. There were two important reasons for using the statistical approach. First, the statistical approach would indicate the important dimensionless variables influencing the variation of experimental data. Thus, a check on the results of dimensional analysis would be provided. Second, a correlation equation might be obtained to represent the data variation by means of regression analysis.

Statistical considerations

Both the statistical analysis of data and regression analysis were made by Mrs. Gretchen Snowden of the Iowa State University Statistical Laboratory on the computation center's IBM 360 Model-50 digital computer by means of a "stepwise" regression analysis.

Detailed explanation of statistical testing procedures including regression analysis are contained in standard textbooks such as Snedecor (68) and Bartee (69). Only a brief summary follows. The analysis was carried out by first determining the most significant independent variable and then, in turn, according to a preselected mathematical model fitting a curve through the data by the method of least squares. This process was then repeated using both the most significant and second most significant independent variables. Repetition of this process (hence, the reason for the connotation "stepwise") was continued until all significant independent variables were determined and used in the least-squares curve fit. The equation of the curve passing through the data would then be the

desired correlation equation provided the curve fit was good enough. The so called multiple-correlation coefficient was then calculated since it is typically used as a measure of goodness of fit of the mathematical model (regression equation) to the data (68,69).

In this investigation the Stanton number was taken as the dependent variable while the possible independent variables were selected from several predefined dimensionless numbers such as temperature ratio, pressure ratio, density ratio, Prandtl number and Reynolds number, to name a few.

The form of the mathematical model was chosen as

$$Y = (\text{constant})^{b_o} X_1^{b_1} X_2^{b_2} \ldots X_n^{b_n} \tag{78}$$

where the dependent variable Y is Stanton number, the X's are possible independent variables, and the b's are constants called regression coefficients. This model was chosen because it is the form found most effective in correlation of heat-transfer data from fluids flowing in ducts and pipes (70).

To test the hypothesis that any proposed independent variable had a significant effect on the dependent variable the F test was used. At a preselected probability level (or significance level) calculated values of F were obtained from the variance (standard deviation squared) of the appropriate variables and compared to values of F found in published tables. If the calculated F value exceeded the table value, the hypothesis was accepted. The significance level is the risk the investigator is willing to take in being wrong when accepting the hypothesis. At a significance

level of 0.05 the table value of F was typically close to 2.0 therefore an F value of 2.0 was always used in the computer program for comparison with the calculated F value.

The results of the stepwise regression analysis were not entirely successful in that a correlation equation was not obtained. However, the significant variables from a statistical viewpoint were determined. As expected, Reynolds number was consistently found to be the most important variable in all of the test mixtures. The only other variables consistently included as significant were those that were measures of shock-wave strength such as T_{21}, P_{21} and ρ_{21}. Sometimes two or more measures of shock-wave strength were indicated as significant in a given mixture. This has little practical meaning since one measure of shock-wave strength should have been enough. Sometimes various other dimensionless numbers such as Prandtl number or flow Mach number were indicated as significant but not in any consistant manner and not highly significant compared to Reynolds number or shock-wave strength. At times these inconsistent dimensionless numbers had extremely high b values. It was decided after discussions with G. Snowden[1] that such inconsistencies were invalid. The ratio of induction time to transition time was selected as one of the dimensionless X variables. At the significance level chosen it was found to be unimportant in correlating the data. This verified that boundary-layer transition was not essentially related to initial heat-energy release of the combustion reactions.

---

[1]Snowden, G., Ames, Iowa, Discussions of regression analysis. Private communication. 1966.

A correlation equation to fit all the mixtures could not be obtained because the regression coefficients (b values) kept changing from mixture-to-mixture. For example, the b values on Reynolds number varied from -0.44 to -1.22 in an inconsistent fashion throughout the mixtures. This was partly due to the lack of selecting a single measure of shock-wave strength as mentioned in the previous paragraph. It was also partly due to the dimensionless variables which were not consistently significant throughout all test mixtures. However, it should be noted that multiple-correlation coefficients were always greater than 0.77 and as high as 0.96. Values close to 0.85 were common. This means that typically about 85% of the variation in the dependent variable was accounted for by variation of the independent variables according to the mathematical model selected. The other 15% was attributed to lack of fit of the mathematical model, unconsidered variables and experimental error. Thus, at least the form of the mathematical model was approximately correct.

These results from statistical analysis surely complement those from dimensional analysis in that Reynolds number and a measure of shock-wave strength (perhaps shock-wave Mach number) should combine with Stanton number to correlate the experimental data. Further, by fixing some of the b values and dropping unimportant variables from the regression equation one might obtain a correlation equation to fit all test mixtures. However, in doing this, the multiple regression coefficient (goodness of fit) would be expected to drop as the number of variables and therefore degrees-of-freedom would be decreased. With these ideas in mind a trial-and-error approach was then attempted.

Final correlation

A parameter for which there is some theoretical basis (70) and is sometimes used for correlation of heat-transfer data in laminar flow (32,70) up to boundary-layer transition is the product of Stanton number and square root of Reynolds number. The use of this parameter was attempted according to the following expression

$$(St\sqrt{Re})_t = F(M_s) \tag{79}$$

The form of the function $F(M_s)$ was determined from the data. A very simple result was found which would approximately correlate the data of all test mixtures. It is

$$(St\sqrt{Re_\delta})_t = m(M_s-1) \tag{80}$$

where m is a particular constant for each given mixture.

In obtaining this correlation equation there were three important findings. First, either absolute flow velocity (u_2) or flow velocity relative to the wall ($u_2 - u_w$) yields the same value for this correlation parameter. Thus, one does not have to worry about which velocity best characterizes the flow in using $St\sqrt{R_e}$ for a correlation parameter.

Second, evaluation of fluid properties at a temperature other than the free-stream value had little effect on obtaining better data correlation for a given mixture and heat-flux gage. This is illustrated in the top two plots of Figure 11. Free-stream temperature (T_2) was used for fluid property evaluation in the first plot while Eckert's (71) "reference temperature" (T^*) was used in the second plot.

Third, and probably most important, the appropriate transition length

to use in the Reynolds number was found to be boundary-layer thickness at transition rather than the distance from the shock wave to the transition point. This fact is illustrated in the bottom plot of Figure 11 where considerable improvement in correlation can be observed compared to the top plot of that figure. Furthermore, it seems reasonable that a boundary-layer thickness should be the important length because this is the length over which the thermal resistance to the incident heat-energy flux occurs. Strictly speaking the appropriate boundary layer thickness to use would be that of the thermal boundary layer (Δ). However, the thickness of the velocity-boundary layer (δ) should correlate the data just as well because the two thicknesses vary approximately according to the relation (72)

$$\frac{\Delta}{\delta} = (Pr)^{-1/4} \tag{81}$$

when frictional dissipation is not neglected for steady flow of a constant property fluid over a flat plate. Thus, for the conditions stated, when the Prandtl number is 0.6 the thicknesses differ by approximately 11%. In this investigation, where the flow model is different by one boundary condtition from that of a flat plate, Δ cannot be obtained without solving a non-linear differential equation. However, δ can be determined as shown in Appendix D by the following relation as developed from a Karman-Pohlhausen integral approach.

$$\frac{\delta}{x} = \frac{a}{\sqrt{Re_x}\sqrt{1 + bU}} \tag{82}$$

In this relation the constants a and b depend on the degree of polynomial used for the velocity profile in the Karman-Pohlhausen technique of

Figure 11. Illustration of correlation improvement

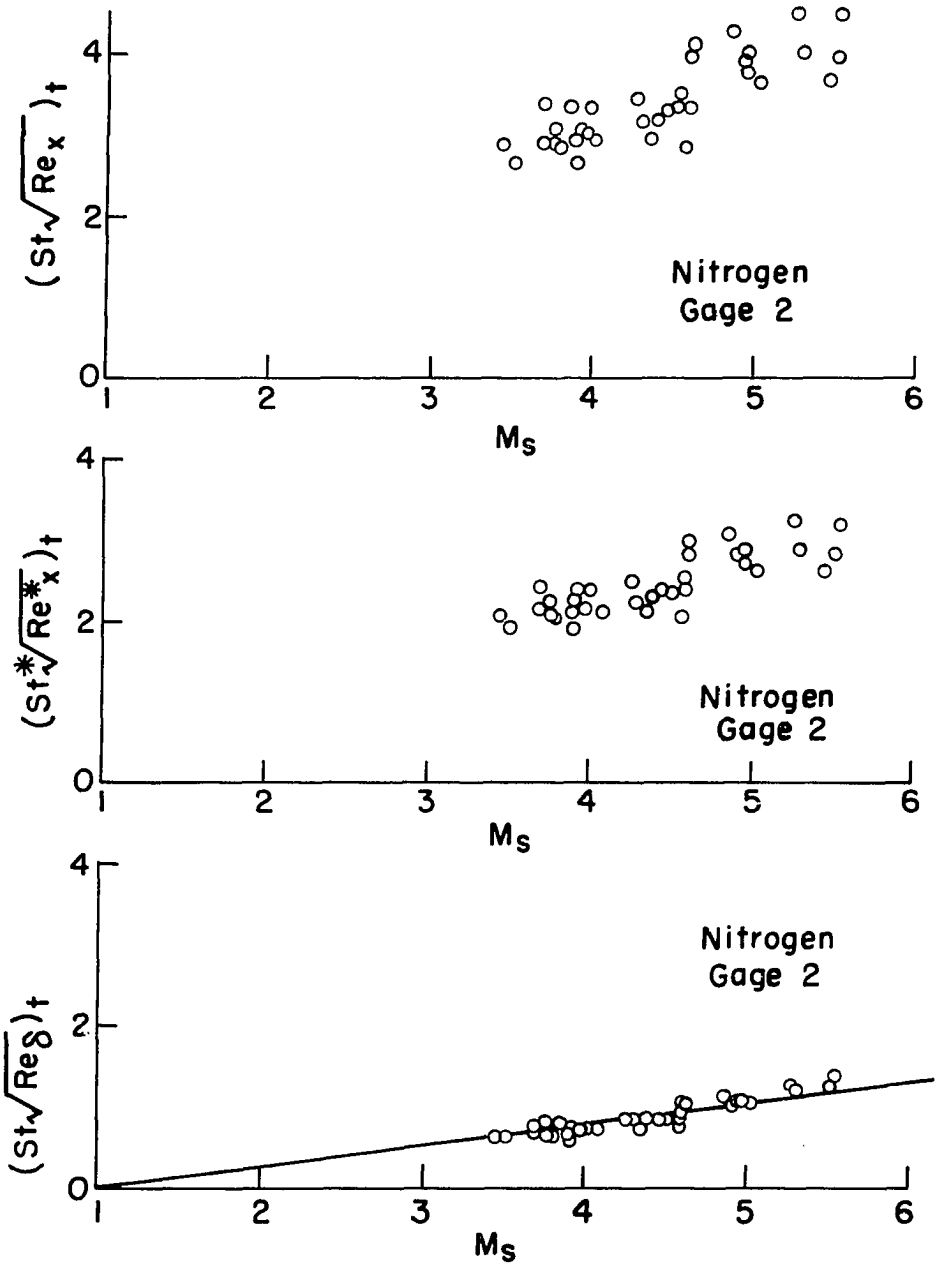
$(St\sqrt{Re_x})_t$
Nitrogen
Gage 2
M_S
$(St^*\sqrt{Re^*_x})_t$
Nitrogen
Gage 2
M_S
$(St\sqrt{Re_\delta})_t$
Nitrogen
Gage 2
M_S

solving the boundary-layer equations in integral form. It is interesting to note that these constants are identical to those obtained in conventional flat-plate flow for a given degree polynomial representing the velocity profile and, for a third degree polynomial, become 4.64 and 1.693 respectively. Also, the difference between shock-tube boundary-layer thickness and that of conventional flat-plate flow is the factor $\sqrt{1 + bU}$. Consequently, a shock-tube boundary layer is thinner than that of conventional flat-plate flow for corresponding x values.

Experimental Results

Presentation of data

The data in final form is presented in Figures 12 through 19. For each figure the top three plots represent data from thin-film gages 1, 2 and 4 respectively and the bottom plot is the average data of the three plots above. The heat-transfer data from gage 3 was not used because it gave erratic results compared to the heat-transfer data of the other gages. Furthermore, as indicated in Appendix B, gage 3 would not recalibrate properly for β after the experimental runs had been made. However, gage 3 was still useful as a shock-wave detector and its output was used for determining shock-wave velocities and corresponding shock-wave Mach numbers.

The experimental data from each individual gage follows the same general trend as can be observed in Figures 12 through 19. However, there is some variation in the correlation parameter $St\sqrt{Re_\delta}$ among gages from a given run. No consistent pattern to this variation was noticed and it

Figure 12. Correlation results for pure nitrogen

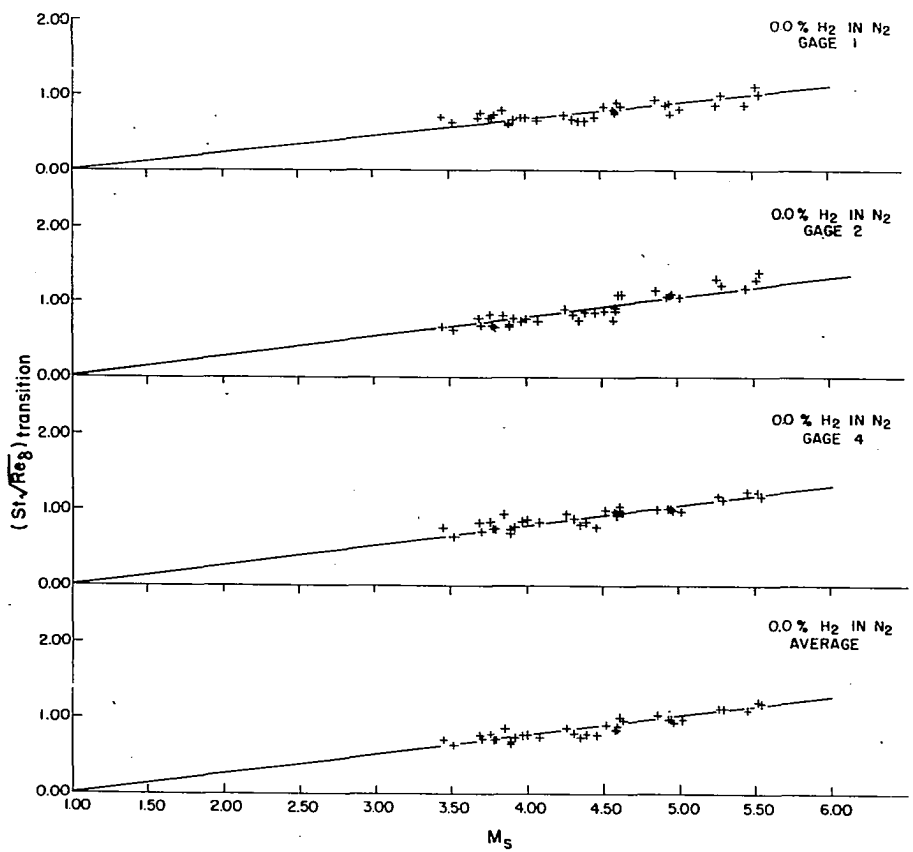
0.0 % H2 IN N2
GAGE 1
0.0 % H2 IN N2
GAGE 2
0.0 % H2 IN N2
GAGE 4
0.0 % H2 IN N2
AVERAGE
(St√Re8) transition
2.00
1.00
0.00
1.00
1.50
2.00
2.50
3.00
3.50
4.00
4.50
5.00
5.50
6.00
Ms

Figure 13. Correlation results for 4.0% hydrogen in nitrogen

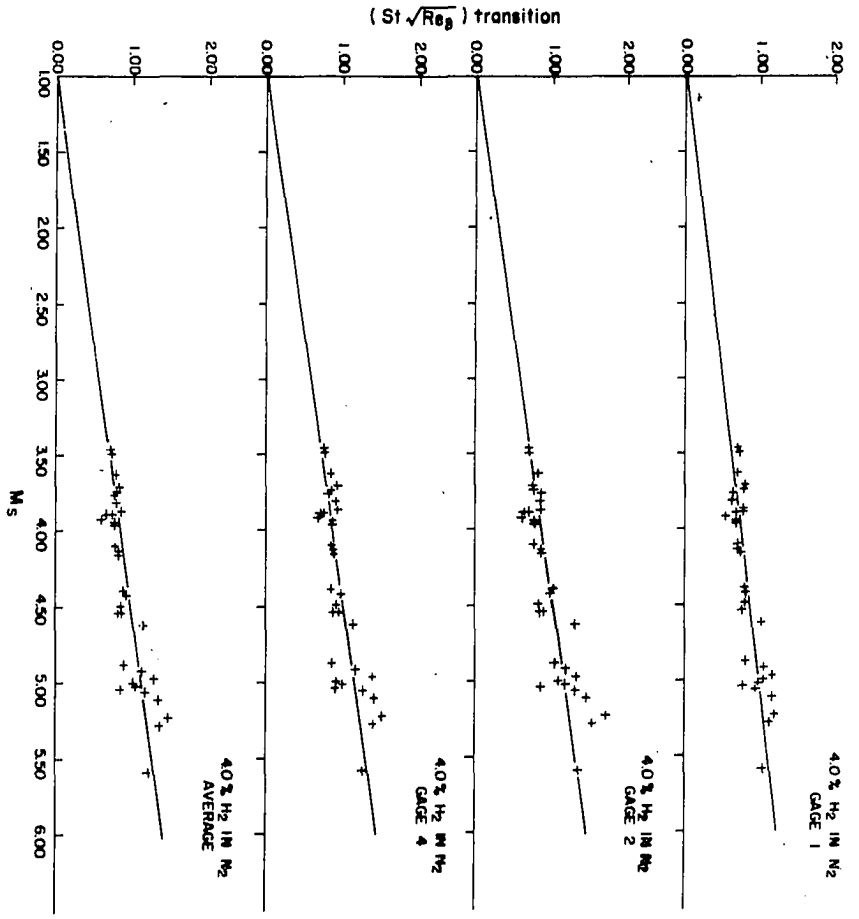
(St √Re$_s$) transition
M_s
0.00
1.00
1.50
2.00
2.50
3.00
3.50
4.00
4.50
5.00
5.50
6.00
4.0 % H_2 IN N_2 GAGE 1
4.0 % H_2 IN N_2 GAGE 2
4.0 % H_2 IN N_2 GAGE 4
4.0 % H_2 IN N_2 AVERAGE

Figure 14. Correlation results for 8.2% hydrogen in nitrogen

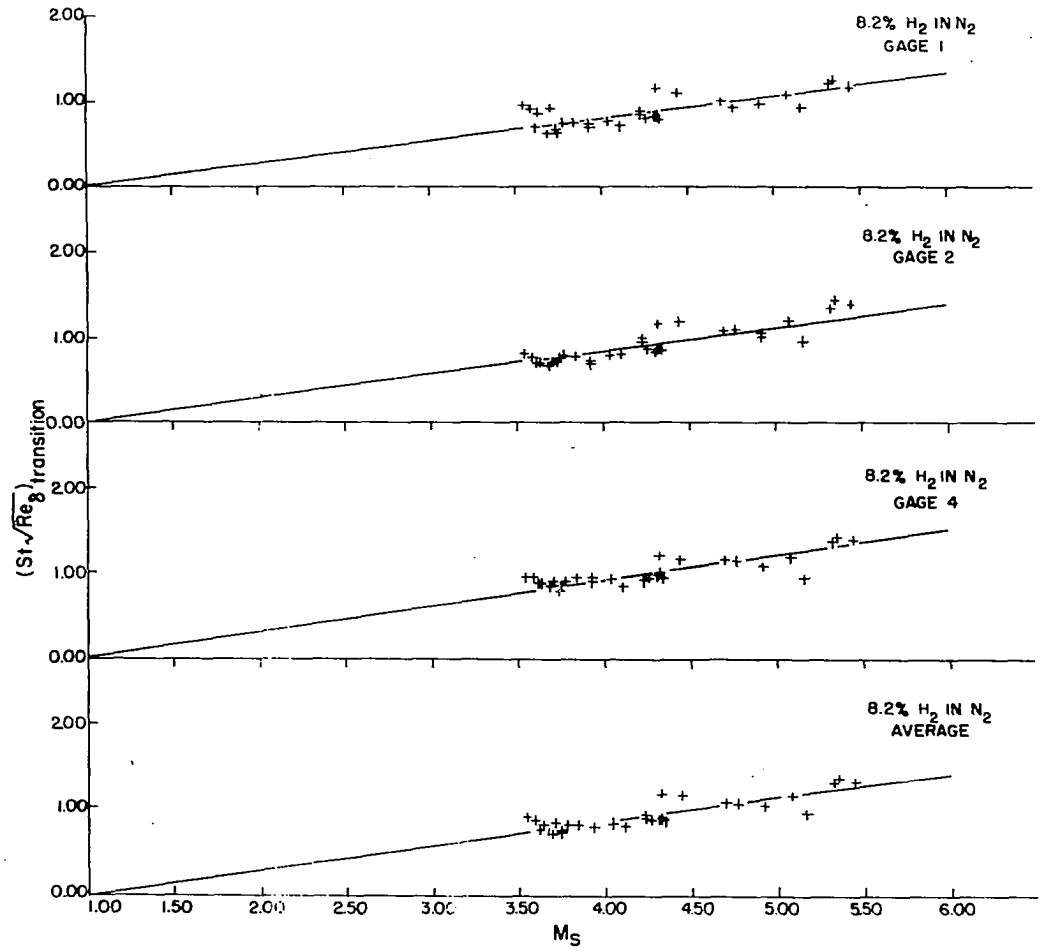
8.2% H_2 IN N_2
GAGE 1
8.2% H_2 IN N_2
GAGE 2
8.2% H_2 IN N_2
GAGE 4
8.2% H_2 IN N_2
AVERAGE
$(St\sqrt{Re_\delta})_{transition}$
M_S
2.00
1.00
0.00
1.00
1.50
2.00
2.50
3.00
3.50
4.00
4.50
5.00
5.50
6.00

Figure 15. Correlation results for 12.3% hydrogen in nitrogen

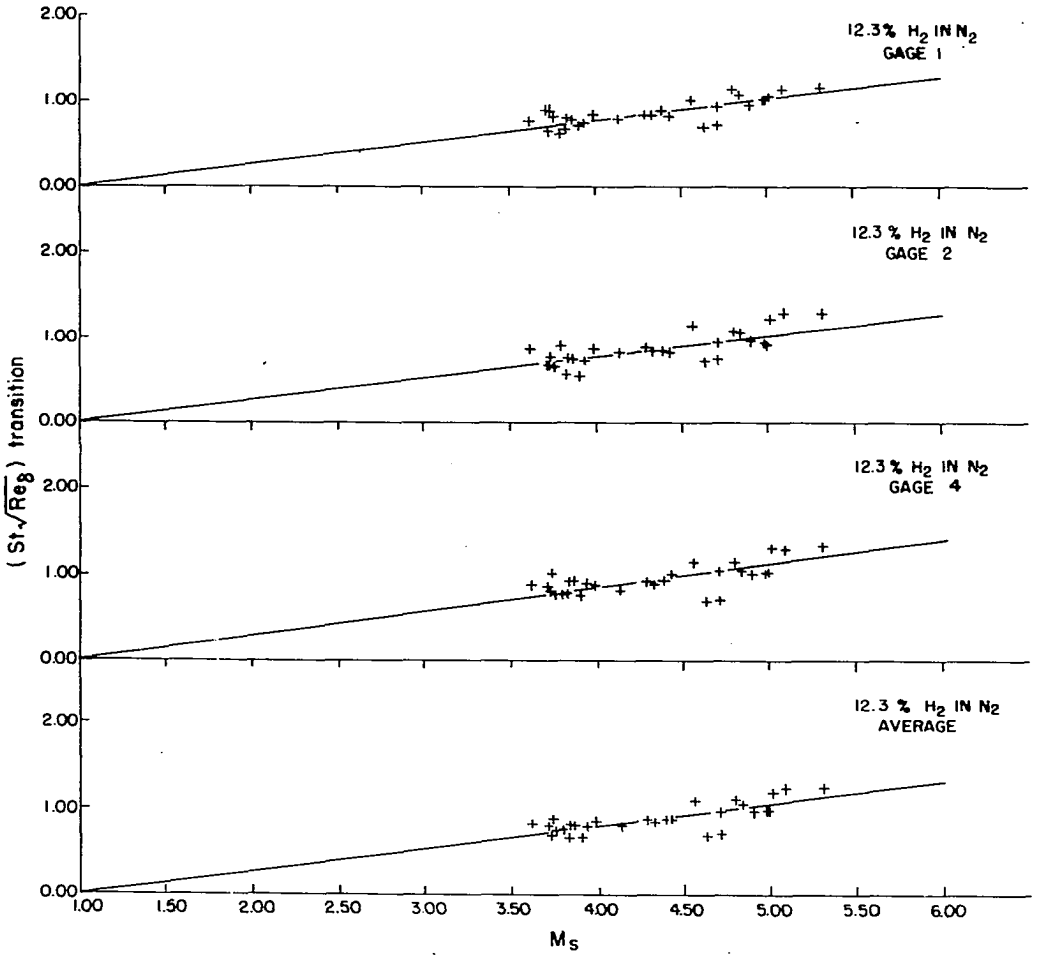
12.3% H_2 IN N_2
GAGE 1
12.3 % H_2 IN N_2
GAGE 2
12.3 % H_2 IN N_2
GAGE 4
12.3 % H_2 IN N_2
AVERAGE
$(St\sqrt{Re_\delta})$ transition
M_s
2.00
1.00
0.00
1.00
1.50
2.00
2.50
3.00
3.50
4.00
4.50
5.00
5.50
6.00

Figure 16. Correlation results for 3.1% hydrogen in air

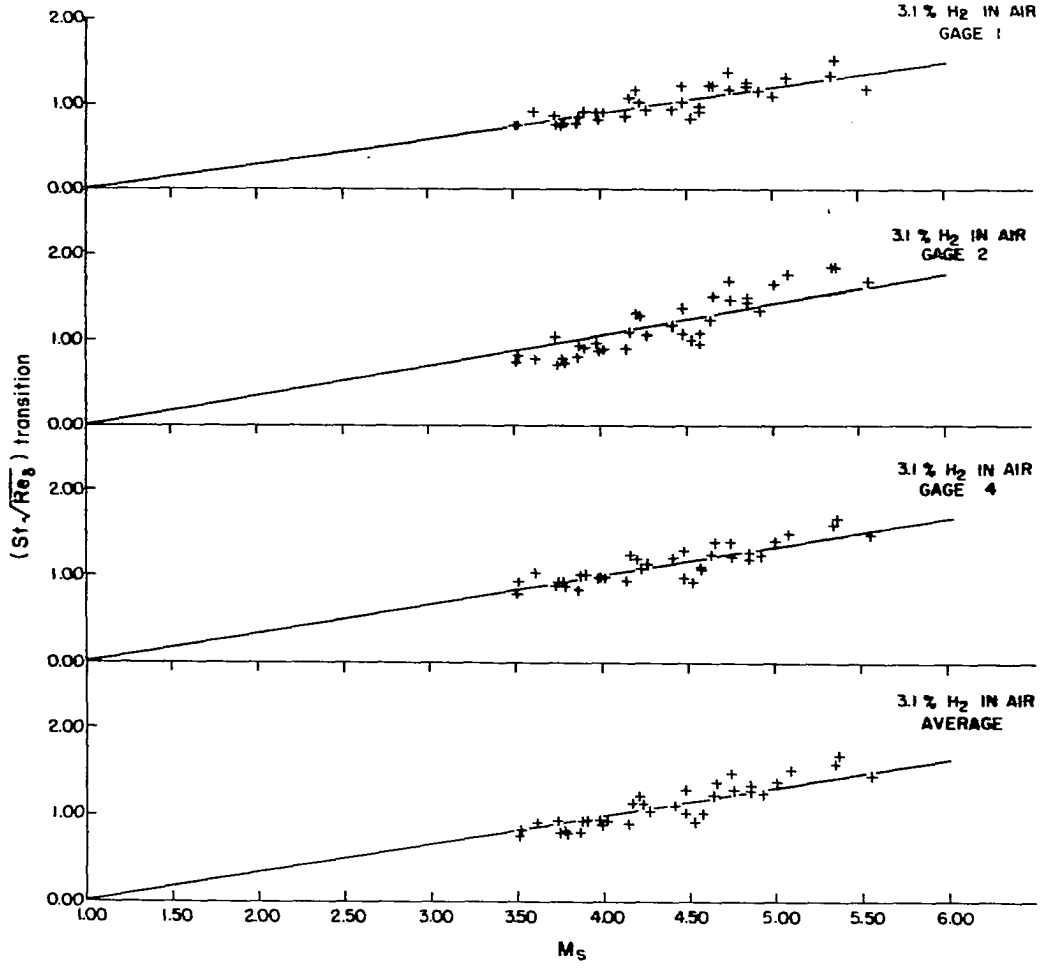
3.1 % H_2 IN AIR
GAGE 1
3.1 % H_2 IN AIR
GAGE 2
3.1 % H_2 IN AIR
GAGE 4
3.1 % H_2 IN AIR
AVERAGE
$(St\sqrt{Re_\delta})$ transition
2.00
1.00
0.00
1.00
1.50
2.00
2.50
3.00
3.50
4.00
4.50
5.00
5.50
6.00
M_s

Figure 17. Correlation results for 7.0% hydrogen in air

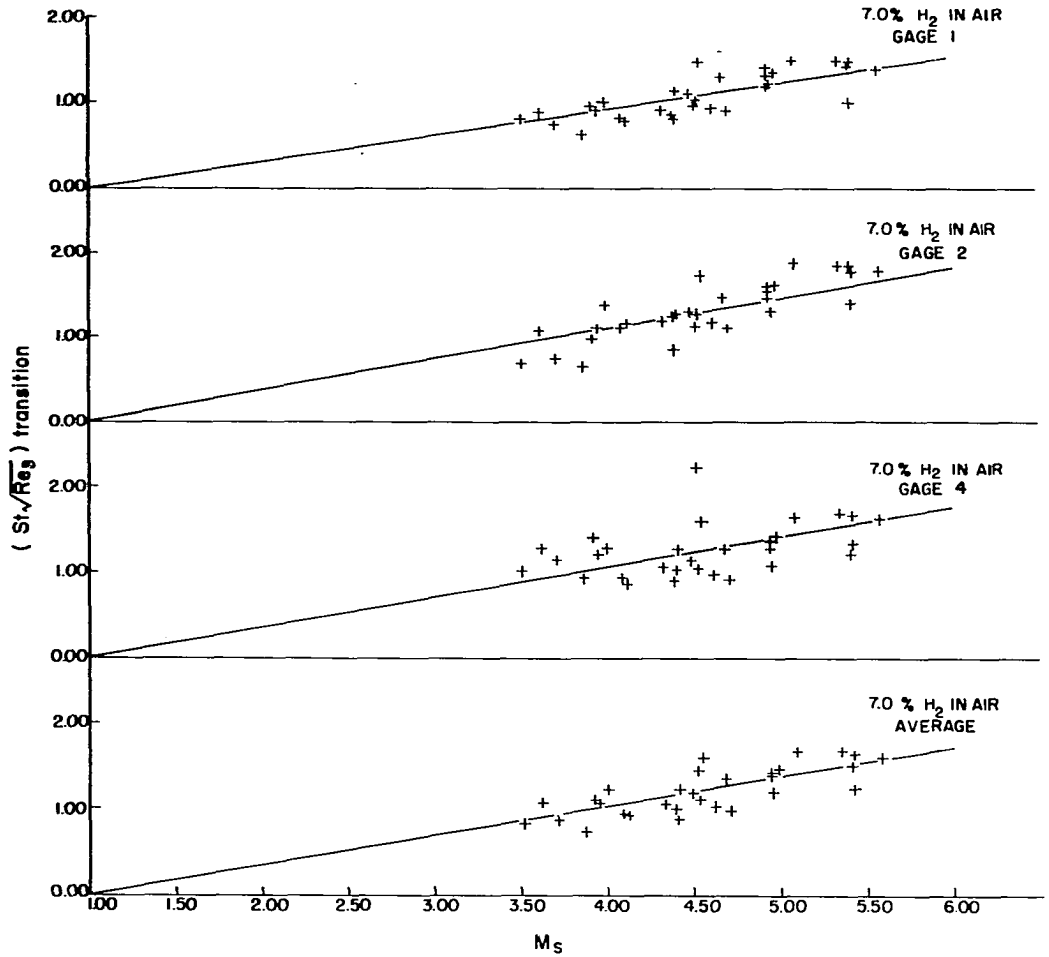
7.0% H_2 IN AIR
GAGE 1
7.0% H_2 IN AIR
GAGE 2
7.0% H_2 IN AIR
GAGE 4
7.0 % H_2 IN AIR
AVERAGE
$(St\sqrt{Re_s})$ transition
2.00
1.00
0.00
1.00
1.50
2.00
2.50
3.00
3.50
4.00
4.50
5.00
5.50
6.00
M_S

Figure 18. Correlation results for 11.0% hydrogen in air

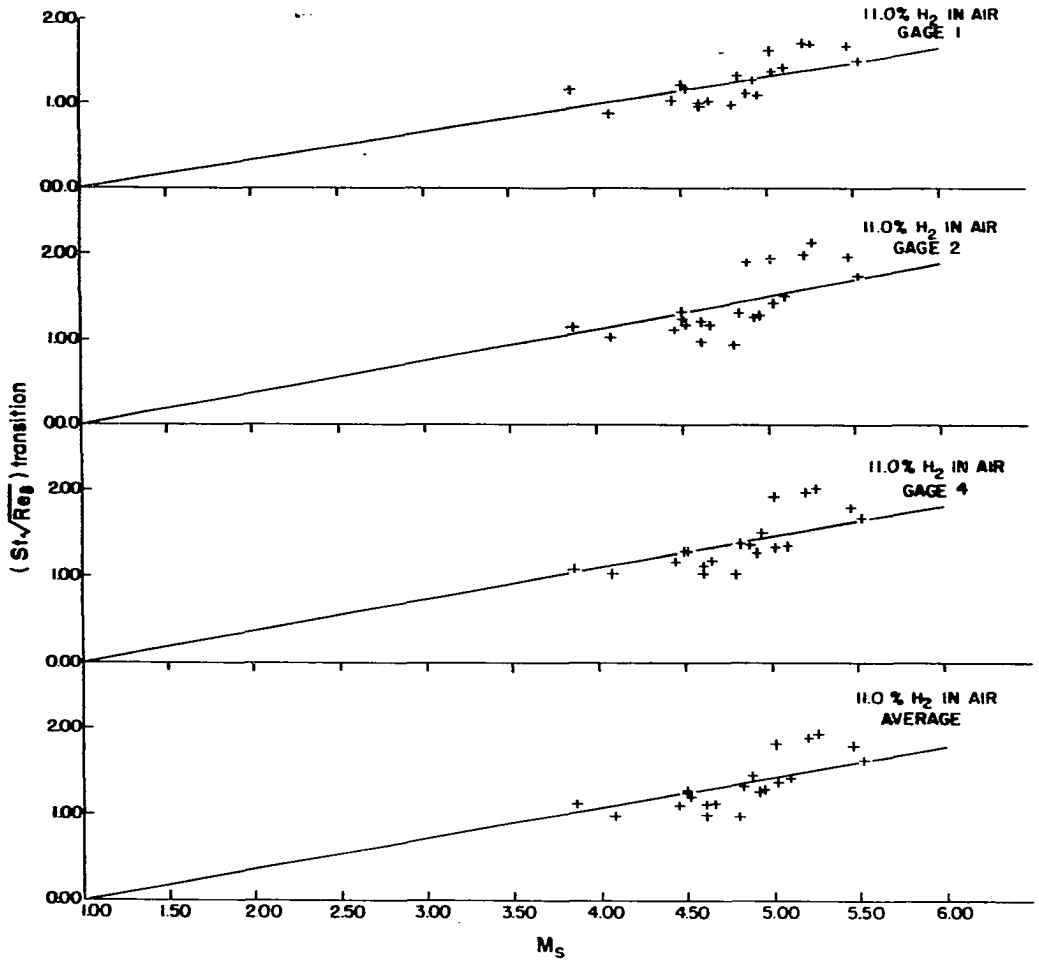
11.0% H_2 IN AIR
GAGE 1
11.0% H_2 IN AIR
GAGE 2
11.0% H_2 IN AIR
GAGE 4
11.0 % H_2 IN AIR
AVERAGE
$(St\sqrt{Re_s})$ transition
2.00
1.00
00.0
2.00
1.00
00.0
2.00
1.00
0.00
2.00
1.00
0.00
1.00
1.50
2.00
2.50
3.00
3.50
4.00
4.50
5.00
5.50
6.00
M_s

Figure 19. Correlation results for 15.0% hydrogen in air

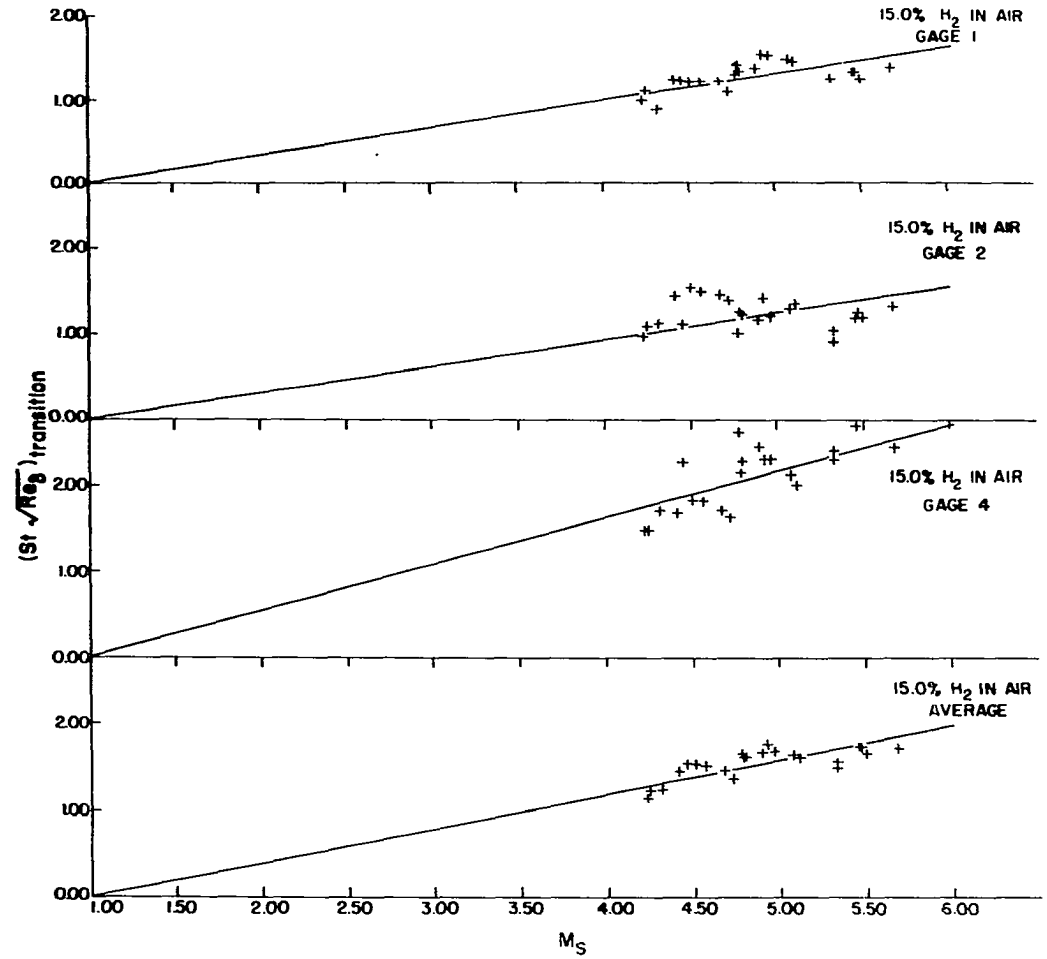
15.0% H_2 IN AIR
GAGE 1
15.0% H_2 IN AIR
GAGE 2
15.0% H_2 IN AIR
GAGE 4
15.0% H_2 IN AIR
AVERAGE
$(St\sqrt{Re_\delta})_{transition}$
M_S
2.00
1.00
0.00
1.00
1.50
2.00
2.50
3.00
3.50
4.00
4.50
5.00
5.50
6.00

was therefore presumed to be random. If this variation is random, the average data as presented will be a better representation of the results of an experimental run than results from any one of the individual gages. Thus, conclusions drawn from this investigation are based on trends of the average data.

Precision of data

The precision or measure of uncertainty in the data has been found by the suggested technique of Kline and McClintock (73) and Beers (74) for single-sample experiments. This technique is described and used in Appendix C to determine the precision of the correlation parameter $St\sqrt{Re}$ and shock-wave Mach number M_s. These precisions are $\pm$ 10% and $\pm$ 3% of the variable values respectively and they represent the range or uncertainty interval within which the actual values of the variables are believed to be according to a specified probability level. Herein the experimenter is establishing 20-to-1 odds (95% probability) that the value of the variable is within the range (uncertainty interval) given.

The scale factors and smallest scale division on the data plots were selected according to these respective values of uncertainty so that the data presented would not be unduly distorted by any particular plotting technique.

Data trends

An apparent trend of the data is that the correlation parameter $St\sqrt{Re_\delta}$ increases nearly linearly with M_s and is zero when M_s is one. This trend is different from that of Hartunian et al. (32) in that they found no effect of M_s within the scatter of their data. To check this

trend so the data would "speak for itself" a straight line was fit by the method of least squares to the average data of each mixture and a test of the goodness of fit was performed by a method presented in References 75 and 76. First, a correlation coefficient ε was obtained by the following relation as given in Reference 75.

$$\varepsilon = \frac{N\Sigma xy - \Sigma x\Sigma y}{[\{N\Sigma x^2 - (\Sigma x)^2\}\{N\Sigma y^2 - (\Sigma y)^2\}]^{\frac{1}{2}}} \tag{83}$$

In this equation, x and y represent M_s and $St\sqrt{Re_\delta}$ respectively, N represents the number of data points, and the summations are carried from 1 to N. An ε of one represents perfect correlation and an ε of zero represents no correlation. Because of random error ε will be somewhere between zero and one. After ε had been determined for each mixture it was necessary to know how large it must be in order to indicate a significant correlation between the variables M_s and $St\sqrt{Re_\delta}$. Thus, it was necessary to find the probability of obtaining by chance the value of ε for each mixture if the variables were not really related. Equivalently, for a given probability level it was necessary to find the value of ε expected if the variables were not really related. Tables have been presented (75,76) to obtain such information. A "rule-of-thumb" presented in Reference 76 in interpreting values of ε is to regard the correlation significant if there is less than 1 chance in 20 (a probability of 5%) that the value will occur by chance. Thus, if the calculated ε exceeds the table value of ε a significant correlation exists with a probability of 5% of having drawn the wrong conclusion. Table 4 is a tabulation of the calculated values of ε for each mixture and corresponding values of ε at both the 5% and 1%

Table 4. Correlation coefficients for goodness of fit test

Mixture	No. Runs	ε Calculated	ε at 5% probability	ε at 1% probability
100% N_2	35	0.927	.337	.435
4.0% H_2 in N_2	33	0.829	.344	.442
8.2% H_2 in N_2	31	0.847	.355	.456
12.3% H_2 in N_2	29	0.769	.367	.470
3.1% H_2 in Air	36	0.901	.330	.424
7.0% H_2 in Air	31	0.769	.355	.456
11.0% H_2 in Air	21	0.762	.433	.549
15.0% H_2 in Air	23	0.743	.413	.526

probability levels.

As shown in the above table the straight lines fitted to the data give a significant correlation of the data with less than a 1% probability of being wrong.

Within the precision of the data, five of eight mixtures had straight lines passing through zero for $St\sqrt{Re_\delta}$ at an M_s of one. Two other mixtures had values close to this zero but not zero within the precision of the data. It is interesting to note that all of the inert runs were in the group that had slopes passing through this zero. A plausible explanation of the data passing through this point might include the following reasoning.

When M_s is one the shock wave becomes an acoustic wave with only extremely small changes in pressure, temperature and velocity across the wave. This would result in essentially zero heat-transfer to the wall of the shock tube since the initial test-gas temperature is the same as the

wall temperature. Consequently, the Stanton number would be expected to be zero and the product $St\sqrt{Re_\delta}$ would also be zero for finite Reynolds number and a shock-wave Mach number of one.

By plotting the data in the manner shown, one then gains the advantage of an additional point through which any curve or line fitted to the data must pass. Straight lines passing through this point were then obtained by the method of least squares for the average data of all mixtures. This was to provide a consistent form of correlation equation for all mixtures. These straight lines are shown on all of the average data plots. Similarly obtained lines are shown on the data plots of individual gages and follow the indicated trend of the average data. It is significant to note that, within the precision of the data, the slopes of straight lines passing through average data of all inert mixtures are nearly identical. The slopes of straight lines passing through average data of the combustible mixtures increase with percentage of hydrogen contained in each combustible mixture. A tabulation of the straight line slopes is presented in Table 5 below. The ratio of combustible mixture slope to the average of the inert mixture slope is also presented.

The following equation has been found to relate the slope m_c to hydrogen content of the combustible mixture and is illustrated in Figure 20.

$$m_c = 0.327 + 2.79 \left(\frac{\%H_2}{100}\right)^2 \qquad (84)$$

Equation 84 is only valid between 3% and 15% hydrogen in air. This corresponds approximately to the range of hydrogen content between the

Figure 20. Variation of slope m_c with hydrogen content

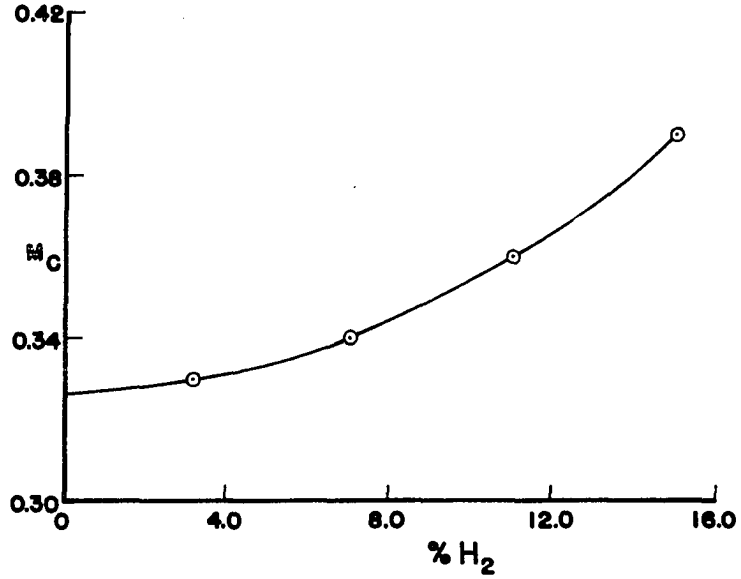
0.42
0.38
M_C
0.34
0.30
0
4.0
8.0
12.0
16.0
% H_2

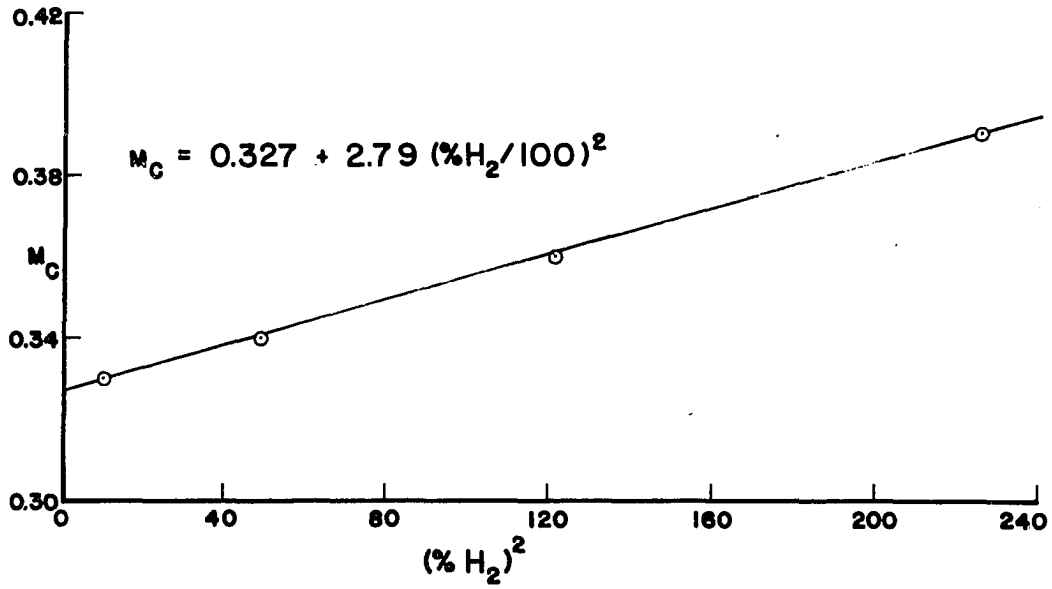
M_C = 0.327 + 2.79 (%H_2/100)^2
0.42
0.38
M_C
0.34
0.30
0
40
80
120
160
200
240
(% H_2)^2

Table 5. Slopes of correlation lines through data of Figures 12 through 19

Inert Compositions	Slope, m_i	Combustible Compositions	Slope, m_c	m_c/m_i Slope ratio
100% N_2	0.26	3.1% H_2 in Air	0.33	1.22
4.0% H_2 in N_2	0.28	7.0% H_2 in Air	0.34	1.26
8.2% H_2 in N_2	0.28	11.0% H_2 in Air	0.36	1.33
12.3% H_2 in N_2	0.26	15.0% H_2 in Air	0.39	1.44

lower flammability limit and the lower detonation limit for hydrogen in air mixtures. Equation 84 allows data from all combustible mixtures composed of hydrogen in air and containing more than 3% hydrogen but less than 15% hydrogen to be represented by the correlation equation

$$(St\sqrt{Re_\delta})_t = \left(0.327 + 2.79\left\{\frac{\%H_2}{100}\right\}^2\right)(M_s - 1) \tag{85}$$

The data of all inert mixtures of this investigation may be represented by Equation 86 given below

$$(St\sqrt{Re_\delta})_t = 0.27\,(M_s - 1) \tag{86}$$

Effect of heat-flux on transition

To arrive at a relation which would indicate the effect of heat-flux on transition the ratio of the correlation equation for a combustible mixture to that of its matched inert mixture was formed. This equation is

$$\frac{(St\sqrt{Re_\delta})_{t_c}}{(St\sqrt{Re_\delta})_{t_i}} = \frac{m_c}{m_i}\,\frac{(M_s - 1)_c}{(M_s - 1)_i} \tag{87}$$

where the subscripts c and i represent "combustible" and "inert" respectively. The ratio form of Equation 87 is extremely important in that uncontrolled factors in the experiment would tend to be cancelled out and only the effects of heat-flux on transition indicated. Such uncontrolled factors include shock-tube wall surface roughness, free-stream turbulence level other than that caused by combustion, and any other anomalous factor unique to the particular shock tube used in this investigation.

The slope ratio m_c/m_i is a constant greater than one for a given set of matched mixtures as shown in Table 5 and it increases parabolically with percent hydrogen according to the following relation

$$\frac{m_c}{m_i} = \left[1.21 + 10.33 \left(\frac{\%H_2}{100}\right)\right]^2 \tag{88}$$

One can show explicitly the effects of heat-flux on boundary-layer transition by simplifying Equation 87 according to the following restrictions.

1. Select any given set of matched mixtures herein so that molecular weight M fixed. This will allow the velocity-of-sound a_1 at a given value of T_1 to be identical for both mixtures since the matched mixtures have the same specific heat ratio of 1.4 in this investigation.

2. Select P_1, T_1 and M_s. These are to be the same for both mixtures.

These restrictions are important because they involve the exact variables an experimenter can fix or control in a shock-tube experiment. The dimensionless parameters in Equation 87 can be rewritten in terms of actual flow

variables so appropriate quantities can be cancelled according to the restrictions listed. Thus using the continuity and state equations respectively in combination with the Stanton number from Equation 76 yield

$$St_t = \frac{q_t \; R_u \; T_1}{M \quad P_1 u_1 (h_r - h_w)} \tag{89}$$

The steady flow energy equation across the shock-wave in the free-stream combined with the definition of recovery factor can be used as shown below to replace $(h_r - h_w)$ in Equation 89.

$$r \equiv \frac{h_r - h_2}{h_o - h_2}$$

$$h_r - h_w = h_r - h_1 = (h_r - h_2) - (h_1 - h_2)$$

$$= r(h_o - h_2) - (h_1 - h_2)$$

$$= \frac{r}{2}(u_2)^2 - \frac{1}{2}\{(u_2)^2 - (u_1)^2\}$$

$$= \frac{(u_1)^2}{2} \left\{1 - \frac{(1-r)}{U^2}\right\} \tag{90}$$

Comtination of Equation 89 with Equation 90 and forming the ratio of Stanton numbers one obtains

$$\frac{(St_t)_c}{(St_t)_i} = \frac{(q_t)_c}{(q_t)_i} \frac{\{1 - (1-r)/U^2\}_i}{\{1 - (1-r)/U^2\}_c} \tag{91}$$

The Reynolds number may be manipulated by using Equation 82 to yield

$$(Re_\delta)_t = (Re_x)_t \frac{\delta_t}{x_t} = \frac{a\sqrt{(Re_x)_t}}{\sqrt{1 + bU}} \tag{92}$$

From the definition of Reynolds number and mass conservation across the shock wave we have from Equation 77

$$(Re_x)_t = \left(\frac{\rho_2}{\rho_1}\right) \frac{\rho_1 u_2 x_t}{\mu_2} = \frac{p_1 M u_1 x_t}{R_u T_1 \mu_2} \tag{93}$$

By combining Equation 92 with 93 and forming the ratio of Reynolds numbers one obtains

$$\left\{\frac{(Re_{\delta_t})_c}{(Re_{\delta_t})_i}\right\}^{1/2} = \left\{\frac{(\sqrt{1+bU})_i}{(\sqrt{1+bU})_c} \frac{\sqrt{(x_t)_c}}{\sqrt{(x_t)_i}} \frac{\sqrt{(\mu_2)_i}}{\sqrt{(\mu_2)_c}}\right\}^{1/2} \tag{94}$$

Substitution of Equations 88, 91 and 94 into Equation 87 yields

$$\frac{(q_t)_c}{(q_t)_i} = \frac{F_c(U,r_2,\mu_2)}{F_i(U,r_2,\mu_2)} \left[\frac{(x_t)_i}{(x_t)_c}\right]^{\frac{1}{4}} \left[1.21 + 10.33 \left(\frac{\%H_2}{100}\right)^2\right] \tag{95}$$

where the function $F(r,U,\mu_2)$ is given by

$$F(U,r_2,\mu_2) = [1 - \{(1-r_2)/U^2\}][(1 + bU)\mu_2]^{\frac{1}{4}}[10^6]^{\frac{1}{4}} \tag{96}$$

Figures 21 through 24 show there is insignificant difference between the functions F_c and F_i at any given value of shock-wave Mach number for the matched sets of mixtures in this investigation. Tables 23 through 30 of Appendix A are detailed tabulations of data used in Equation 96 to evaluate $F(U, r_2, \mu_2)$. Table 6 below is a summary of slopes, ordinates and correlation coefficients for straight lines fit through the data presented in Figures 21 through 24.

Taking the ratio F_c/F_i to be unity allows Equation 95 to reduce to the following significant result of this investigation

Figure 21. Variation of F with M_s for a molecular weight of 28.0

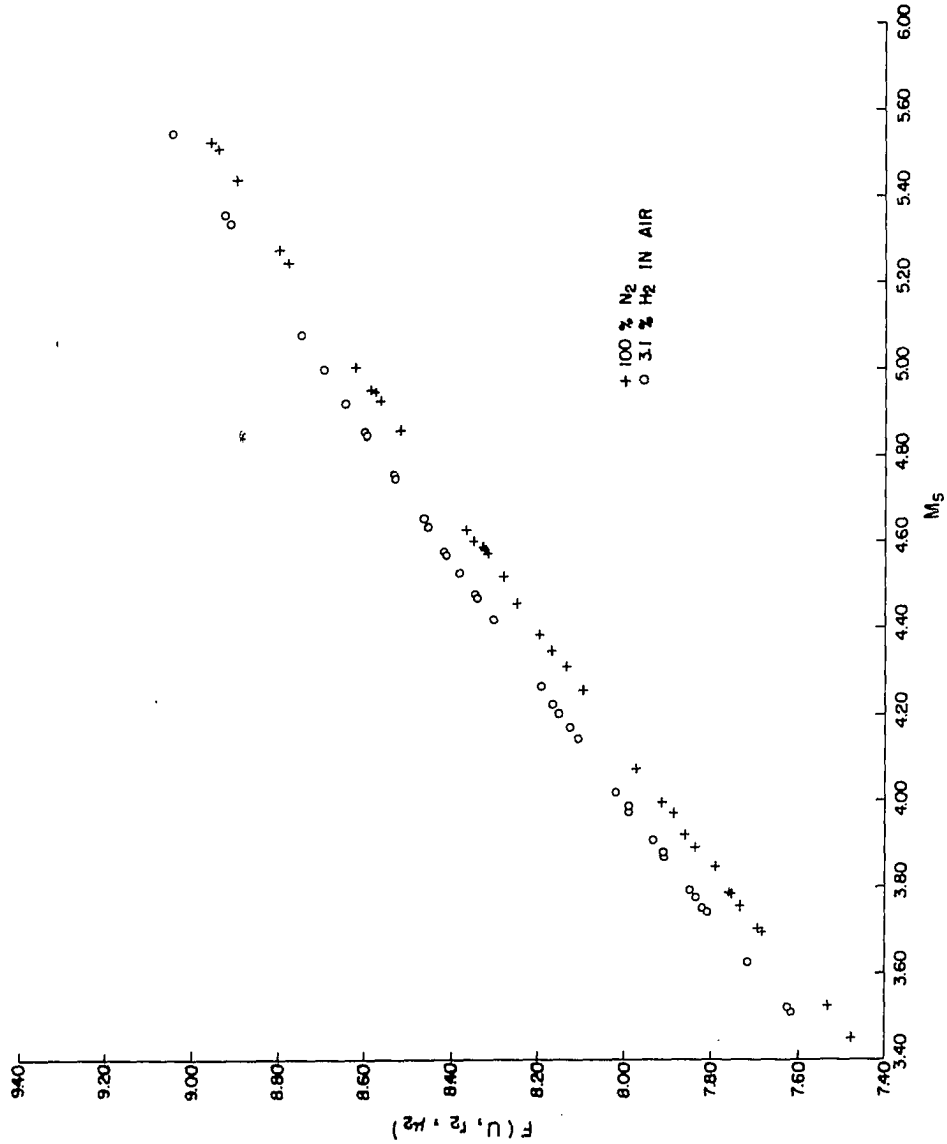
+ 100 % N2
o 3.1 % H2 IN AIR
F (U, r2 , ρ2)
Ms
9.40
9.20
9.00
8.80
8.60
8.40
8.20
8.00
7.80
7.60
7.40
3.40
3.60
3.80
4.00
4.20
4.40
4.60
4.80
5.00
5.20
5.40
5.60
6.00

Figure 22. Variation of F with M_s for a molecular weight of 27.0

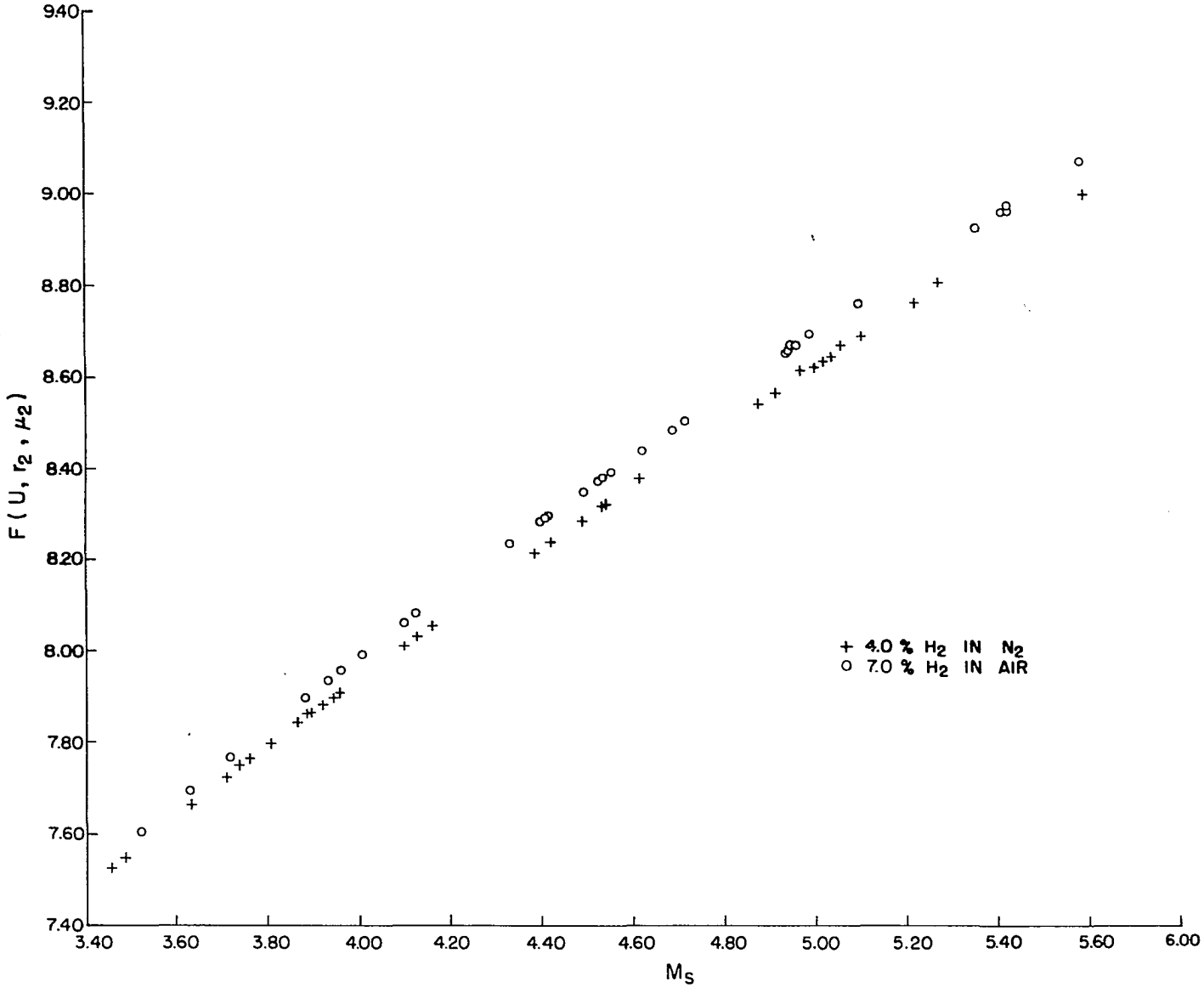
9.40
9.20
9.00
8.80
8.60
8.40
8.20
8.00
7.80
7.60
7.40
F (U, r2 , μ2)
3.40
3.60
3.80
4.00
4.20
4.40
4.60
4.80
5.00
5.20
5.40
5.60
6.00
Ms
+ 4.0 % H2 IN N2
o 7.0 % H2 IN AIR

Figure 23. Variation of F with M_s for a molecular weight of 25.9

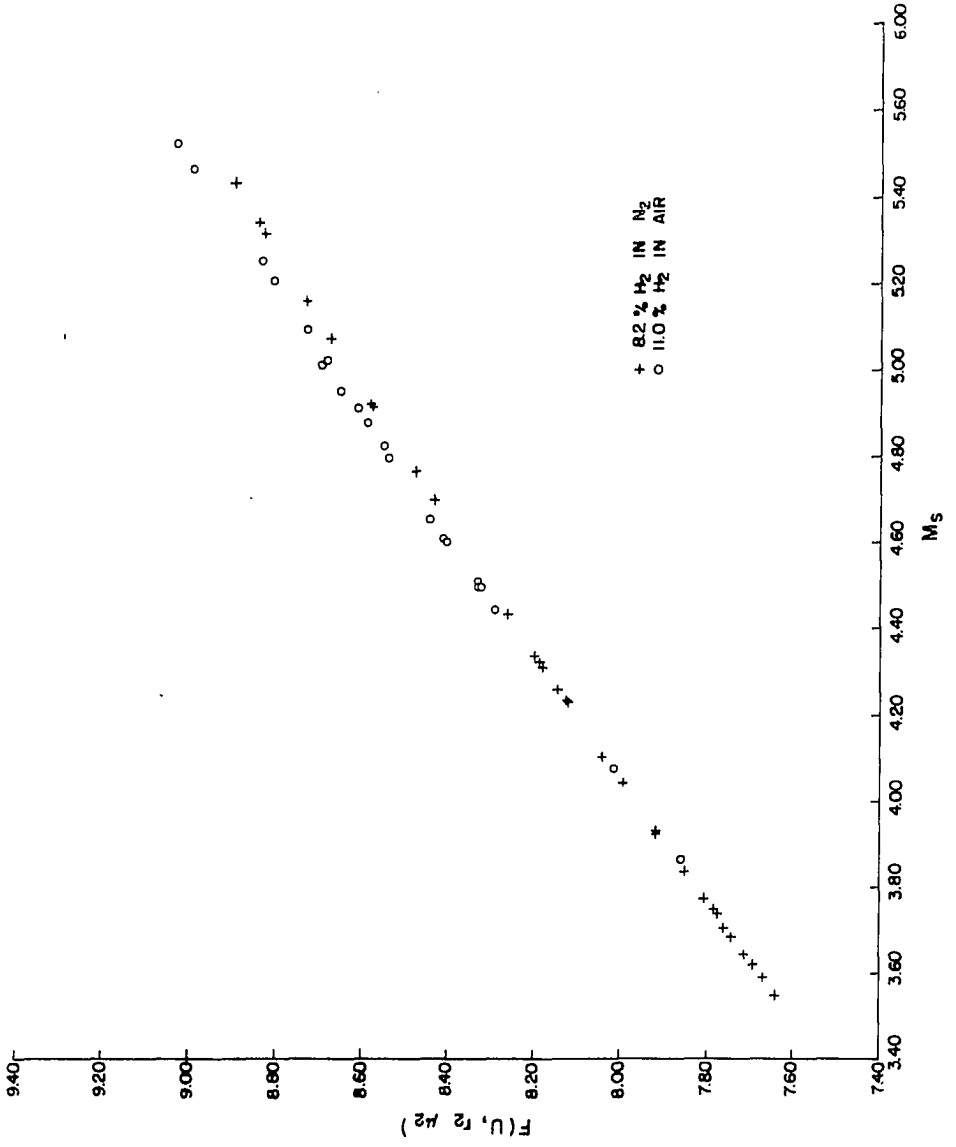
+ 8.2 % H2 IN N2
o 11.0 % H2 IN AIR
F(U, r2 μ2)
Ms
9.40
9.20
9.00
8.80
8.60
8.40
8.20
8.00
7.80
7.60
7.40
3.40
3.60
3.80
4.00
4.20
4.40
4.60
4.80
5.00
5.20
5.40
5.60
6.00

Figure 24. Variation of F with M_s for a molecular weight of 24.8

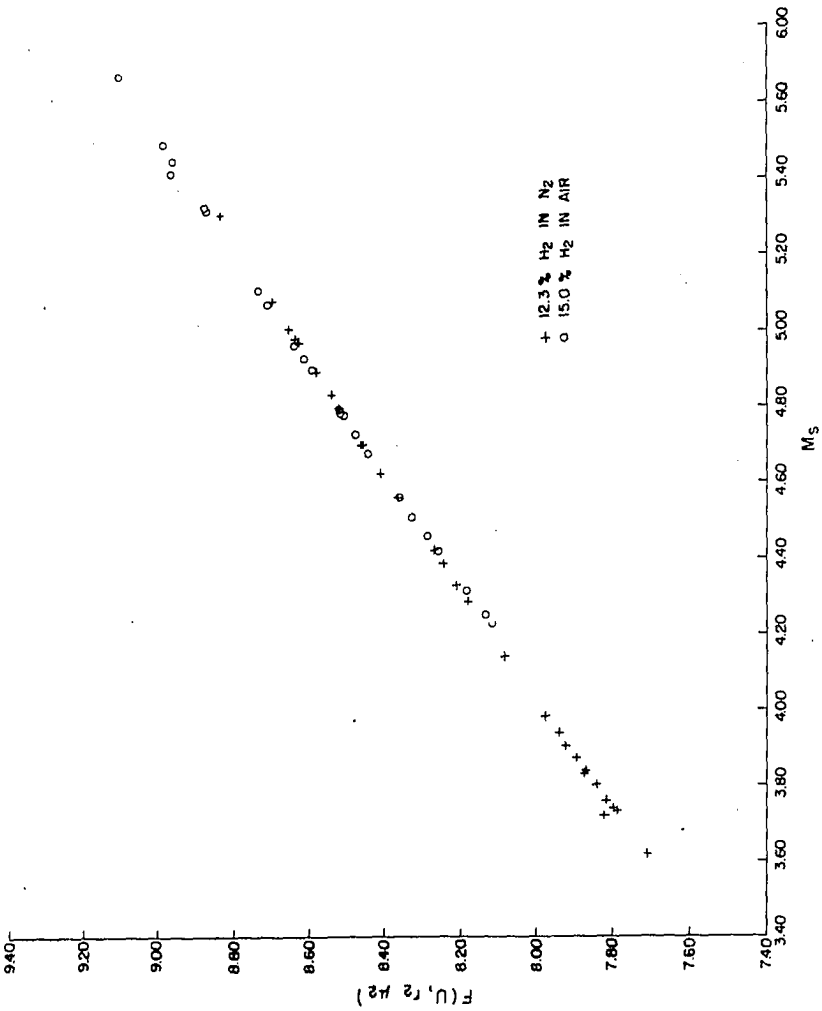
+ 12.3 % H2 IN N2
o 15.0 % H2 IN AIR
F(U, r2 μ2)
Ms
9.40
9.20
9.00
8.80
8.60
8.40
8.20
8.00
7.80
7.60
7.40
3.40
3.60
3.80
4.00
4.20
4.40
4.60
4.80
5.00
5.20
5.40
5.60
6.00

Table 6. Summary of least squares fit of straight lines to data of Figures 21 through 24

Mixture Composition	Ordinate	Slope	Correlation Coefficient
100% N_2	5.12	0.70	0.99
4.0% H_2 in N_2	5.17	0.70	0.99
8.2% H_2 in N_2	5.29	0.67	0.99
12.3% H_2 in N_2	5.52	0.66	0.99
3.1% H_2 in air	5.21	0.70	0.99
7.0% H_2 in air	5.18	0.70	0.99
11.0% H_2 in air	5.21	0.69	0.99
15.0% H_2 in air	5.26	0.68	0.99

$$\frac{(q_t)_c}{(q_t)_i} = \left[\frac{m_c}{m_i}\right]\left[\frac{(x_t)_i}{(x_t)_c}\right]^{\frac{1}{4}} = \left[1.21 + 10.33\left\{\frac{\%H_2}{100}\right\}^2\right]\left[\frac{(x_t)_i}{(x_t)_c}\right]^{\frac{1}{4}} \qquad (97)$$

Equation 97 shows explicitly the effect of heat-energy flux on boundary-layer transition for a given value of hydrogen content in the combustible mixture. It should be emphasized that Equation 97 is only valid for hydrogen contents between 3% and 15% and may not be extrapolated outisde this range because of the flammability and detonation limits previously mentioned. Examination of this result shows the boundary layer is stabilized (longer transition distance x_t) by heat-energy release above the boundary layer only as long as the additional heat energy due to combustion does not allow $(q_t)_c/(q_t)_i$ to be larger than m_c/m_i. Otherwise, the boundary layer is destabilized and the transition distance $(x_t)_c$ becomes less than $(x_t)_i$.

Although transition reversal has not been observed in shock tube flows, Equation 97 indicates it is possible. Further, such explicitness in showing the effects of heat-energy passing through the boundary layer on boundary-layer transition has not been presented in available literature. Instead, plots of the ratio of free-stream to wall temperatures as a function of Reynolds number have been used (32). This temperature ratio alone does not necessarily indicate the actual quantity of heat-energy passing through the boundary layer to the wall. This is especially true if radiation modes of heat-energy exchange are present. Furthermore, results of dimensional analysis do not show temperature ratio to be important in correlating data but instead show Stanton number to be important along with Reynolds number, Mach number and Prandtl number. Thus, measurements of heat-energy transfer to the wall are necessary before one can be quantitative as well as qualitative in determining the effects of incident heat energy on boundary layer transition.

SIGNIFICANT FINDINGS AND RECOMMENDATIONS

In attempting to satisfy the objectives of this investigation the following items were found.

1. Boundary-layer transition could be correlated with heat-energy transfer through the boundary layer to the wall in terms of dimensionless parameters by the relation

$$(St\sqrt{Re_\delta})_t = m(M_s - 1) .$$

The factor m was found to be approximately constant at a value of 0.27 for the inert test gases used in this investigation. For the combustible mixtures m was found to vary parabolically with percent hydrogen according to

$$m_c = \left[0.327 + 2.79\left\{\frac{\%H_2}{100}\right\}^2\right]$$

2. For a fixed set of initial shock-tube conditions and a given shock-wave Mach number the effect of heat-energy release above the boundary layer on boundary-layer transition was governed by the relation

$$\frac{(q_t)_c}{(q_t)_i} = \left[\frac{m_c}{m_i}\right]\left[\frac{(x_t)_i}{(x_t)_c}\right]^{\frac{1}{4}} = \left[1.21 + 10.33\left\{\frac{\%H_2}{100}\right\}^2\right]\left[\frac{(x_t)_i}{(x_t)_c}\right]^{\frac{1}{4}}$$

This relation indicates the boundary layer may be either stabilized or destabilized depending on the magnitude of the heat-transfer ratio relative to the ratio m_c/m_i.

3. The significant length in transition Reynolds number was found to be boundary-layer thickness at transition rather than

distance from the shock wave to the transition point. No attempts were made in this investigation to use either "momentum" or "energy" thicknesses for characteristic lengths. Further work should include such attempts.

4. Evaluation of fluid properties at Eckert's reference temperature had little effect on improving data correlation over that based on fluid properties evaluated at free-stream temperature.

5. Surface heat-transfer rates are more sensitive than surface temperature in determining boundary-layer transition. In addition, heat-transfer rate histories provide measures of time for the entire transition process to occur while surface-temperature histories do not. Thus, surface heat-transfer histories yield more information than do surface-temperature histories. Further comparison between these two techniques for determining boundary-layer transition are needed.

6. Free-stream properties behind the shock-wave and before combustion were calculated equilibrium values. No other measure of flow temperature during the induction period or during combustion was obtained. Continuous temperature measurements, possibly by optical means, should be considered in further studies of this nature. Measurements of turbulence level in the free-stream should also be attempted.

7. Heat-energy release above the boundary layer was obtained by means of hydrogen burning in air. Additional experiments should be made using some other mode of energy release in

order to check the results herein. Combustible gases with specific heats different from 1.4 should also be tried.

8. Experiments such as these should be obtained in shock tubes of different geometry to determine if geometric factors cause an important variation of the data or if the techniques used in these experiments have indeed cancelled geometric factors.

9. Uncertainties in the correlation parameter $St\sqrt{Re}$ and shock-wave Mach number M_s were found to be $\pm$ 10% and $\pm$ 3% respectively. Uncertainties in heat-transfer rates were the predominant factor in causing the stated uncertainty of the correlation parameter. Thus, efforts to improve uncertainties in the correlation parameter should start with improvement of uncertainties in heat-transfer rates.

ACKNOWLEDGMENTS

The author would like to express his sincere appreciation to the following people and organizations:

Dr. George K. Serovy for his advice, counsel, and patience while directing the author's thesis work, and for his unique ability in expediting funds, correspondence, computer time and other things necessary for the completion of this investigation.

The author's graduate study committee for their guidance, teaching and encouragement during the years of the author's graduate study. This committee consisted of: Dr. George K. Serovy, Chairman; Dr. Cheng T. Hsu, co-chairman, Professor Henry M. Black; Dr. Ernest W. Anderson; Professor Robert C. Fellinger; and Dr. Harry J. Weiss.

Frank E. Belles of Lewis Research Center of the National Aeronautics and Space Administration for suggesting the problem and allowing the author to use experimental facilities located there under his supervision. His cooperation, interest in the problem and suggestions for its solution were extremely gratifying.

Milton R. Lauver of Lewis Research center of National Aeronautics and Space Administration for helping prepare the experimental facility, enlarge data traces and fruitful discussions.

Professor Henry M. Black for providing the support necessary to allow certain data reduction techniques as well as the understanding attitude and environment which allowed the author to pursue graduate studies.

Mrs. Gretchen Snowden and the Iowa State University Statistical

Laboratory for performing a stepwise regression analysis of the data through the use of a digital computer program.

The Iowa State University Computation Center for providing the large amount of computer time necessary for the data reduction of this experiment.

Numerous colleagues and staff members of both the Mechanical Engineering Department at Iowa State University and the Chemical Kinetics section of Lewis Research Center, NASA, who have provided assistance through discussions and suggestions during the course of this work.

A very special note of appreciation and gratitude is given the author's wife and family for their encouragement, support and untiring sacrifices made throughout the years of the author's graduate work.

LITERATURE CITED

1. Wilson, R. E. Viscosity and heat transfer effects. Handbook of Supersonic Aerodynamics. Vol. 5, Sections 13 and 14. U.S. Bureau of Naval Weapons NAVORD Report 1488. 1966.

2. Mirels, H. Laminar boundary layer behind a strong shock moving into air. U.S. National Aeronautics and Space Administration Technical Note D-291. 1961.

3. Bromberg, R. Use of the shock tube wall boundary layer in heat transfer studies. Jet Propulsion 26: 737-740. 1956.

4. Soloukhin, R. I. Shock waves and detonations in gases. Mono Book Corp., Baltimore, Maryland. 1966.

5. Low, G. M. Stability of compressible laminar boundary layer with internal heat sources and sinks. Journal of the Aeronautical Sciences 22: 329-336. 1955.

6. Jack, J. R., Wisniewski, R. J. and Diaconis, N. S. Effects of extreme surface cooling on boundary-layer transition. U.S. National Advisory Committee for Aeronautics Technical Note 4094. 1957.

7. Sichel, M. and David, T. S. Transfer behind detonations in H_2-O_2 mixtures. American Institute of Aeronautics and Astronautics Journal 4: 1089-1090. 1966.

8. Glass, I. I. and Hall, J. G. Shock tubes. Handbook of Supersonic Aerodynamics. Vol. 6, Section 18. U.S. Bureau of Naval Weapons NAVORD Report 1488. 1959.

9. Bernstein, L. Notes on some experimental and theoretical results for the boundary layer development aft of the shock in a shock tube. Great Britain Aeronautical Research Council Current Paper 625. 1963.

10. Bernstein, L. Some measurements of shock-wave attenuation in channels of various cross-sections. Great Britain Aeronautical Research Council Reports and Memoranda 3321. 1963.

11. Hollyer, R. N., Jr. A study of attenuation in the shock tube. Unpublished Ph.D. thesis. Library, University of Michigan, Ann Arbor, Michigan. 1953.

12. Hollyer, R. N., Jr. Attenuation in the shock tube. I. Laminar flow. Journal of Applied Physics 27: 254-261. 1956.

13. Mirels, H. Laminar boundary layer behind shock advancing into stationary fluid. U.S. National Advisory Committee for Aeronautics Technical Note 3401. 1955.

14. Mirels, H. Boundary layer behind shock or thin expansion wave moving into stationary fluid. U.S. National Advisory Committee for Aeronautics Technical Note 3712. 1956.

15. Mirels, H. The wall boundary layer behind a moving shock wave. In Gortler, H., ed. Grenzschichtforschung (Boundary Layer Research). pp. 281-293. Springer Verlag, Berlin, Germany. 1958.

16. Schlichting, H. Boundary layer theory. 4th ed. McGraw-Hill Book Co., Inc., New York, New York. 1960.

17. Low, G. M. The compressible laminar boundary layer with heat transfer and small pressure gradient. U.S. National Advisory Committee for Aeronautics Technical Note 3028. 1953.

18. Bershader, D. and Allport, J. On the laminar boundary layer induced by a travelling shock wave. Princeton University Department of Physics Technical Report II-22. 1956.

19. Trimpi, R. L. and Cohen, N. B. An integral solution to the flat-plate laminar boundary-layer flow existing inside and after expansion waves and after shock waves moving into quiescent fluid with particular application to the complete shock-tube flow. U.S. National Advisory Committee for Aeronautics Technical Note 3944. 1957.

20. Duff, R. E. Laminar boundary layer development behind shock waves in argon. Physics of Fluids 1: 546-547. 1958.

21. Vidal, R. Model instrumentation techniques for heat transfer and force measurements in a hypersonic shock tunnel. Cornell Aeronautical Laboratory Report AD-917-A-1. 1956.

22. Martin, M. A. An experimental study of the boundary layer behind a moving plane shock wave. University of Toronto Institute of Aerophysics Report 47. 1957.

23. Gooderum, P. B. An experimental study of the turbulent boundary layer on a shock-tube wall. U.S. National Advisory Committee for Aeronautics Technical Note 4243. 1958.

24. Becker, E. Instationare Grenzschichten hinter Verdichtungsstossen und Expansionswellen. Zeitschrift fur Flugwissenschaften 7: 61-72. 1959.

25. Daiber, J. W. An optical boundary-layer probe. Journal of the Aerospace Sciences 27: 836-840. 1960.

26. Chen, C. J. and Emrich, R. J. Investigation of the shock-tube boundary layer by a tracer method. Physics of Fluids 6: 1-9. 1963.

27. Gion, E. J. Measured velocity profiles in the laminar boundary layer behind a shock. Physics of Fluids 8: 546-547. 1965.

28. Mirels, H. and Hamman, J. Laminar boundary layer behind strong shock moving with nonuniform velocity. Physics of Fluids 5: 91-96. 1962.

29. Bertin, J. J. Analysis of test times and boundary layer induced property variations in a circular shock tube. U.S. National Aeronautics and Space Administration Technical Note D-3759. 1967.

30. Roshko, A. On flow duration in low pressure shock tubes. Physics of Fluids 3: 835-842. 1960.

31. Sandborn, V. A. Measurements of flow duration in a low-pressure shock tube. National Aeronautics and Space Administration Technical Note D-1218. 1962.

32. Hartunian, R. A., Russo, A. L. and Marrone, P. V. Boundary-layer transition and heat transfer in shock tubes. Journal of the Aerospace Sciences 27: 587-594. 1960.

33. Kurzrock, J. W. and Mates, R. E. Exact numerical solutions of the time-dependent compressible navier-stokes equation. American Institute of Aeronautics and Astronautics Paper 66-30. 1966.

34. Breeze, J. C. and Ferriso, C. C. Duration of laminar flow in a shock wave boundary layer. Physics of Fluids 7: 1071-1073. 1964.

35. Van Driest, E. R. and Boison, J. C. Experiments on boundary-layer transition at supersonic speeds. Journal of the Aeronautical Sciences 24: 885-900. 1957.

36. Higgins, R. W. and Pappas, C. C. An experimental investigation of the effect of surface heating on boundary-layer transition on a flat plate in supersonic flow. U.S. National Advisory Committee for Aeronautics Technical Note 2351. 1951.

37. Kline, S. J. and Shapiro, A. H. Experimental investigation of the effects of cooling on friction and on boundary-layer transition for low-speed gas flow at the entry of a tube. U.S. National Advisory Committee for Aeronautics Technical Note 3048. 1953.

38. Stetson, K. F. Boundary layer transition on blunt bodies with highly cooled boundary layers. Journal of the Aerospace Sciences 27: 81-91. 1960.

39. Ostrach, S. and Thornton, P. R. Stability of compressible boundary layers induced by a moving wave. Journal of the Aerospace Sciences 29: 289-296. 1962.

40. Sheetz, N. W., Jr. Free-flight boundary layer transition investigations at hypersonic speeds. American Institute of Aeronautics and Astronautics Paper 65.127. 1965.

41. Rumsey, C. B. and Lee, D. B. Measurements of aerodynamic heat transfer and boundary layer transition on a 10° cone in free flight at supersonic Mach numbers up to 5.9. National Aeronautics and Space Administration Technical Note D-745. 1961.

42. Brinich, P. F. Recovery temperature, transition and heat transfer measurements at Mach 5. National Aeronautics and Space Administration Technical Note D-1047. 1961.

43. Deem, R. E. and Murphy, J. S. Flat plate boundary layer transition at hypersonic speeds. American Institute of Aeronautics and Astronautics Paper 65-128. 1965.

44. Richards, B. E. and Stollery, J. L. Transition reversal on a flat plate at hypersonic speeds. North Atlantic Treaty Organization, Advisory Group for Aerospace Research and Development AGARDograph 97. Recent Developments in Boundary Layer Research, Part 1: pp. 477-501. 1965.

45. Wisniewski, R. J. and Jack, J. R. Recent studies on the effect of cooling on boundary-layer transition at Mach 4. Journal of the Aerospace Sciences 28: 250. 1961.

46. Reshotko, E. Transition reversal and Tollmien-Schlichting instability. Physics of Fluids 6: 335-342. 1963.

47. Belles, F. E. and Lauver, M. R. Origin of OH chemiluminescence during the induction period of the H_2-O_2 reaction behind shock waves. Journal of Chemical Physics 40:415-422. 1964.

48. Hall, J. L. Shock tube investigation of heat transfer in two-dimensional laminar separated flow behind a backward-facing step. Unpublished M.S. thesis. Library, Iowa State University of Science and Technology, Ames, Iowa. 1963.

49. Henshall, B. D. and Schultz, D. L. Some notes on the use of resistance thermometers for measurement of heat-transfer rates in shock tubes. Great Britain Aeronautical Research Council Current Paper 408. 1959.

50. Taylor, B. W. Development of a thin film heat-transfer gauge for shock tube flows. University of Toronto, Canada, Institute of Aerophysics Technical Note 27. 1959.

51. Belles, F. E. Detonability and chemical kinetics: prediction of limites of detonability of hydrogen. Symposium (International) on Combustion 7: 745-751. 1959.

52. Brokaw, R. S. Analytic solutions to the ignition kinetics of the hydrogen-oxygen reaction. Symposium (International) on Combustion 10: 269-278. 1965.

53. Lewis, B. and von Elbe, G. Combustion, flames and explosions of gases. 2nd ed. Academic Press, Inc., New York, New York. 1961.

54. Belles, F. E. and Lauver, M. R. Effects of concentration and vibrational relaxation on induction period of hydrogen-oxygen reaction. National Aeronautics and Space Administration Technical Note D-2540. 1964.

55. Cook, W. J. and Felderman, E. J. Reduction of data from thin-film heat-transfer gages: a concise numerical technique. American Institute of Aeronautics and Astronautics Journal 4: 561-562. 1966.

56. Svehla, R. A. Thermodynamic and transport properties for the hydrogen-oxygen system. National Aeronautics and Space Administration Special Publication 3011. 1964.

57. Zeleznik, F. J. and Gordon, S. A general IBM 704 or 7090 computer program for computation of chemical equilibrium compositions, rocket performance, and Chapman-Jouguet detonations. National Aeronautics and Space Administration Technical Note D-1454. 1962.

58. Markstein, G. H. Graphical computation of shock and detonation waves in real gases. ARS (American Rocket Society) Journal 29: 588-590. 1959.

59. Bernstein, L. Tabulated solutions of the equilibrium gas properties behind the incident and reflected normal shock wave in a shock tube; I-nitrogen; II-oxygen. Great Britain Aeronautical Research Council Current Paper 626. 1963.

60. Schott, G. L., and Kinsey, J. L. Kinetic studies of hydroxyl radicals in shock waves. II. Induction times in the hydrogen-oxygen reaction. Journal of Chemical Physics 29: 1177-1182. 1958.

61. McBride, B. J., Heimel, S., Ehlers, J. G. and Gordon S. Thermodynamic properties to 6000°K for 210 substances involving the first 18 elements. National Aeronautics and Space Administration Special Publication 3001. 1963.

62. Kaufman, F. and DelGreco, F. P. Fast reactions of OH radicals. Symposium (International) on Combustion 9: 659-666. 1963.

63. Millikan, R. C. and White, D. R. Systematics of vibrational relaxation. Journal of Chemical Physics 39: 3209-3213. 1963.

64. White, D. R. and Millikan, R. C. Oxygen vibrational relaxation in O_2-H_2 mixtures. Journal of Chemical Physics 39: 2107-2108. 1963.

65. Asaba, T., Gardiner, W. C., Jr., and Stubbeman, R. F. Shock-tube study of the hydrogen-oxygen reaction. Symposium (International) on Combustion 10: 295-302. 1965.

66. White, D. R. and Moore, G. E. Structure of gaseous detonation. IV. Induction zone studies in H_2-O_2 and CO-O_2 mixtures. Symposium (International) on Combustion 10: 785-795. 1965.

67. Shepherd, D. G. Elements of fluid mechanics. Harcourt, Brace and World, Inc., New York, New York. 1965.

68. Snedecor, G. W. Statistical methods. 5th ed. The Iowa State University Press, Ames, Iowa. 1956.

69. Bartee, E. M. Statistical methods in engineering experiments. Charles E. Merrill Book, Inc., Columbus, Ohio. 1966.

70. Knudsen, J. G. and Katz, D. L. Fluid dynamics and heat transfer. McGraw-Hill Book Company, Inc., New York, New York. 1958.

71. Eckert, E. R. G. Survey of boundary layer heat transfer at high velocities and high temperatures. U.S. Air Research and Development Center Technical Report 59-624. 1960.

72. Fillo, A. Approximate solution to the flat plate thermometer problem. American Institute of Aeronautics and Astronautics Journal 4: 1876. 1966.

73. Kline, S. J. and McClintock, F. Describing uncertainty in single sample experiments. Mechanical Engineering 75: 3-8. 1953.

74. Beers, Y. Introduction to the theory of errors. 2nd ed. Addison-Wesley Publishing Company, Inc., Reading, Massachusetts. 1962.

75. Neville, A. M. and Kennedy, J. B. Basic statistical methods for Engineers and Scientists. International Textbook Company, Scranton, Pennsylvania. 1964.

76. Young, H. D. Statistical treatment of data. McGraw-Hill Book Company, Inc., New York, New York. 1962.

77. Skinner, G. T. A new method of calibrating thin-film gauge backing materials. Cornell Aeronautical Laboratory Report CAL-105. 1962.

78. Bogdan, L. High-temperature, thin-film resistance thermometers for heat transfer measurement. Cornell Aeronautical Laboratory Report HM-1510-Y-6. 1963.

79. Somers, L. M. The variation of $(k\ \rho\ c)^{\frac{1}{2}}$ with temperature in "pyrex". Cornell Aeronautical Laboratory Report CAL-106. 1961.

80. Sokolnikoff, I. S. and Redheffer, R. M. Mathematics of physics and modern engineering. McGraw-Hill Book Company, Inc., New York, New York. 1958.

APPENDIX A: TABULATED DATA

Table 7. Flow properties for 100% N_2

Run Code	P_1 Torr	T_1 °K	M_s	P_{21}	T_{21}	μ_2 x 10^6	k_2 x 10^6	Pr_2
1001	50	300	3.695	15.90	3.457	409.6	164.9	0.695
1002	50	300	3.787	16.72	3.576	418.6	169.6	0.695
751	50	300	3.783	16.69	3.571	418.2	169.9	0.695
752	50	300	3.703	15.97	3.467	410.4	165.3	0.695
501	50	302	3.447	13.77	3.159	386.6	153.3	0.695
303	35	304	3.521	14.36	3.265	394.9	157.4	0.695
503	35	300	3.893	17.70	3.715	428.7	175.0	0.695
504	35	300	3.894	17.71	3.717	428.9	175.1	0.695
753	35	300	4.077	19.45	3.966	446.6	184.7	0.695
754	35	300	3.998	18.69	3.858	439.0	180.5	0.695
1003	35	305	3.975	18.41	3.866	439.6	180.8	0.695
1004	35	305	3.848	17.22	3.694	427.2	174.2	0.695
1005	20	305	4.524	24.00	4.662	495.9	210.2	0.695
1006	20	305	4.594	24.76	4.769	503.2	213.9	0.695
755	20	305	4.587	24.68	4.758	502.5	213.6	0.695
756	20	305	4.579	24.59	4.745	501.6	213.1	0.695
505	20	304	4.315	21.79	4.339	473.3	198.5	0.695
506	20	304	4.258	21.21	4.257	467.5	195.5	0.695
507	20	300	4.349	22.21	4.350	474.1	199.0	0.695
305	20	299	3.755	16.45	3.527	414.9	167.7	0.695
306	20	299	3.922	17.98	3.748	431.1	176.3	0.695
307	10	301	4.463	23.41	4.529	486.7	205.4	0.695
308	10	301	4.390	22.63	4.422	479.1	201.5	0.695
508	10	301	4.609	25.00	4.750	501.9	213.3	0.695
509	10	301	4.634	25.27	4.787	504.5	214.6	0.695
757	10	302	4.934	28.71	5.271	537.6	231.6	0.694
1007	10	302	4.865	27.90	5.160	530.0	227.7	0.694
1008	10	302	4.954	28.96	5.305	539.9	232.8	0.694
1009	5	302	5.521	36.13	6.267	604.8	266.2	0.693
1010	5	302	5.452	35.26	6.147	596.8	262.0	0.693
759	5	301	5.540	36.41	6.286	606.1	266.8	0.693
510	5	300	5.257	32.73	5.781	572.3	249.4	0.694
511	5	300	5.287	33.12	5.832	575.7	251.2	0.694
309	5	300	5.015	29.73	5.379	545.0	235.4	0.694
310	5	300	4.958	29.04	5.286	538.7	232.1	0.694

Table 8. Flow properties for 4.0% H_2 in N_2

Run Code	P_1 Torr	T_1 °K	M_s	P_{21}	T_{21}	μ_2 x 10^6	k_2 x 10^6	Pr_2
1001	50	297	3.887	17.84	3.579	417.7	186.6	0.653
1002	50	297	3.739	16.49	3.384	403.1	178.4	0.653
752	50	298	3.894	17.89	3.596	419.0	187.3	0.653
753	50	298	3.711	16.23	3.355	400.9	177.1	0.653
501	50	298	3.455	14.05	3.035	375.8	163.5	0.653
502	50	298	3.485	14.30	3.072	378.7	165.1	0.653
503	35	298	3.632	15.54	3.255	393.2	172.9	0.653
504	35	299	3.921	18.13	3.640	422.3	189.1	0.653
754	35	299	3.943	18.34	3.670	424.5	190.4	0.653
755	35	299	3.960	18.49	3.691	426.0	191.3	0.653
1003	35	299	3.867	17.63	3.568	417.0	186.1	0.653
1004	35	299	4.099	19.84	3.884	439.8	136.6	0.651
1005	35	299	4.422	23.14	4.347	472.9	218.4	0.652
1006	20	299	4.537	24.39	4.520	485.0	225.5	0.652
756	20	299	4.544	24.46	4.531	485.8	225.9	0.652
757	20	299	4.492	23.89	4.452	480.3	222.7	0.652
505	20	299	4.163	20.47	3.973	446.1	202.9	0.653
506	20	299	4.130	20.14	3.926	442.8	201.0	0.653
305	20	299	3.808	17.09	3.490	411.1	182.8	0.653
306	20	299	3.762	16.68	3.430	406.6	180.3	0.653
307	10	299	4.388	22.78	4.297	469.3	216.3	0.652
507	10	299	5.040	30.19	5.309	539.0	258.7	0.647
508	10	299	4.880	28.27	5.050	521.5	247.2	0.650
758	10	299	5.022	29.97	5.280	537.1	257.4	0.648
1007	10	299	5.003	29.75	5.249	535.0	256.0	0.648
1008	10	299	4.917	28.72	5.111	525.6	249.9	0.649
1009	5	299	5.107	31.02	5.420	546.5	263.7	0.646
1010	5	299	5.225	32.49	5.617	559.7	272.8	0.643
760	5	294	5.595	37.45	6.176	596.7	303.4	0.628
761	5	294	5.277	33.25	5.635	560.9	273.6	0.643
509	5	295	5.061	30.52	5.291	537.8	257.9	0.647
510	5	295	4.973	29.46	5.150	528.2	251.6	0.649
309	5	296	4.618	25.33	4.610	491.3	229.1	0.651

Table 9. Flow properties for 8.2% H_2 in N_2

Run Code	P_1 Torr	T_1 °K	M_s	P_{21}	T_{21}	μ_2 x 10^6	k_2 x 10^6	Pr_2
1001	50	296	3.589	15.39	3.069	377.5	181.2	0.616
1002	50	296	3.708	16.40	3.221	389.4	188.3	0.616
751	50	296	3.550	15.04	3.020	373.7	179.0	0.616
752	50	296	3.644	15.85	3.139	383.0	184.5	0.616
503	35	297	3.687	16.21	3.201	387.8	187.3	0.616
504	35	297	3.622	15.64	3.118	381.4	183.5	0.616
753	35	297	3.776	17.00	3.317	396.4	192.7	0.616
754	35	297	3.926	18.38	3.517	411.8	201.9	0.616
1003	35	298	3.932	18.42	3.533	412.9	202.6	0.616
1004	35	298	3.839	17.56	3.409	403.7	196.9	0.616
1005	20	298	4.323	22.28	4.083	451.9	227.7	0.615
1006	20	298	4.260	21.63	3.991	445.5	223.6	0.615
755	20	298	4.337	22.43	4.103	453.4	228.7	0.615
756	20	298	4.311	22.16	4.066	450.7	227.0	0.615
505	20	298	4.107	20.10	3.775	430.4	213.7	0.615
506	20	299	4.044	19.47	3.695	424.7	210.1	0.615
305	20	299	3.751	16.75	3.299	395.4	191.9	0.616
306	20	299	3.740	16.65	3.285	394.3	191.2	0.616
307	10	299	4.231	21.33	3.959	443.2	222.2	0.615
308	10	299	4.234	21.36	3.964	443.5	222.3	0.615
507	10	299	4.437	23.46	4.261	464.6	235.8	0.614
508	10	299	4.325	22.28	4.095	452.8	228.3	0.615
757	10	300	4.919	28.86	5.021	517.4	270.0	0.611
758	10	300	4.924	28.93	5.029	518.0	270.5	0.611
1008	10	300	5.164	31.84	5.424	544.8	291.1	0.606
1010	5	300	5.438	35.35	5.892	575.9	317.6	0.597
759	5	300	5.322	33.85	5.693	562.8	306.1	0.601
760	5	300	5.346	34.15	5.733	565.4	308.3	0.600
511	5	301	5.076	30.74	5.291	535.8	284.0	0.608
309	5	301	4.769	27.10	4.794	501.9	259.8	0.613
310	5	301	4.702	26.34	4.688	494.6	255.1	0.613

Table 10. Flow properties for 12.3% H_2 in N_2

Run Code	P_1 Torr	T_1 °K	M_s	P_{21}	T_{21}	μ_2 x 10^6	k_2 x 10^6	Pr_2
1001	50	297	3.835	17.70	3.279	391.8	208.1	0.583
1002	50	297	3.719	16.79	3.038	373.0	195.9	0.583
751	50	298	3.759	17.00	3.186	384.6	203.4	0.583
752	50	298	3.907	18.36	3.385	399.8	213.5	0.583
503	35	301	3.731	16.73	3.172	383.5	202.7	0.583
504	35	301	3.802	17.36	3.266	390.8	207.5	0.583
753	35	300	3.840	17.71	3.309	394.0	209.7	0.583
754	35	300	3.940	18.64	3.446	404.4	216.6	0.583
1003	35	300	3.741	16.82	3.177	383.9	202.9	0.583
1004	35	300	3.874	18.03	3.355	397.6	212.0	0.583
1005	20	300	4.427	23.50	4.145	454.4	252.3	0.582
1006	20	300	4.389	23.10	4.088	450.3	249.4	0.582
755	20	299	4.333	22.54	3.996	443.7	244.8	0.582
756	20	299	4.289	22.08	3.932	439.3	241.5	0.582
505	20	299	3.986	19.09	3.501	408.4	219.4	0.583
506	20	299	4.144	20.62	3.723	424.6	230.8	0.583
306	20	299	3.617	15.76	3.008	370.9	194.4	0.583
307	10	296	4.706	26.62	4.529	481.5	271.6	0.581
308	10	297	4.630	25.75	4.422	474.0	266.2	0.581
507	10	298	4.564	25.01	4.332	467.7	261.7	0.581
508	10	298	4.705	26.58	4.551	483.1	272.7	0.581
758	10	299	4.978	29.73	5.000	514.0	295.0	0.579
1007	10	298	4.838	28.10	4.763	497.7	283.2	0.580
1008	10	298	4.803	27.70	4.705	493.8	280.3	0.580
1009	5	298	5.315	33.94	5.551	550.9	327.7	0.570
509	5	298	5.015	30.19	5.047	517.2	297.7	0.578
510	5	298	5.088	31.09	5.169	525.4	304.6	0.576
309	5	298	4.988	29.87	5.003	514.2	295.2	0.579
310	5	298	4.901	28.83	4.863	504.6	288.2	0.579

Table 11. Flow properties for 3.1% H_2 in air

Run Code	P_1 Torr	T_1 °K	M_s	P_{21}	T_{21}	μ_2 x 10^6	k_2 x 10^6	Pr_2
1001	50	298	3.750	16.47	3.522	431.9	174.8	0.694
1002	50	298	3.625	15.36	3.363	419.2	168.2	0.694
751	50	299	3.795	16.31	3.587	436.9	177.4	0.694
752	50	299	3.779	16.71	3.566	435.3	176.6	0.694
501	50	300	3.510	14.35	3.234	408.7	162.9	0.694
502	50	300	3.521	14.44	3.247	409.7	163.4	0.694
503	35	300	3.742	16.37	3.526	432.2	175.0	0.694
504	35	300	3.873	17.55	3.699	445.6	182.0	0.694
753	35	301	4.148	20.13	4.071	473.3	196.9	0.693
754	35	301	3.979	18.55	3.849	456.9	188.0	0.693
1003	35	301	3.910	17.90	3.756	449.9	184.3	0.695
1004	35	301	4.023	18.98	3.909	461.3	190.4	0.693
1005	20	301	4.583	24.79	4.714	519.5	223.3	0.692
1006	20	301	4.577	24.73	4.705	518.9	222.9	0.692
755	20	302	4.423	23.04	4.487	503.5	213.9	0.692
756	20	302	4.476	23.61	4.565	509.1	217.2	0.692
505	20	302	4.532	24.21	4.648	514.9	220.6	0.692
511	20	303	4.268	21.39	4.268	488.0	205.1	0.693
506	20	303	4.174	20.43	4.135	478.1	199.5	0.693
305	20	303	3.990	18.63	3.879	459.1	189.2	0.693
306	20	303	3.883	17.62	3.733	448.2	183.4	0.694
307	10	303	4.227	20.97	4.211	483.7	202.7	0.693
308	10	303	4.207	20.78	4.183	481.6	201.5	0.693
507	10	303	4.641	25.41	4.824	527.1	227.8	0.692
508	10	303	4.483	23.66	4.585	510.5	218.0	0.692
757	10	303	4.928	28.74	5.271	557.7	247.1	0.690
758	10	303	4.861	27.94	5.164	550.4	242.3	0.691
1007	10	303	4.857	27.90	5.159	550.0	242.1	0.691
1008	10	303	4.755	26.70	4.999	538.9	235.0	0.691
1009	5	304	5.559	36.80	6.316	627.9	303.5	0.680
1010	5	304	5.368	34.25	6.000	607.0	282.0	0.686
759	5	304	5.348	33.98	5.966	604.8	280.3	0.686
509	5	304	5.089	30.68	5.540	576.1	259.6	0.689
510	5	304	5.010	29.71	5.413	567.5	253.7	0.690
309	5	304	4.765	26.80	5.026	540.8	236.1	0.691
310	5	304	4.661	25.6	4.866	529.9	229.5	0.692

Table 12. Flow properties for 7.0% H_2 in air

Run Code	P_1 Torr	T_1 °K	M_s	P_{21}	T_{21}	μ_2 x 10^6	k_2 x 10^6	Pr_2
752	50	297	3.628	15.34	3.385	418.0	172.9	0.694
501	50	297	3.522	14.43	3.252	407.1	167.1	0.694
503	35	298	3.884	17.63	3.723	444.5	187.4	0.693
504	35	298	3.719	16.13	3.508	427.7	178.2	0.694
753	35	298	3.934	18.11	3.792	449.7	190.3	0.693
754	35	298	3.964	18.39	3.833	452.7	192.0	0.693
1003	35	298	4.414	22.93	4.467	499.8	219.1	0.691
1004	35	298	4.009	18.82	3.894	457.2	194.6	0.693
1005	20	298	4.722	26.33	4.928	532.9	238.9	0.689
1006	20	298	4.539	24.28	4.651	513.2	227.0	0.690
755	20	298	4.627	25.26	4.784	522.7	232.7	0.690
756	20	298	4.530	24.19	4.638	512.3	226.4	0.690
505	20	298	4.404	22.82	4.452	498.7	218.4	0.691
506	20	298	4.337	22.11	4.354	491.6	214.2	0.691
305	20	298	4.102	19.73	4.022	466.6	199.9	0.692
306	20	298	4.127	19.97	4.057	469.3	201.4	0.692
307	10	298	4.420	22.99	4.476	500.5	219.5	0.691
308	10	298	4.498	23.84	4.591	508.9	224.4	0.690
507	10	298	4.693	26.01	4.884	529.8	237.0	0.690
508	10	298	4.965	29.19	5.305	559.2	256.9	0.688
757	10	298	4.946	28.97	5.276	557.3	255.4	0.688
758	10	298	4.558	24.49	4.680	515.3	228.2	0.690
1007	10	296	4.995	29.59	5.328	560.8	258.0	0.687
1008	10	296	4.954	29.10	5.264	556.4	254.8	0.688
1009	5	296	5.592	37.35	6.294	625.6	317.1	0.675
1010	5	296	5.417	34.97	6.008	606.5	294.6	0.682
759	5	297	5.360	34.20	5.928	601.3	289.0	0.683
760	5	297	5.431	35.14	6.045	609.0	297.3	0.681
509	5	298	5.430	35.11	6.058	609.9	298.2	0.681
510	5	298	5.103	30.90	5.525	574.3	268.2	0.686
309	5	298	4.951	29.03	5.284	557.8	255.9	0.688

Table 13. Flow properties for 11.0% H_2 in air

Run Code	P_1 Torr	T_1 °K	M_s	P_{21}	T_{21}	μ_2 x 10^6	k_2 x 10^6	Pr_2
1005	20	299	4.801	27.18	5.091	542.4	254.6	0.687
1006	20	299	4.501	23.79	4.636	510.0	233.4	0.689
755	20	299	4.612	25.01	4.801	521.9	241.0	0.689
756	20	299	4.657	25.52	4.870	526.8	244.1	0.688
506	20	300	4.609	24.97	4.808	522.4	241.3	0.689
507	20	300	4.449	23.21	4.569	505.1	230.4	0.689
305	20	300	4.080	19.43	4.037	465.3	206.2	0.692
306	20	300	3.868	17.41	3.746	443.4	193.2	0.693
307	10	301	4.503	23.78	4.659	511.7	234.5	0.689
308	10	301	4.515	23.92	4.678	513.0	235.3	0.689
508	10	302	4.828	27.44	5.167	547.8	258.6	0.687
509	10	302	4.916	28.48	5.307	557.6	266.0	0.686
757	10	302	4.882	28.07	5.252	553.8	263.1	0.686
1007	10	303	5.029	29.82	5.499	571.0	276.6	0.684
1008	10	303	5.099	30.68	5.614	578.9	283.1	0.683
1009	5	303	5.259	32.69	5.878	596.8	298.6	0.681
1010	5	303	5.214	32.12	5.803	591.8	294.2	0.681
759	5	295	5.475	35.69	6.125	613.5	316.5	0.676
760	5	295	5.532	36.48	6.219	619.9	325.0	0.672
510	5	296	5.019	29.83	5.397	563.9	271.0	0.685
309	5	297	4.955	29.03	5.308	557.7	266.1	0.686

Table 14. Flow properties for 15.0% H_2 in air

Run Code	P_1 Torr	T_1 °K	M_s	P_{21}	T_{21}	μ_2 x 10^6	k_2 x 10^6	Pr_2
1005	20	297	4.683	25.77	4.933	529.3	254.8	0.687
1006	20	297	4.732	26.32	5.009	534.6	258.5	0.686
755	20	297	4.422	22.90	4.538	500.7	235.8	0.689
756	20	297	4.513	23.88	4.674	510.7	242.4	0.688
505	20	298	4.319	21.80	4.395	490.0	228.9	0.689
305	20	298	4.230	20.88	4.266	480.3	222.7	0.690
306	20	298	4.253	21.12	4.299	482.9	224.4	0.690
307	10	298	4.566	24.44	4.765	517.2	246.7	0.688
308	10	298	4.460	23.29	4.605	505.6	239.0	0.688
507	10	298	4.789	26.97	5.109	541.9	264.0	0.686
508	10	298	4.797	27.06	5.121	542.7	264.6	0.685
757	10	298	4.970	29.11	5.393	562.0	280.2	0.683
758	10	298	4.932	28.65	5.333	557.8	276.7	0.684
1007	10	299	5.078	30.41	5.579	575.0	291.3	0.681
1008	10	299	5.113	30.84	5.636	579.0	294.7	0.681
1009	5	299	5.683	38.40	6.567	642.8	378.7	0.652
1010	5	299	5.461	35.35	6.207	618.2	337.9	0.669
759	5	299	5.472	35.49	6.224	619.4	339.7	0.668
760	5	299	5.503	35.91	6.275	622.9	345.0	0.666
509	5	299	5.333	33.65	5.997	603.8	317.8	0.676
510	5	299	5.325	33.55	5.984	602.9	316.9	0.676
309	5	299	4.905	28.31	5.302	555.6	274.9	0.684
310	5	299	4.784	26.89	5.113	542.1	264.2	0.686

Table 15. Transition data for 100% N_2

Run Code	GAGE 1			GAGE 2			GAGE 4		
	q_t	$(t_t)_q$	$(t_t)_T$	q_t	$(t_t)_q$	$(t_t)_T$	q_t	$(t_t)_q$	$(t_t)_T$
1001	23.4	19.6	19.6	25.5	21.1	18.4	27.1	20.7	22.1
1002	26.0	20.6	20.6	22.7	21.6	19.9	27.2	17.5	25.4
751	25.7	17.8	26.8	23.5	20.6	17.7	25.8	23.5	25.3
752	25.6	20.6	12.8	22.7	20.4	25.8	23.1	23.1	24.3
501	19.5	22.1	25.1	17.4	24.1	25.0	20.1	24.2	25.2
303	13.3	29.3	30.3	12.8	29.5	30.4	13.0	32.7	34.1
503	18.0	20.1	21.8	18.5	28.6	29.9	19.8	27.1	25.6
504	17.7	23.6	25.1	18.9	21.6	28.4	18.5	26.6	29.0
753	22.4	19.6	23.3	23.4	22.1	27.0	26.1	24.8	26.6
754	21.4	22.4	22.6	22.0	28.8	29.0	25.9	23.5	23.9
1003	21.4	21.7	23.2	21.6	24.6	25.4	25.3	23.9	25.3
1004	22.1	23.8	24.8	22.3	23.8	24.9	24.9	26.6	27.9
1005	21.5	33.4	35.3	23.0	28.4	30.2	25.1	34.0	29.4
1006	23.2	21.5	22.7	24.8	29.1	30.1	24.6	36.8	38.1
755	22.0	23.5	25.8	24.0	27.7	30.2	25.1	28.7	30.4
756	21.0	34.1	32.7	20.4	28.0	28.1	26.0	31.0	31.6
505	16.5	24.8	26.4	18.8	29.9	30.0	20.5	28.7	31.2
506	15.7	35.8	38.2	19.7	30.7	32.6	19.5	39.0	40.8
507	15.8	25.9	26.9	17.3	31.3	31.8	18.1	32.7	33.9
305	9.3	58.7	60.0	12.9	30.7	31.9	12.9	32.3	35.3
306	11.3	35.9	34.8	13.0	37.0	41.7	12.8	36.3	33.2
307	9.5	44.6	49.4	10.5	62.5	60.5	8.4	98.5	107.7
308	8.2	50.3	45.6	10.6	52.3	58.7	9.1	82.2	90.3
508	14.0	35.6	39.2	15.7	46.6	48.6	13.5	68.8	68.9
509	12.7	45.8	48.1	15.1	55.7	56.3	12.2	82.9	91.6
757	16.0	36.6	37.6	18.5	45.8	48.7	15.6	74.2	76.4
1007	17.2	33.7	36.4	18.9	49.3	55.0	15.0	72.2	73.7
1008	16.5	37.4	35.2	18.4	50.2	50.8	15.6	72.7	74.4
1009	14.7	57.5	61.4	18.4	42.1	40.7	14.5	86.9	90.5
1010	10.7	69.1	71.9	15.9	45.6	44.9	14.4	84.0	85.9
759	13.5	57.2	57.9	18.7	53.4	49.0	13.8	91.6	92.3
510	9.4	75.5	87.9	14.2	70.7	69.4	11.3	113.6	124.0
511	11.8	56.0	64.5	14.0	60.3	55.3	11.9	83.5	89.2
309	7.7	82.7	78.2	10.0	75.0	77.3	8.3	112.5	113.3
310	6.8	81.6	92.7	10.0	75.0	78.7	8.8	87.4	119.6

Table 16. Transition data for 4.0% H_2 in N_2

Run Code	GAGE 1			GAGE 2			GAGE 4		
	q_t	$(t_t)_q$	$(t_t)_T$	q_t	$(t_t)_q$	$(t_t)_T$	q_t	$(t_t)_q$	$(t_t)_T$
1001	26.1	32.0	31.9	26.7	21.4	23.8	27.6	22.5	22.5
1002	24.0	30.6	35.1	25.4	23.4	26.6	28.5	22.5	24.7
752	23.3	28.6	30.8	24.6	20.9	20.2	26.2	21.5	22.4
753	24.4	29.6	26.6	25.3	20.9	21.7	32.6	18.3	15.3
501	16.8	36.8	36.8	19.0	24.0	25.1	20.2	24.1	24.9
502	18.4	32.7	27.6	19.4	26.2	28.4	21.1	24.3	25.6
503	14.7	37.2	37.2	18.7	28.2	28.6	19.0	28.2	28.8
504	14.4	31.0	32.8	17.3	26.4	21.8	18.9	27.0	28.9
754	18.1	31.8	31.8	23.1	22.6	24.5	24.9	25.7	26.5
755	18.7	29.6	30.4	23.7	22.4	21.7	25.1	25.4	27.6
1003	19.9	31.7	30.9	23.6	24.7	25.2	25.8	24.8	21.1
1004	20.7	33.6	34.0	25.1	23.4	23.7	27.1	24.9	23.1
1005	19.6	30.1	35.8	25.7	23.3	24.5	24.4	28.5	29.3
1006	19.5	30.5	31.2	23.7	29.9	24.0	25.6	27.6	29.5
756	18.9	36.0	35.4	23.3	25.7	28.2	23.3	28.5	30.1
757	19.8	32.4	32.2	23.0	22.4	26.2	23.5	30.8	30.7
505	14.6	37.6	39.8	18.4	27.9	29.0	17.9	34.5	34.5
506	14.1	30.5	30.6	17.8	29.3	31.9	17.5	33.5	34.2
305	9.3	43.4	43.8	13.2	37.3	37.4	14.2	36.5	31.2
306	9.2	43.5	43.6	13.2	37.4	38.2	11.5	48.8	52.3
307	10.4	42.2	45.2	12.3	56.7	58.4	9.2	86.8	91.4
507	14.6	40.8	43.0	15.3	54.2	54.3	15.4	63.4	65.2
508	14.9	32.8	36.4	16.7	55.3	54.5	13.0	71.0	75.9
758	18.6	36.9	38.1	20.9	52.2	53.8	16.8	66.2	66.3
1007	19.3	40.4	43.0	20.0	42.5	44.8	14.9	70.6	70.6
1008	18.5	41.1	41.1	20.2	47.0	49.9	18.2	69.2	72.1
1009	12.3	60.2	59.5	15.0	68.7	69.5	13.2	100.7	103.1
1010	13.9	51.7	54.1	19.5	58.9	60.7	16.0	81.5	85.3
760	14.8	44.6	43.3	18.7	51.9	54.6	16.2	68.2	72.9
761	13.1	54.5	56.5	16.6	75.0	74.9	15.1	77.8	78.0
509	9.1	73.9	77.0	12.8	72.1	72.3	11.8	89.3	93.1
510	11.4	59.1	63.0	12.3	72.4	72.4	12.3	92.0	94.9
309	8.0	65.3	76.2	9.4	94.0	93.8	8.2	98.4	100.0

Table 17. Transition data for 8.2% H_2 in N_2

Run Code	GAGE 1			GAGE 2			GAGE 4		
	q_t	$(t_t)_q$	$(t_t)_T$	q_t	$(t_t)_q$	$(t_t)_T$	q_t	$(t_t)_q$	$(t_t)_T$
1001	24.5	34.5	35.1	22.2	24.4	23.4	29.4	19.5	19.9
1002	27.8	30.6	32.4	23.6	20.2	20.6	29.9	20.7	22.3
751	25.6	31.2	33.0	23.7	20.8	22.4	28.8	19.6	20.8
752	24.9	30.3	31.4	21.8	21.4	20.9	28.6	19.5	21.2
503	13.8	34.4	35.7	15.4	27.4	28.9	19.2	30.6	31.9
504	14.7	36.4	36.4	16.0	24.7	26.5	20.1	26.0	27.6
753	18.0	30.1	30.3	20.9	22.2	23.4	23.6	22.3	24.1
754	19.0	30.5	31.4	20.7	20.4	20.3	27.2	23.7	24.9
1003	20.1	32.4	32.8	20.9	23.3	24.4	25.9	24.6	26.1
1004	19.0	31.1	34.7	21.2	22.2	23.5	25.7	23.2	28.3
1005	18.2	33.9	35.2	19.4	31.9	35.0	22.1	35.8	38.3
1006	17.4	34.3	35.3	19.0	30.6	32.6	19.0	42.8	45.2
755	18.2	31.5	33.3	19.7	29.9	32.6	21.0	37.5	38.0
756	18.3	35.5	36.2	19.0	30.4	33.9	21.4	34.8	38.1
505	13.9	35.5	35.5	15.6	34.7	36.5	15.2	44.9	43.9
506	14.0	37.8	39.4	14.9	34.1	36.2	16.5	42.5	45.4
305	9.2	43.0	43.1	11.5	36.9	40.7	11.4	59.1	49.4
306	9.8	41.0	41.1	10.2	40.1	41.4	11.0	48.6	60.4
307	10.1	41.7	42.4	10.4	58.9	60.7	8.9	86.3	90.9
308	10.1	49.4	50.2	10.5	69.0	74.1	9.2	86.0	89.7
507	14.7	43.7	43.7	15.2	51.0	50.2	13.5	76.0	77.0
508	14.5	42.1	42.1	14.3	46.7	40.4	13.0	78.0	77.9
757	18.3	34.7	35.3	17.6	44.1	47.1	17.4	61.0	63.3
758	18.2	35.5	38.1	17.9	51.9	52.6	17.4	63.0	63.9
1008	18.9	41.7	43.3	19.0	44.7	48.2	17.2	63.5	65.0
1010	15.5	48.7	48.7	18.1	54.0	56.3	16.5	75.9	76.3
759	15.5	45.2	45.4	16.5	53.7	54.2	15.2	79.2	83.6
760	17.1	36.4	35.4	18.0	51.3	51.3	17.0	61.5	61.2
511	11.9	48.8	48.8	13.0	53.1	54.4	11.7	77.0	77.7
309	7.8	78.2	78.5	9.0	84.1	84.6	9.1	93.3	93.0
310	8.1	76.4	76.5	9.0	66.6	76.5	8.9	94.3	93.3

Table 18. Transition data for 12.3% H_2 in N_2

Run Code	GAGE 1			GAGE 2			GAGE 4		
	q_t	$(t_t)_q$	$(t_t)_T$	q_t	$(t_t)_q$	$(t_t)_T$	q_t	$(t_t)_q$	$(t_t)_T$
1001	22.3	28.3	28.7	19.8	22.3	24.9	28.0	21.2	22.0
1002	26.1	31.4	32.7	20.2	24.9	26.2	27.5	21.2	21.2
751	25.6	30.4	30.4	21.6	23.5	24.0	27.4	18.5	18.4
752	24.9	29.3	29.5	21.1	18.2	25.0	27.6	23.8	24.2
503	14.8	33.0	33.2	18.7	15.5	15.3	19.7	25.4	25.9
504	15.1	33.7	33.9	23.8	23.8	23.8	27.6	23.8	27.4
753	19.6	34.9	36.0	20.6	22.0	22.2	24.6	25.5	26.2
754	20.1	30.9	33.3	21.3	22.1	22.8	25.4	26.8	27.1
1003	20.8	31.3	31.3	21.3	16.2	16.0	25.7	24.4	25.6
1004	20.4	29.8	25.6	22.8	15.2	15.3	25.1	25.8	26.9
1005	19.6	33.2	33.2	21.8	21.8	21.7	21.6	51.1	51.7
1006	20.6	33.3	34.8	22.0	21.5	26.6	19.7	50.0	52.8
755	18.9	33.9	28.2	19.9	25.9	26.0	17.6	55.2	55.8
756	18.3	33.6	33.5	20.8	24.9	29.6	18.2	48.7	48.4
505	15.0	34.9	36.8	16.1	29.2	30.3	13.9	54.8	55.8
506	15.5	35.1	37.6	17.6	25.5	26.2	14.3	59.2	62.8
306	9.9	42.8	43.4	11.7	36.8	37.0	10.2	65.5	63.9
307	10.9	51.0	54.8	10.8	56.4	57.1	9.4	78.5	82.2
308	10.0	51.5	52.5	10.2	52.0	53.3	8.5	90.8	91.0
507	14.8	39.9	39.5	15.7	51.7	57.5	14.6	69.3	71.5
508	14.7	43.9	44.0	14.2	15.1	54.4	14.5	69.7	75.6
758	19.1	38.1	44.0	16.4	51.4	53.1	16.2	74.8	74.9
1007	19.7	30.8	30.9	17.0	53.1	52.2	15.8	69.5	69.7
1008	19.9	34.1	38.0	17.4	45.6	48.1	17.2	63.4	66.6
1009	14.5	47.5	47.7	15.7	53.1	52.6	14.9	77.8	78.3
509	10.5	63.2	64.1	11.8	73.8	77.3	12.0	92.8	93.4
510	13.0	42.8	42.9	13.9	56.9	57.5	12.4	88.7	90.3
309	9.8	69.4	69.8	9.2	60.1	60.4	9.4	86.0	86.5
310	9.1	59.2	61.4	8.8	72.4	73.0	8.7	90.7	91.7

Table 19. Transition and induction time data for 3.1% H_2 in air

		GAGE 1			GAGE 2			GAGE 4		
Run Code	Induction Time	q_t	$(t_t)_q$	$(t_t)_T$	q_t	$(t_t)_q$	$(t_t)_T$	q_t	$(t_t)_q$	$(t_t)_T$
1001	15.4	26.7	19.8	19.5	24.4	22.8	23.2	31.5	21.6	21.8
1002	23.0	31.0	16.0	21.7	24.1	24.6	24.7	32.1	22.4	23.0
751	13.0	30.7	13.7	21.5	25.3	24.5	25.2	30.4	22.7	23.2
752	13.6	30.6	11.1	19.8	27.4	22.2	24.6	32.3	21.9	24.6
501	32.0	22.4	19.8	21.7	21.1	24.7	26.1	22.2	24.7	24.9
502	30.8	23.3	17.5	18.2	23.2	24.8	27.4	26.5	24.5	22.4
503	21.9	21.7	25.1	25.2	26.0	26.8	26.9	22.6	24.1	26.9
504	14.8	21.3	26.3	26.5	22.3	25.0	24.7	22.6	28.4	28.5
753	7.0	29.8	20.2	22.7	29.4	26.7	29.1	30.8	25.7	25.8
754	10.7	28.8	18.2	19.3	29.5	22.6	27.3	28.5	25.9	26.2
1003	12.9	27.5	18.6	19.1	26.3	24.8	27.5	28.8	24.6	25.7
1004	9.5	27.8	23.9	25.9	27.3	25.7	27.4	29.8	25.6	26.2
1005	4.9	25.9	24.7	25.8	29.5	29.1	29.9	28.4	32.1	32.4
1006	4.9	26.6	27.9	29.5	26.8	26.6	28.7	29.8	29.3	30.8
755	6.6	23.3	29.9	31.6	29.4	29.1	30.2	28.7	34.6	35.0
756	5.9	28.5	20.4	21.1	27.7	28.8	28.9	23.5	36.7	36.6
505	5.3	20.8	36.5	39.5	26.7	28.9	33.2	23.7	32.5	33.6
511	9.2	20.3	34.7	33.5	23.8	31.6	32.1	25.3	30.6	31.4
506	11.5	22.2	32.6	35.6	23.3	30.7	32.1	25.3	35.5	31.4
305	18.3	15.5	29.8	30.1	16.8	28.6	30.8	18.6	29.8	33.7
306	24.5	15.1	28.3	19.0	16.7	29.6	32.1	18.0	28.6	29.3
307	21.8	12.6	36.6	34.0	14.2	59.7	65.8	11.4	69.3	71.7
308	22.8	13.0	50.7	51.2	14.5	55.2	76.4	11.4	97.9	100.7
507	9.2	18.3	43.5	49.4	18.1	51.5	56.2	16.8	72.0	72.1
508	12.5	18.3	31.8	30.0	19.0	43.2	45.8	15.6	75.2	72.2
757	5.5	20.1	45.8	44.0	23.3	48.8	49.2	19.3	74.1	73.8
758	6.2	22.0	34.5	35.9	24.5	44.6	47.8	18.1	70.6	70.9
1007	6.2	22.6	34.7	37.4	25.5	44.0	45.8	19.8	62.9	63.3
1008	7.4	22.3	41.2	44.2	26.5	49.7	50.1	20.4	64.9	60.5
1009	4.8	17.0	45.5	46.5	23.6	51.5	54.4	18.9	71.8	72.2
1010	6.1	20.4	40.3	42.4	24.1	46.7	50.0	19.5	72.5	72.9
759	6.3	16.3	57.6	58.6	23.2	51.7	56.3	18.9	65.9	72.5
509	9.2	14.9	44.2	44.5	19.2	55.0	57.2	14.8	79.5	77.5
510	10.5	10.3	81.5	88.2	16.0	74.3	78.0	12.7	95.0	95.6
309	15.7	10.0	72.0	72.2	12.7	69.7	82.5	9.5	105.7	105.7
310	18.9	10.8	48.8	49.4	12.5	65.3	67.7	10.5	95.2	94.5

Table 20. Transition and induction time data for 7.0% H_2 in air

Run Code	Induction Time	GAGE 1 q_t	GAGE 1 $(t_t)_q$	GAGE 1 $(t_t)_T$	GAGE 2 q_t	GAGE 2 $(t_t)_q$	GAGE 2 $(t_t)_T$	GAGE 4 q_t	GAGE 4 $(t_t)_q$	GAGE 4 $(t_t)_T$
752	16.2	26.3	28.3	27.7	35.9	17.9	18.0	38.0	28.3	28.3
501	23.8	21.9	29.5	30.6	22.3	15.0	15.2	29.6	22.6	25.1
503	5.9	15.8	37.7	35.7	17.5	29.2	30.5	23.9	36.2	31.1
504	10.1	16.3	44.3	47.6	18.2	27.2	29.5	28.0	28.2	29.1
753	8.7	24.2	41.7	10.2	32.2	15.0	13.9	36.1	42.0	40.2
754	8.0	23.7	40.7	41.6	31.9	27.6	29.6	33.0	35.7	36.4
1003	2.4	27.5	43.8	29.4	32.3	26.7	26.8	41.8	21.3	18.8
1004	7.0	28.3	34.4	35.2	43.3	22.8	19.8	38.4	27.3	28.7
1005	2.3	25.0	36.5	37.8	32.3	30.5	32.1	22.4	63.6	61.8
1006	3.5	26.2	35.3	36.2	33.5	30.8	34.4	23.1	63.2	62.0
755	2.9	24.7	35.3	35.4	32.2	32.0	34.7	22.7	62.5	65.6
756	3.5	24.2	36.2	35.3	28.6	36.2	37.3	64.0	22.0	63.9
505	4.7	19.4	40.4	41.7	28.8	38.0	35.2	17.7	73.9	74.3
506	5.5	19.6	41.1	43.7	27.3	33.2	34.8	20.0	74.0	77.2
305	10.0	15.2	42.5	32.6	20.9	41.1	43.4	14.6	86.4	89.8
306	9.4	15.0	41.5	42.4	21.5	45.3	49.4	13.9	87.7	87.3
307	9.8	15.2	44.3	44.1	15.6	64.0	65.3	14.2	92.5	94.3
308	8.3	14.8	50.2	50.2	16.6	64.2	63.7	13.5	87.0	90.2
507	5.5	19.2	53.5	56.1	21.4	59.5	62.8	16.7	90.6	95.0
508	3.3	20.7	54.3	55.4	22.6	54.4	54.8	16.7	82.4	88.0
757	3.4	23.4	57.4	60.4	25.1	54.3	54.9	20.0	77.7	76.9
758	7.3	20.7	49.5	49.4	23.5	58.5	61.4	20.2	75.7	67.0
1007	3.2	24.5	44.2	45.9	28.2	55.2	58.2	24.0	61.0	66.4
1008	3.5	23.2	44.9	46.6	27.0	49.7	52.1	21.5	76.5	74.6
1009	2.8	18.8	56.5	57.6	25.2	51.1	51.0	21.0	72.1	67.2
1010	3.6	18.0	56.7	58.7	22.9	61.0	59.6	13.7	89.9	92.3
759	3.8	18.6	51.7	50.3	22.6	59.3	61.4	19.2	77.4	72.7
760	3.5	17.4	75.7	76.0	21.9	65.0	63.5	20.2	70.5	69.9
509	3.4	11.3	90.5	90.2	15.9	91.3	93.5	14.5	105.5	107.2
510	5.7	15.5	64.7	73.5	19.5	69.7	61.4	16.0	86.5	88.6
309	7.4	10.3	102.2	102.3	15.9	59.9	68.5	12.1	93.4	92.8

Table 21. Transition and induction time data for 11.0% H_2 in air

Run Code	Induction Time	GAGE 1 q_t	GAGE 1 $(t_t)_q$	GAGE 1 $(t_t)_T$	GAGE 2 q_t	GAGE 2 $(t_t)_q$	GAGE 2 $(t_t)_T$	GAGE 4 q_t	GAGE 4 $(t_t)_q$	GAGE 4 $(t_t)_T$
1005	1.5	30.0	31.7	31.4	27.3	42.4	44.8	25.1	81.5	81.8
1006	2.9	30.2	37.0	38.3	29.8	44.6	46.7	27.3	76.6	77.4
755	2.3	26.4	39.7	40.1	31.9	40.4	41.1	25.6	72.5	72.5
756	2.0	27.8	37.3	37.3	31.2	42.0	42.1	27.2	77.6	80.1
506	2.2	26.2	32.4	33.3	24.5	49.3	55.4	22.8	83.2	26.5
507	3.2	24.8	37.2	36.8	26.3	42.7	42.8	24.6	71.1	72.8
305	8.2	13.9	83.7	82.8	17.0	71.4	72.6	15.3	115.5	113.8
306	15.1	19.2	40.0	40.6	18.6	45.1	45.0	14.2	105.7	120.8
307	6.0	15.8	65.4	66.8	16.7	75.8	76.6	15.0	102.7	102.5
308	5.9	15.8	58.8	58.1	15.1	70.3	70.4	15.7	92.2	95.2
508	3.0	20.9	61.6	64.7	20.3	70.3	72.7	19.6	97.0	96.8
509	2.6	22.2	50.6	52.7	21.0	60.7	61.1	19.0	97.7	97.7
757	2.7	17.0	79.3	45.5	28.5	87.0	62.3	22.6	60.0	83.3
1007	2.0	25.0	53.3	54.6	25.7	57.0	69.7	22.7	74.0	74.4
1008	1.8	27.3	50.7	52.0	28.4	56.3	57.4	23.7	76.0	75.1
1009	3.1	18.5	87.0	87.2	24.5	70.3	93.9	23.0	73.9	73.3
1010	3.3	21.0	49.0	48.8	23.0	62.2	65.0	22.0	74.6	75.2
759	2.5	20.2	80.2	67.9	24.4	72.4	73.3	22.0	77.0	77.4
760	2.3	20.4	55.0	55.4	22.8	64.7	66.3	20.3	90.3	95.5
510	5.3	15.4	83.3	80.0	18.5	84.6	85.5	17.7	97.3	98.5
309	5.8	8.9	136.3	138.4	10.1	160.0	160.0	13.4	100.1	98.5

Table 22. Transition and induction time data for 15.0% H_2 in air

		GAGE 1			GAGE 2			GAGE 4		
Run Code	Induction Time	q_t	$(t_t)_q$	$(t_t)_T$	q_t	$(t_t)_q$	$(t_t)_T$	q_t	$(t_t)_q$	$(t_t)_T$
1005	1.8	40.0	20.7	20.7	41.2	37.2	32.9	45.3	49.7	49.5
1006	1.6	32.3	35.1	34.8	41.3	34.3	35.3	42.6	57.6	21.6
755	3.2	28.8	44.9	45.1	34.1	42.3	43.4	38.2	50.1	49.9
756	2.6	30.7	40.5	31.2	44.4	23.7	23.6	44.5	47.2	28.8
505	4.0	19.9	40.5	44.2	26.7	32.3	32.8	37.2	46.7	43.6
305	5.0	23.3	27.1	27.4	18.5	63.3	37.2	26.6	80.9	24.2
306	4.8	25.3	32.3	25.4	20.7	67.0	35.4	26.8	82.7	22.6
307	4.9	17.0	62.1	76.3	18.7	95.6	99.4	24.2	76.2	79.5
308	6.2	13.4	131.4	132.0	12.7	107.2	118.3	26.2	104.1	106.3
507	3.0	22.6	58.2	58.3	19.7	63.3	65.0	35.0	55.6	56.5
508	3.0	21.5	58.8	59.7	19.0	68.5	69.9	41.9	35.1	38.6
757	2.1	27.9	52.7	61.2	20.5	69.6	80.0	40.5	60.4	33.0
758	2.3	28.2	48.1	48.1	24.5	59.5	62.9	41.8	49.9	59.0
1007	1.7	30.2	42.8	46.6	24.2	60.1	63.5	42.4	46.2	44.8
1008	1.6	29.8	45.5	49.3	26.5	50.0	50.1	38.9	55.3	55.8
1009	1.5	20.0	68.6	63.6	17.5	95.7	95.6	39.4	43.6	41.8
1010	2.0	15.1	121.5	120.2	12.7	147.7	147.3	40.4	38.8	38.7
759	2.0	16.4	88.8	89.5	14.7	103.1	103.9	38.8	40.0	40.0
760	1.9	14.4	120.1	108.0	13.1	142.8	143.0	37.4	45.2	45.6
509	2.5	13.0	124.2	127.2	9.6	134.9	135.8	30.8	47.7	49.0
510	2.5	12.7	133.6	133.5	10.7	130.8	131.0	32.3	46.2	46.0
309	5.2	10.8	168.7	170.0	9.2	164.2	171.9	25.8	51.6	51.6
310	6.6	9.6	166.4	166.9	7.5	158.6	165.4	24.3	66.2	67.5

Figure 25. Estimated testing time between the shock wave and the interface at gage 2 in the test section

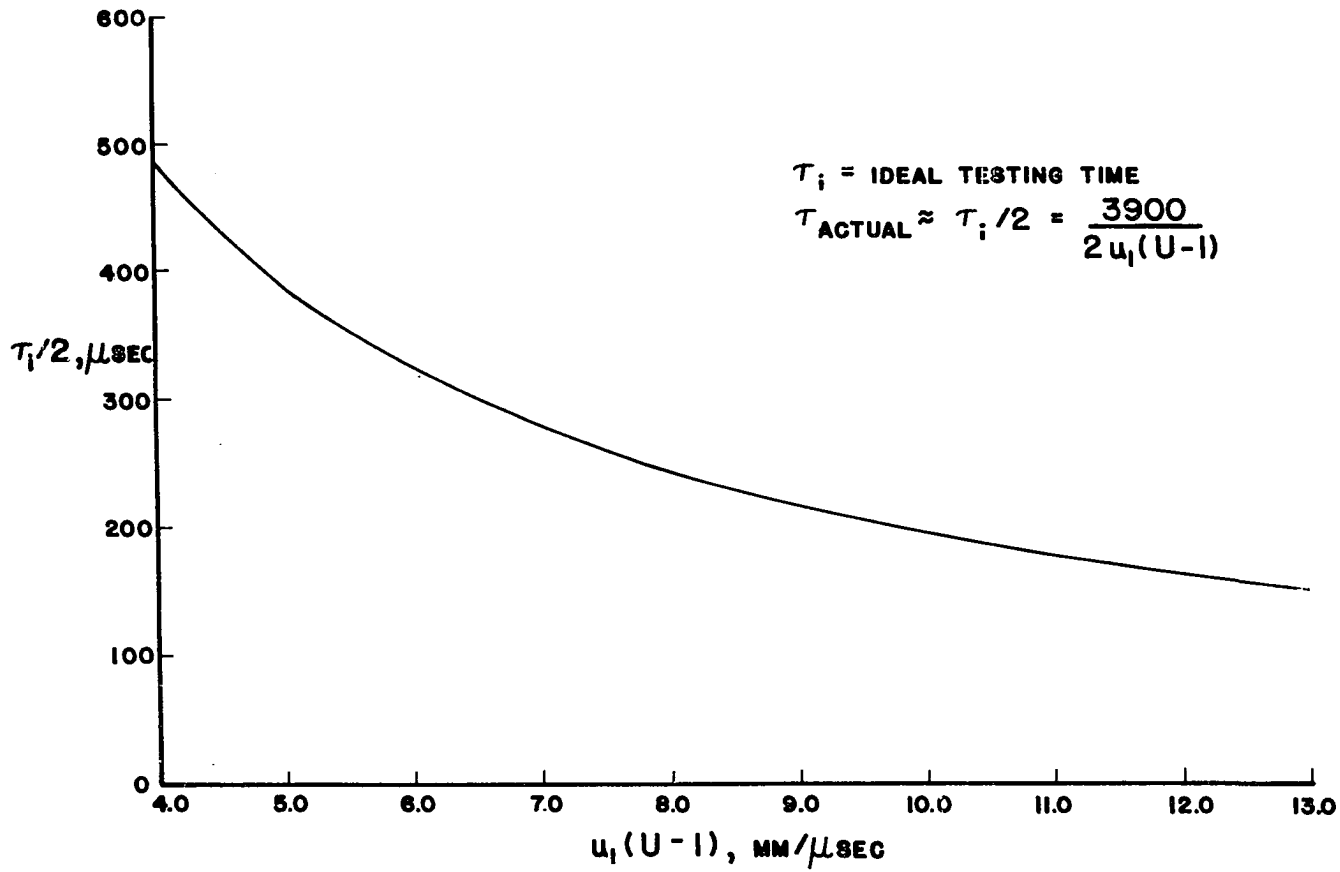
600
500
400
300
200
100
0
$\tau_i/2$, μSEC
τ_i = IDEAL TESTING TIME
$\tau_{ACTUAL} \approx \tau_i/2 = \frac{3900}{2u_1(U-1)}$
4.0
5.0
6.0
7.0
8.0
9.0
10.0
11.0
12.0
13.0
$u_1(U-1)$, MM/μSEC

Table 23. $F(U,\mu_2,r_2)$ for 100% N_2

Run	M_s	U	$\mu_2 \times 10^6$	r_2	F
501	3.45	4.36	386.6	0.83	7.48
303	3.52	4.40	394.9	0.83	7.53
1001	3.69	4.60	409.6	0.83	7.68
752	3.70	4.61	410.4	0.83	7.69
305	3.75	4.66	414.9	0.83	7.73
751	3.78	4.67	418.2	0.83	7.75
1002	3.79	4.68	418.6	0.83	7.76
1004	3.85	4.66	427.2	0.83	7.79
503	3.89	4.76	428.7	0.83	7.84
504	3.89	4.76	428.5	0.83	7.84
306	3.92	4.80	431.1	0.83	7.86
1003	3.97	4.76	439.6	0.83	7.89
754	4.00	4.84	439.0	0.83	7.92
753	4.08	4.90	446.6	0.83	7.97
506	4.26	4.98	467.5	0.83	8.10
505	4.31	5.02	473.3	0.83	8.14
507	4.35	5.10	474.1	0.83	8.17
308	4.39	5.12	479.1	0.83	8.20
307	4.46	5.17	486.7	0.83	8.25
1005	4.52	5.15	495.9	0.83	8.28
756	4.58	5.18	501.6	0.83	8.32
1006	4.59	5.19	503.2	0.83	8.33
755	4.59	5.19	502.5	0.83	8.32
508	4.61	5.26	501.9	0.83	8.35
509	4.63	5.28	504.5	0.83	8.36
1007	4.86	5.41	530.0	0.83	8.52
757	4.93	5.45	537.6	0.83	8.56
1008	4.95	5.46	539.9	0.83	8.58
310	4.96	5.49	538.7	0.83	8.58
309	5.01	5.53	545.0	0.83	8.62
510	5.26	5.66	572.3	0.83	8.78
511	5.29	5.68	575.7	0.83	8.80
1010	5.45	5.73	596.8	0.83	8.89
1009	5.52	5.76	604.8	0.83	8.94
759	5.54	5.79	606.1	0.83	8.95

Table 24. $F(U,\mu_2,r_2)$ for 4.0% H_2 in N_2

Run	M_s	U	$\mu_2 \times 10^6$	r_2	F
501	3.45	4.63	375.8	0.81	7.52
502	3.48	4.66	378.7	0.81	7.55
503	3.63	4.78	393.2	0.81	7.67
753	3.71	4.84	400.9	0.81	7.73
1002	3.74	4.87	403.1	0.81	7.75
306	3.76	4.86	406.6	0.81	7.76
305	3.81	4.90	411.1	0.81	7.80
1003	3.87	4.94	417.0	0.81	7.84
752	3.89	4.98	419.0	0.81	7.87
1001	3.89	4.99	417.8	0.81	7.86
504	3.92	4.98	422.3	0.81	7.88
754	3.94	5.00	424.5	0.81	7.90
755	3.96	5.01	426.0	0.81	7.91
1004	4.10	5.11	439.8	0.81	8.01
506	4.13	5.13	442.8	0.81	8.03
505	4.16	5.15	446.1	0.81	8.06
307	4.39	5.30	469.3	0.81	8.21
1005	4.42	5.32	472.9	0.81	8.24
757	4.49	5.37	480.3	0.81	8.29
1006	4.54	5.39	485.0	0.81	8.32
756	4.54	5.40	485.8	0.81	8.32
309	4.62	5.49	491.3	0.81	8.38
508	4.88	5.60	521.5	0.81	8.54
1008	4.92	5.62	525.6	0.81	8.57
510	4.97	5.72	528.2	0.81	8.62
1007	5.00	5.67	535.0	0.80	8.62
758	5.02	5.68	537.1	0.81	8.64
507	5.04	5.69	539.0	0.80	8.65
509	5.06	5.77	537.8	0.80	8.67
1009	5.11	5.72	546.5	0.80	8.69
1010	5.22	5.78	559.7	0.80	8.76
761	5.28	5.90	560.9	0.80	8.81
760	5.59	6.06	596.7	0.79	9.00

Table 25. $F(U,\mu_2,r_2)$ for 8.2% H_2 in N_2

Run	M_s	U	$\mu_2 \times 10^6$	r_2	F
751	3.55	4.98	373.7	0.78	7.64
1001	3.59	5.01	377.5	0.78	7.67
504	3.62	5.02	381.4	0.78	7.69
752	3.64	5.05	383.0	0.78	7.71
503	3.69	5.06	387.8	0.78	7.74
1002	3.71	5.09	389.4	0.78	7.76
306	3.74	5.07	394.3	0.78	7.77
305	3.75	5.08	395.4	0.78	7.78
753	3.78	5.12	396.7	0.78	7.81
1004	3.84	5.15	403.7	0.78	7.85
754	3.93	5.23	411.8	0.78	7.92
1003	3.93	5.21	412.9	0.78	7.92
506	4.04	5.27	424.7	0.78	7.99
505	4.11	5.33	430.4	0.78	8.04
307	4.23	5.39	443.2	0.78	8.12
308	4.23	5.39	443.5	0.78	8.12
1006	4.26	5.42	445.4	0.78	8.14
756	4.31	5.45	450.7	0.78	8.18
1005	4.32	5.46	451.9	0.78	8.19
508	4.32	5.44	452.8	0.78	8.19
755	4.34	5.47	453.4	0.78	8.20
507	4.44	5.51	464.6	0.78	8.26
310	4.70	5.62	494.6	0.78	8.43
309	4.77	5.65	501.9	0.78	8.48
757	4.92	5.75	517.4	0.78	8.58
758	4.92	5.75	518.0	0.78	8.58
511	5.08	5.81	535.8	0.78	8.67
1008	5.16	5.87	544.8	0.78	8.73
759	5.32	5.95	562.8	0.78	8.83
760	5.35	5.96	565.4	0.77	8.84
1010	5.44	6.00	575.9	0.77	8.90

Table 26. $F(U,\mu_2,r_2)$ for 12.3% H_2 in N_2

Run	M_s	U	$\mu_2 \times 10^6$	r_2	F
306	3.62	5.24	370.7	0.76	7.71
1002	3.72	5.52	373.0	0.76	7.82
503	3.73	5.27	383.5	0.76	7.79
1003	3.74	5.29	383.9	0.76	7.80
751	3.76	5.34	384.6	0.76	7.82
504	3.80	5.31	390.8	0.76	7.84
1001	3.83	5.40	391.8	0.76	7.87
753	3.84	5.35	394.0	0.76	7.87
1004	3.87	5.37	397.6	0.76	7.89
752	3.91	5.42	399.8	0.76	7.92
754	3.94	5.41	404.4	0.76	7.94
505	3.99	5.45	408.4	0.76	7.98
506	4.14	5.54	424.6	0.76	8.08
756	4.29	5.62	439.3	0.76	8.18
755	4.33	5.64	443.7	0.76	8.21
1006	4.39	5.65	450.3	0.76	8.24
1005	4.43	5.67	454.4	0.76	8.27
507	4.56	5.77	467.7	0.76	8.36
308	4.63	5.82	474.0	0.76	8.41
307	4.71	5.88	481.5	0.76	8.46
508	4.70	5.84	483.1	0.76	8.46
1008	4.80	5.89	493.8	0.76	8.52
1007	4.84	5.90	497.7	0.76	8.54
310	4.90	5.93	504.6	0.76	8.58
758	4.98	5.95	514.0	0.76	8.63
309	4.99	5.97	514.2	0.-6	8.63
509	5.01	5.98	517.2	0.76	8.65
510	5.09	6.01	525.4	0.76	8.70
1009	5.31	6.11	550.9	0.75	8.83

Table 27. $F(U,\mu_2,r_2)$ for 3.1% H_2 in air

Run	M_s	U	$\mu_2 \times 10^6$	r_2	F
501	3.51	4.44	408.7	0.83	7.62
502	3.52	4.45	409.8	0.83	7.62
1002	3.62	4.57	419.2	0.83	7.72
503	3.74	4.64	432.2	0.83	7.81
1001	3.75	4.67	431.9	0.83	7.82
752	3.78	4.69	435.3	0.83	7.84
751	3.79	4.70	436.9	0.83	7.85
504	3.87	4.75	445.6	0.83	7.91
306	3.88	4.72	448.2	0.83	7.91
1003	3.91	4.76	449.9	0.83	7.93
754	3.98	4.82	456.9	0.83	7.99
305	3.99	4.80	459.1	0.83	7.99
1004	4.02	4.85	461.3	0.83	8.02
753	4.15	4.94	473.3	0.83	8.11
506	4.17	4.94	478.1	0.83	8.12
308	4.21	4.98	481.6	0.83	8.15
307	4.23	4.98	483.7	0.83	8.16
511	4.27	5.01	487.9	0.83	8.19
755	4.42	5.13	503.5	0.83	8.30
508	4.48	5.16	510.5	0.83	8.34
756	4.48	5.17	509.1	0.83	8.34
505	4.53	5.21	514.9	0.83	8.38
1005	4.58	5.26	519.5	0.83	8.42
1006	4.58	5.25	518.9	0.83	8.41
507	4.64	5.27	527.1	0.83	8.45
310	4.66	5.27	529.9	0.83	8.46
1008	4.75	5.34	538.9	0.83	8.53
309	4.76	5.33	540.8	0.83	8.53
758	4.86	5.41	550.4	0.83	8.60
1007	4.86	5.41	550.0	0.83	8.60
757	4.93	5.45	557.7	0.83	8.64
510	5.01	5.49	567.5	0.83	8.69
509	5.09	5.54	576.1	0.83	8.74
759	5.35	5.70	604.8	0.83	8.91
1010	5.37	5.71	607.0	0.83	8.92
1009	5.56	5.83	627.9	0.82	9.04

Table 28. $F(U,\mu_2,r_2)$ for 7.0% H_2 in air

Run	M_s	U	$\mu_2 \times 10^6$	r_2	F
501	3.52	4.44	407.1	0.83	7.61
752	3.63	4.53	418.0	0.83	7.70
504	3.72	4.60	427.7	0.83	7.77
503	3.88	4.74	444.5	0.83	7.90
753	3.93	4.77	449.7	0.83	7.94
754	3.96	4.80	452.8	0.83	7.96
1004	4.01	4.83	457.2	0.83	7.99
305	4.10	4.90	466.0	0.83	8.06
306	4.13	4.92	469.3	0.83	8.08
506	4.34	5.08	491.6	0.83	8.23
505	4.40	5.13	498.7	0.83	8.28
1003	4.41	5.13	499.8	0.83	8.29
307	4.42	5.14	500.5	0.83	8.29
308	4.50	5.19	508.9	0.83	8.35
756	4.53	5.21	512.3	0.83	8.37
1006	4.54	5.22	513.2	0.83	8.38
758	4.56	5.23	515.3	0.83	8.39
755	4.63	5.28	522.7	0.83	8.44
507	4.69	5.32	529.8	0.83	8.48
1005	4.72	5.34	532.9	0.83	8.50
309	4.95	5.49	557.8	0.83	8.66
1008	4.95	5.53	556.4	0.83	8.66
757	4.95	5.49	557.2	0.83	8.65
508	4.96	5.50	559.2	0.83	8.67
1007	4.99	5.55	560.8	0.83	8.69
510	5.10	5.59	574.3	0.84	8.76
759	5.36	5.77	601.3	0.83	8.92
1010	5.42	5.82	606.5	0.83	8.96
760	5.43	5.83	609.0	0.83	8.97
509	5.43	5.80	609.9	0.83	8.96
1009	5.59	5.93	625.6	0.82	9.07

Table 29. $F(U,\mu_2,r_2)$ for 11.0% H_2 in air

Run	M_s	U	$\mu_2 \times 10^6$	r_2	F
306	3.87	4.65	443.4	0.83	7.86
305	4.08	4.81	465.3	0.83	8.02
507	4.45	5.08	505.1	0.83	8.29
1006	4.50	5.13	510.0	0.83	8.33
307	4.50	5.10	511.7	0.83	8.33
308	4.51	5.11	513.0	0.83	8.33
506	4.61	5.19	522.4	0.83	8.40
755	4.61	5.21	521.9	0.83	8.41
756	4.66	5.24	526.8	0.83	8.44
1005	4.80	5.34	542.4	0.83	8.54
508	4.83	5.31	547.8	0.83	8.55
757	4.88	5.34	553.8	0.83	8.59
509	4.92	5.37	557.6	0.83	8.61
309	4.95	5.47	557.7	0.83	8.65
510	5.02	5.53	563.9	0.83	8.69
1007	5.03	5.42	571.0	0.83	8.68
1008	5.10	5.46	578.9	0.83	8.73
1010	5.21	5.53	591.8	0.83	8.80
1009	5.26	5.56	596.8	0.82	8.83
759	5.47	5.83	613.5	0.82	8.99
760	5.53	5.87	619.9	0.82	9.03

Table 30. $F(U,\mu_2,r_2)$ for 15.0% H_2 in air

Run	M_s	U	$\mu_2 \times 10^6$	r_2	F
305	4.23	4.90	480.3	0.83	8.12
306	4.25	4.91	482.9	0.83	8.13
505	4.32	4.96	490.0	0.83	8.18
755	4.42	5.04	500.7	0.83	8.26
308	4.46	5.06	505.6	0.83	8.28
756	4.51	5.11	510.7	0.83	8.32
307	4.57	5.13	517.2	0.83	8.36
1005	4.68	5.22	529.3	0.83	8.44
1006	4.73	5.26	534.6	0.83	8.48
310	4.78	5.26	542.1	0.83	8.51
507	4.79	5.28	541.9	0.83	8.51
508	4.80	5.28	542.7	0.83	8.52
309	4.90	5.34	555.6	0.83	8.59
758	4.93	5.37	557.8	0.83	8.61
757	4.97	5.40	562.0	0.83	8.64
1007	5.08	5.45	575.0	0.83	8.71
1008	5.11	5.47	579.0	0.82	8.73
510	5.32	5.61	602.9	0.82	8.87
509	5.33	5.61	603.8	0.82	8.87
1010	5.46	5.70	618.2	0.82	8.96
759	5.43	5.70	619.4	0.82	8.96
760	5.50	5.72	622.9	0.82	8.98
1009	5.68	5.85	642.8	0.81	9.10

APPENDIX B: CALIBRATION OF THIN-FILM RESISTANCE THERMOMETERS

Theoretical Considerations

Calibration for α

The temperature coefficient of resistance of the thin-film resistance thermometers were obtained by measuring the gage resistance with a bridge circuit when the gage was immersed in a fluid bath at various temperatures. Freon 113 was found to be a very convenient fluid for this purpose because it does not chemically affect the gage, in the form of a resistance drop, as other fluids such as water or alcohol do. A discussion of this adverse chemical effect is included in a later section. Resistance measurements were obtained between temperatures of 0°C (ice point) and 49°C (Freon 113 boiling point). This resistance-temperature data was then plotted and found to be linear as expected as illustrated in Figure 26. Thus, α for the thin-films were found graphically from the relation below for a pure metal.

$$\alpha = (1/R_o)(\Delta R/\Delta T) \tag{B-1}$$

In this equation R_o is a resistance at some reference temperature T_o. Here, T_o is taken as T_1 for any given experimental run.

Since the thin films have negligible heat-energy capacity it is necessary to use a special precaution in obtaining resistance-temperature data to determine α. The current must be limited so that the Joule heating (I^2R dissipation) is not appreciable enough to cause gage temperatures different from the fluid bath temperature. In this case, the current was set at 10 milliamps which resulted in energy dissipations of less than 10^{-2} watts. This value of current was used because it was the same as the

Figure 26. Resistance variation with temperature for the α calibration of a thin-film gage

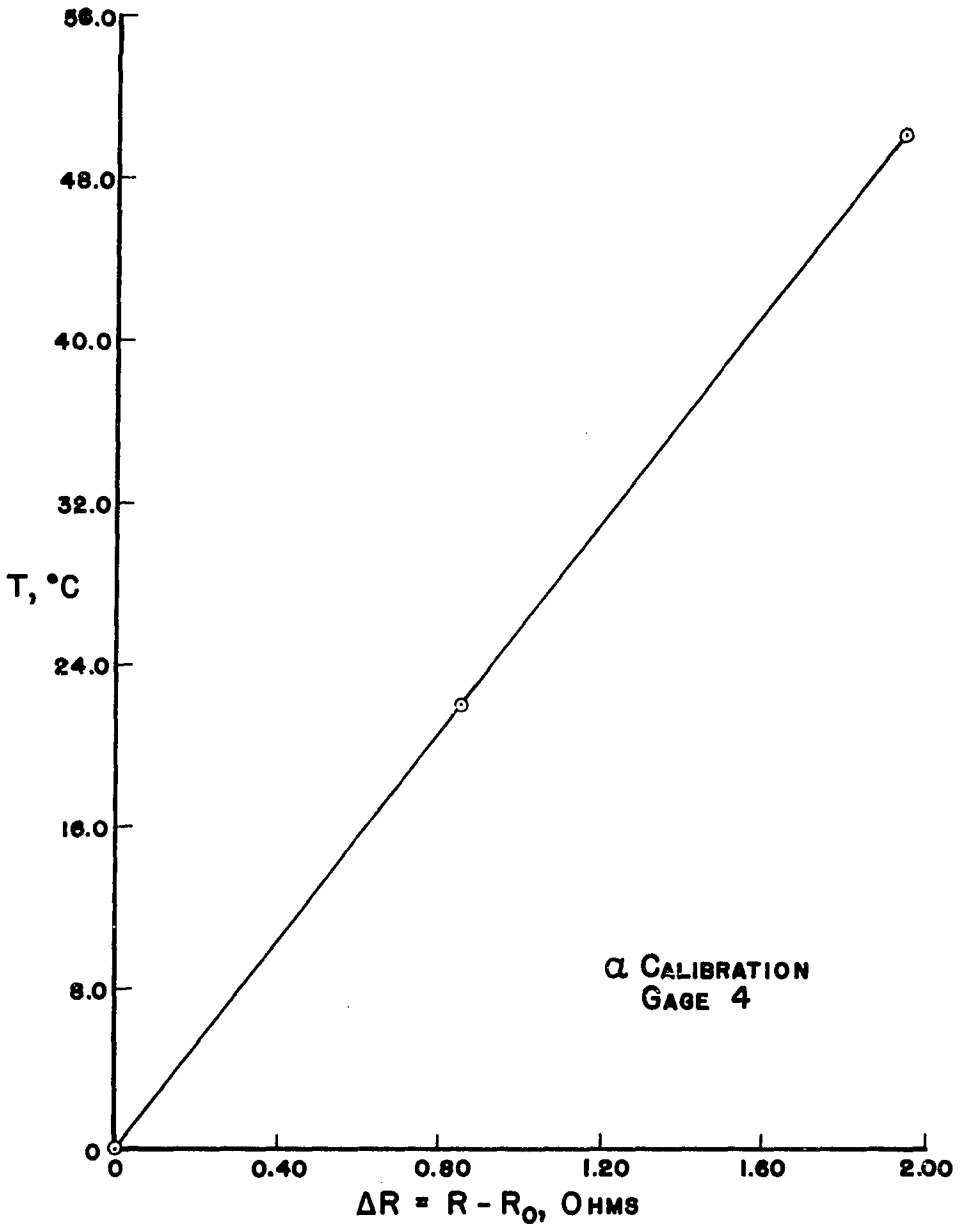
56.0
48.0
40.0
32.0
T, °C
24.0
16.0
8.0
0
0
0.40
0.80
1.20
1.60
2.00
ΔR = R - R0, OHMS
α CALIBRATION
GAGE 4

operating current used during each experimental run.

A special bridge circuit designed to accomplish both α and β calibrations is shown in Figure 27 and the actual calibration apparatus using this circuit is illustrated in Figures 28 and 29. An outline of the procedure followed in using the apparatus is given in a later section.

Calibration for β

To determine the thermal product of the backing material using Equation 44 one must dissipate energy in the gage, first while the gage is immersed in a fluid (such as air) with a known thermal product β_{f_1} and then again while the gage is immersed in another fluid (such as Freon 113 or water) with a known thermal product β_{f_2}. Both of the fluids would be at the same temperature. Since the gage has a negligible heat capacity the electrical energy dissipated in the gage must pass immediately and simultaneously to the backing material on one side of the gage and the fluid medium on the other side of the gage. Further, because the gage is extremely thin (about 0.1 micron) the heat-transter area presented to the backing material and fluid medium is the same. Thus, writing an energy balance around the gage one obtains from Equation 41 the following result in the transform plane.

$$q(o,s) = (\beta_b + \beta_f)\sqrt{s}\ T(o,s) \qquad \text{(B-2)}$$

In Equation B-2, β_b represents the unknown thermal product of the backing material and β_f represents the known thermal product of the fluid medium in which the gage is immersed. The quantities, $q(o,s)$ and $T(o,s)$ are the energy input to the gage and the temperature response of the gage to the energy input respectively in the Laplace transform plane. When the gage

Figure 27. Thin-film gage calibration circuit

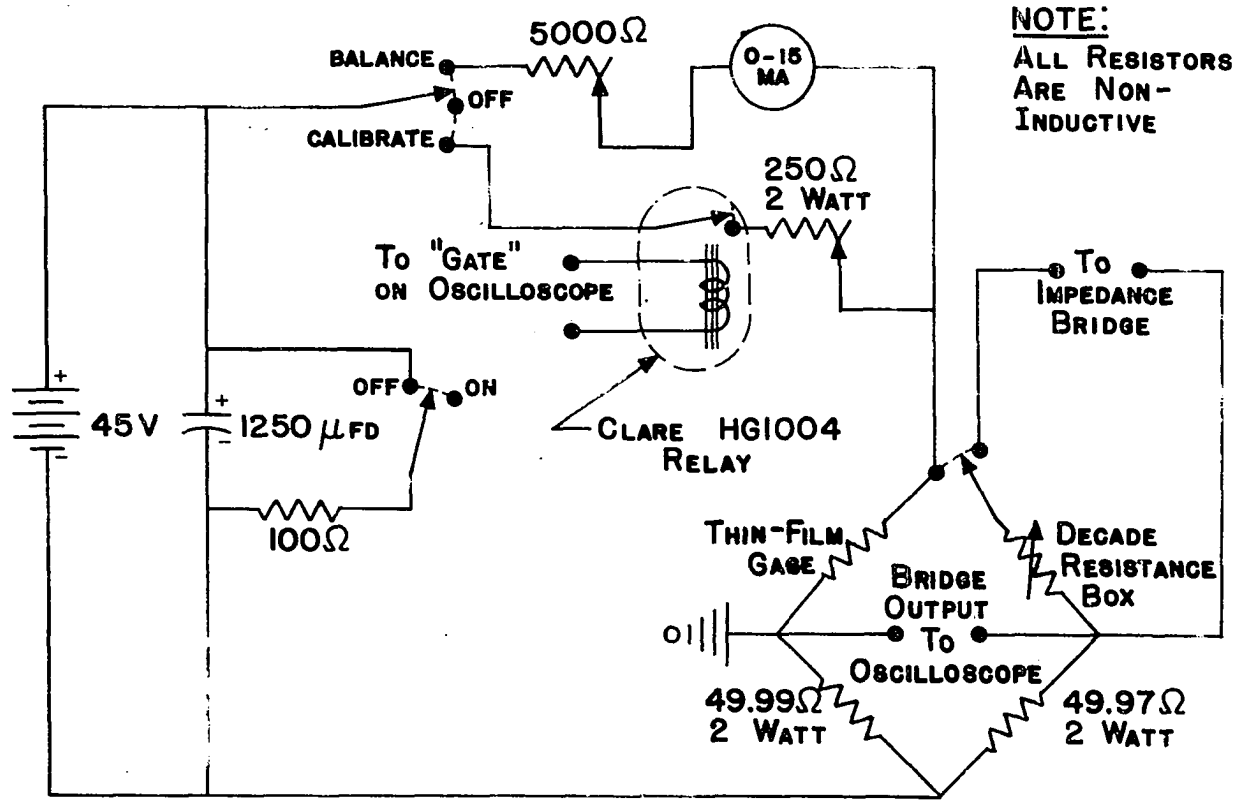
NOTE:
ALL RESISTORS ARE NON-INDUCTIVE
BALANCE
OFF
CALIBRATE
5000Ω
0-15 MA
250Ω 2 WATT
To "GATE" ON OSCILLOSCOPE
To IMPEDANCE BRIDGE
45V
1250 μFD
OFF
ON
100Ω
CLARE HG1004 RELAY
THIN-FILM GAGE
DECADE RESISTANCE BOX
BRIDGE OUTPUT To OSCILLOSCOPE
49.99Ω 2 WATT
49.97Ω 2 WATT

Figure 28. View of calibration apparatus for calibration in air

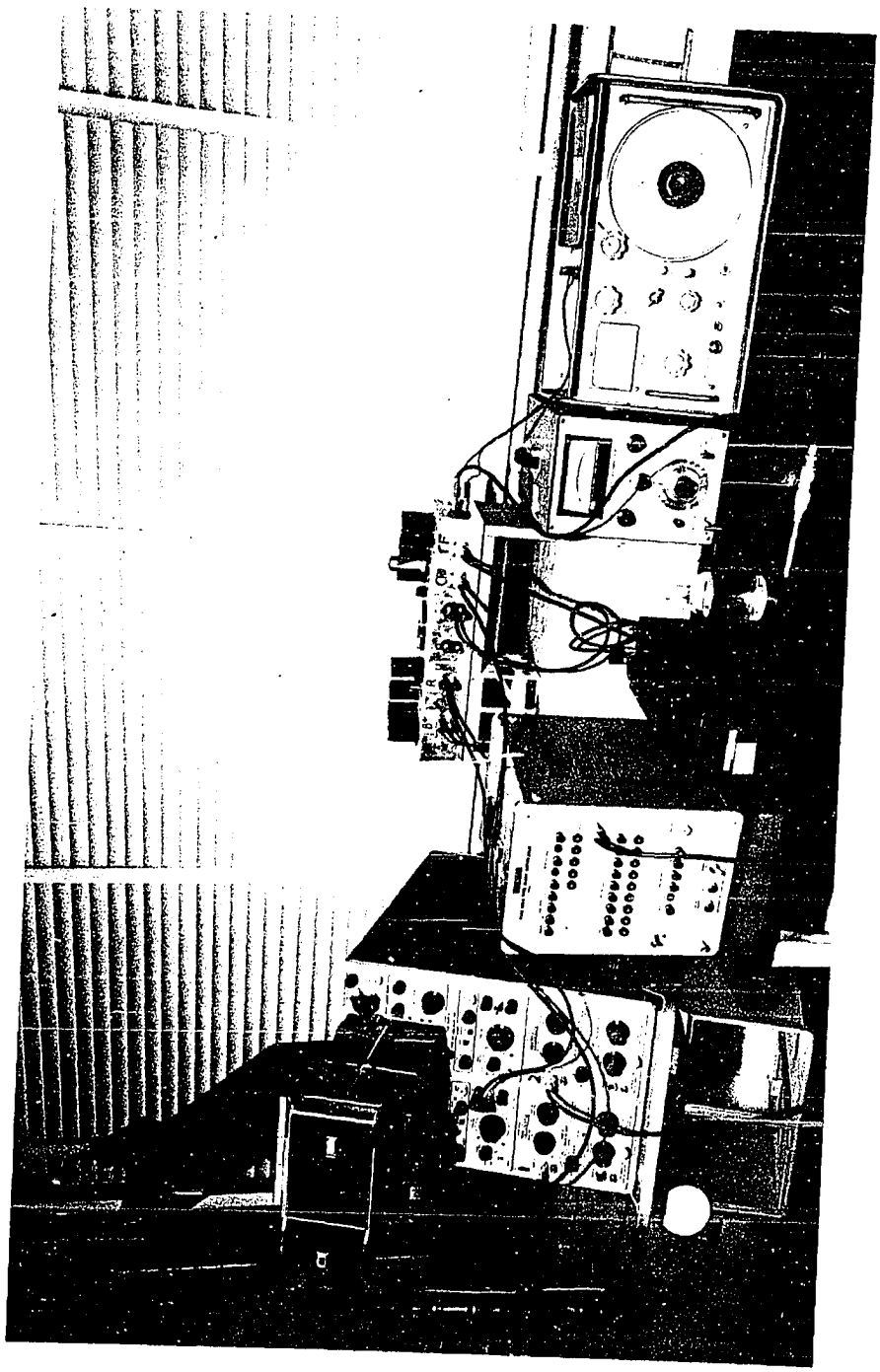

Figure 29. View of calibration apparatus for calibration in Freon 113

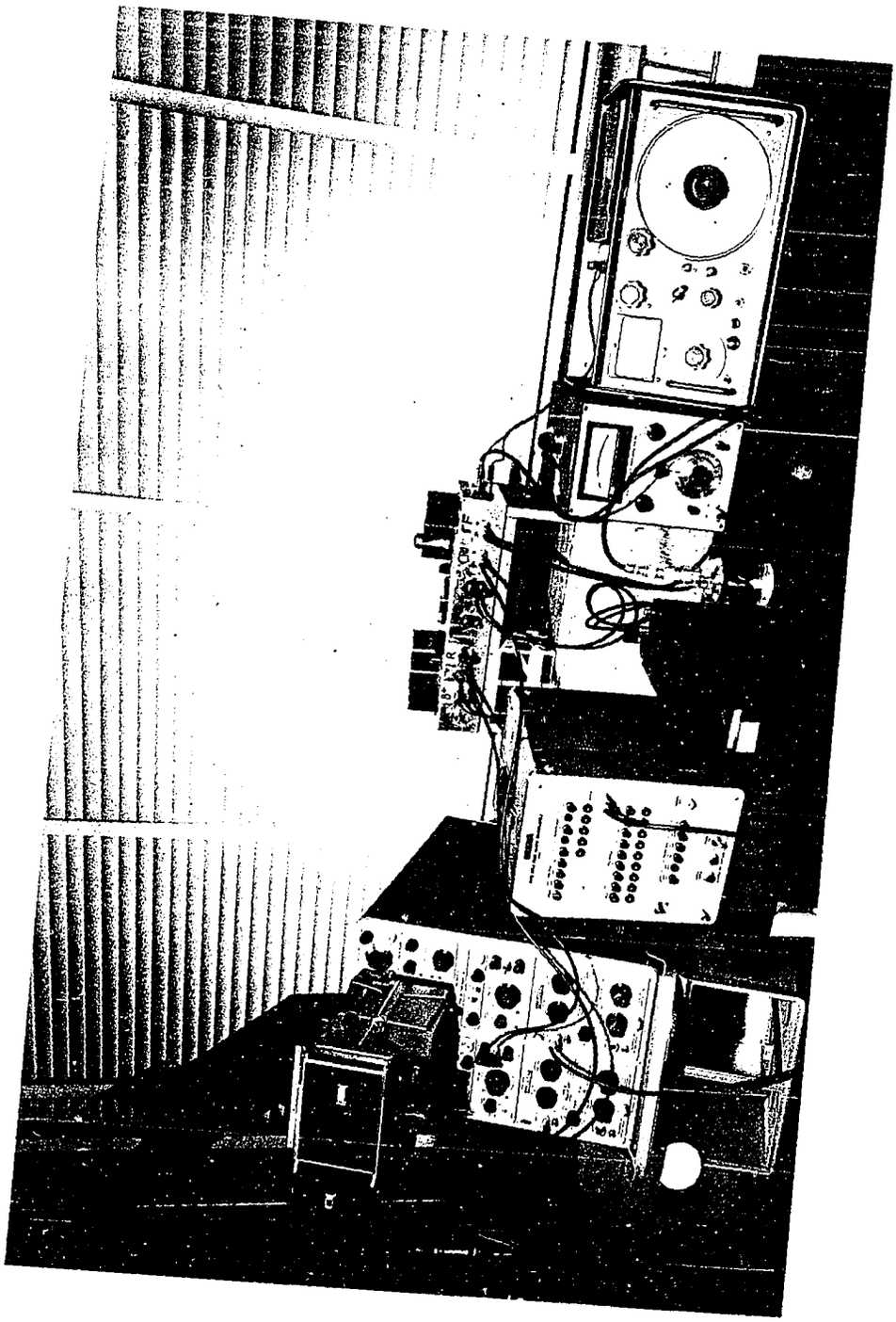

is pulsed electrically in the two different fluid mediums one can write the following two relations:

$$q_1(o,s) = (\beta_{b_1} + \beta_{f_1})\sqrt{s}\ T_1(o,s)$$
$$q_2(o,s) = (\beta_{b_2} + \beta_{f_2})\sqrt{s}\ T_2(o,s) \qquad \text{(B-3)}$$

If the energy input, $q(o,s)$ is the same in form for each fluid medium the tempearture response, $T(o,s)$ will also be the same in form as predicted by Equation B-3. Then, only the magnitudes of $q(o,s)$ and $T(o,s)$ for each fluid medium are different and one can write the following relations:

$$q_1(o,s) = B\ T_1(o,s)$$
$$T_1(o,s) = A\ T_2(o,s) \qquad \text{(B-4)}$$

By dividing Equations B-3 and combining with Equations B-4 one obtains the calibration equation of interest.

$$\frac{B}{A} = \frac{\beta_{b_1} + \beta_{f_1}}{\beta_{b_2} + \beta_{f_2}} \qquad \text{(B-5)}$$

When the fluid mediums are at the same temperature β_{b_1} and β_{b_2} are equal (i.e., $\beta_{b_1} = \beta_{b_2} = \beta_b$). Furthermore, if the temperatures of the fluid mediums are the same the gage resistance will be the same in both fluid mediums. Hence, the energy dissipation (such as might be obtained from a capacitor discharge) in the gage is easily made the same in both form and magnitude and $B = 1$. If one of the fluids (say fluid #1) is air its thermal product β_{f_1} is negligible compared to the substrate thermal product β_{b_1}. Thus, for a given temperature level (usually room temperature) and using air as one of the fluids, the value of the substrate thermal

product β_b is obtained from Equation B-5 and the items above as given below

$$\beta_b = \left(\frac{1}{A-1}\right) \beta_{f_2} \tag{B-6}$$

Distilled water is normally selected for the second fluid medium when obtaining the room temperature substrate thermal product β_b because the thermal properties (hence, β_{f_2}) of water are accurately known and tabulated. However, Freon 113 has been found to work better than water for both α and β calibrations as indicated in the α calibration section and discussed in a later section.

The temperature-response magnitude factor, A, is determined from an oscilloscope recording of the gage-temperature response as it is pulsed electrically in the two different fluid mediums. This technique is demonstrated in Figure 30-a for a calibration time of interest with the gage as one arm of a resistance bridge to give $A = E_1/E_2$. Skinner (77) was the first to apply this calibration technique using thin films.

In actual practice it is virtually impossible to obtain a perfect bridge balance before pulsing the gage and both E_1 and E_2 require initial unbalance corrections. Further, it has been indicated by Bogdan (78) that an initial step, over and above the initial bridge unbalance, occurs when the gage is pulsed. To date, no satisfactory explanation can be given for this additional initial step. Fortunately, by using a nearly constant power dissipation (simulating a constant heat-transfer rate) one can correct for both the initial bridge unbalance and the additional initial step.

It is of interest to note that Equations B-2, B-3, B-4, and B-5 do not stipulate the form of the electrical energy dissipation used to simulate the heat-transfer rate. These equations only require the form of dissipation to be identical for each fluid medium. However, in order to make the initial unbalance corrections mentioned above it is convenient to use a nearly constant power dissipation in the gage. This can be obtained by appropriately discharging a capacitor through the gage as was done in this investigation.

From Equation 44 it is shown that a constant heat-transfer rate q_o gives a constant $\Delta T/\sqrt{\Delta t}$. Also, from Equation 37 it is shown that ΔT is directly related to ΔE. Then, if a plot of ΔE as a function of $\sqrt{t}$ is made from the data obtained on an oscilloscope photograph of the gage response to the electrical pulse, one can obtain the initial correction as shown below in Figure 30-b. The initial correction for each gage voltage response can then be applied to A to yield:

$$A = \frac{E_1 - C_1}{E_2 - C_2} \tag{B-7}$$

This correction method has been used quite satisfactorily by Bogdan (78) and was also used in this investigation. Figure 31-a is an oscilloscope photograph for β calibration and Figure 32 is the plotted results from which A and consequently β_b are determined. Also shown in Figure 31-b is a recalibration photograph taken after the experimental runs were completed.

Special Considerations

Chemical effect of water and alcohol

A disadvantage of using water as one of the fluid media is that the

Figure 30. Correction technique for slight bridge unbalance

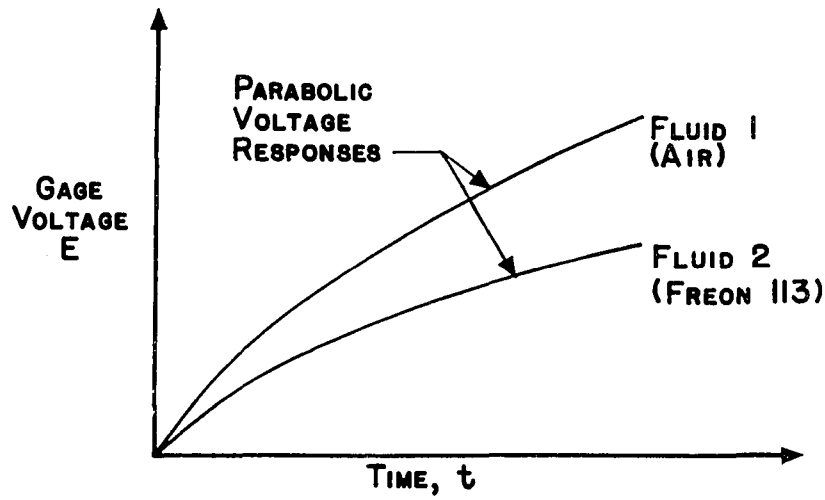

a.) Thin Film Voltage Response

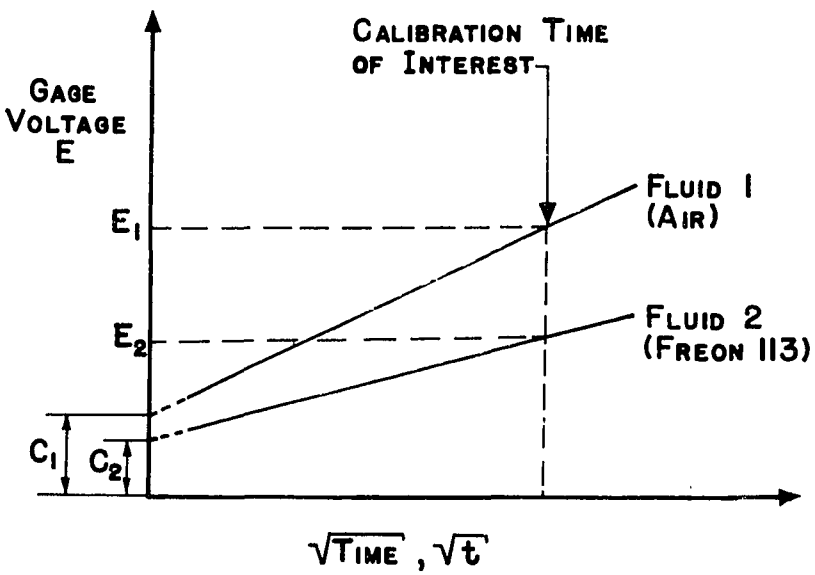

b) Bridge Unbalance Corrections

Figure 31. Voltage response curves for β calibration of a typical thin-flim gage

Note: Traces a and b have the same arbitrary vertical sensitivity. Horizontal sensitivity is 50 micro-seconds per major graticule division. Timing marks are superimposed at intervals of 10 micro-seconds.

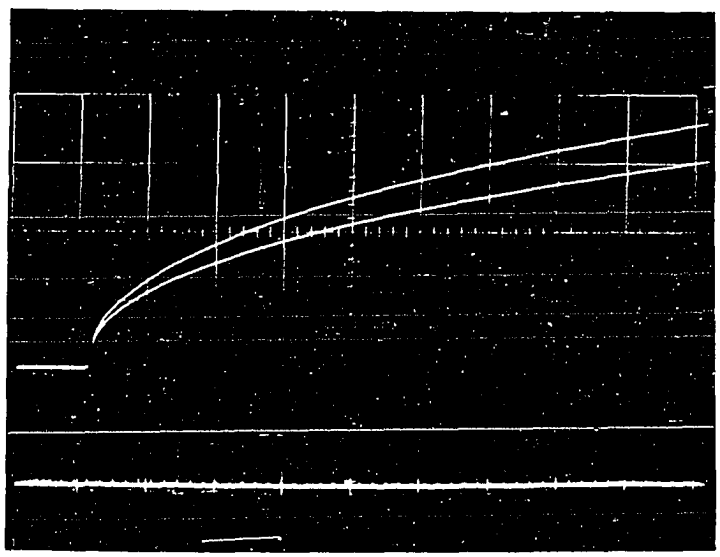

a)Before Experimental Run

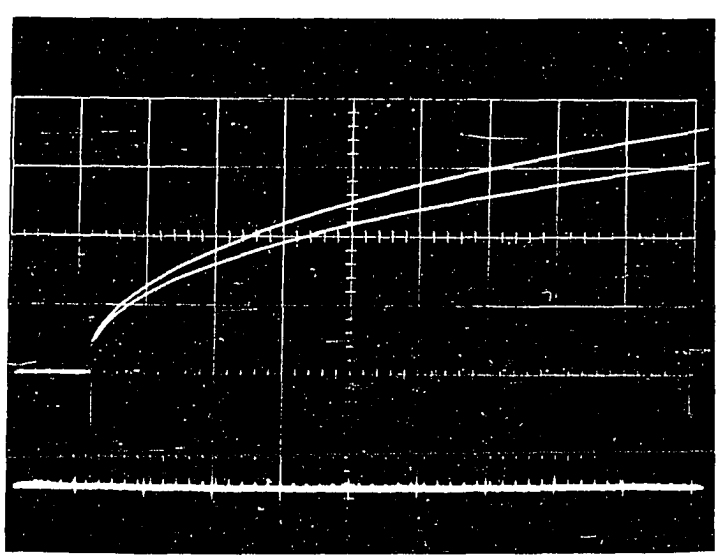

b)After Experimental Run

gage-lead wire combination immediately decreases in resistance when immersed in water. When the gages are removed from the water and allowed to dry the gage resistance does not recover to its initial value precluding any ionization and/or heat-transfer affect caused by the water. Instead, it is believed that the water causes a chemical phenomenon at the interface between the gage and the lead material. Some proof of this is given by the fact that the resistance of the gage-lead wire combination decreases about 1.5 to 4% when silver micropaint is used to attach leads to the gage and about 1 to 2% when the leads are soldered directly to the thin film gages. Another possible explanation of the resistance drop as presented in Reference 77 is that the water molecules adhere to the metal film and fill voids in the surface structure. In any case the resistance change is small, but finite and quite disconcerting when one is trying to calibrate gages.

It has been observed by the author that alcohol also has the same effect as water indicating that possibly the OH radical is responsible for a portion of the effect as well as any polar nature of the fluids. At the same time it has been found that Freon 113 does not cause this effect.

Another method of eliminating the water effect is to coat the gages with a thin insulative layer (about 1 micron or less) of silicon monoxide or calcium flouride before immersion in the water bath. This thin coating has been demonstrated (77,78, and 79) to have a negligible effect on the resulting calibration. Further, if the thin film gage is to be used in an ionized flow the thin insulative coating is necessary, hence, it

need not be a hindrance to Skinner's calibration technique. Also, a fluid other than water could be used in this calibration technique. To date, an effort made along this line indicates that Freon 113 works very satisfactorily.

Two-dimensional effects

The basic equations governing the operation of a thin film gage are obtained from the non-steady, one-dimensional, heat-flux equation. The equations listed herein lose their significance if the heat-flux becomes multi-dimensional in character. Bogdan (78) indicates the calibration time should be kept as small as possible to minimize any two-dimensional effects. For pyrex backing he lists maximum times of 4-5 milliseconds and for substrates of higher thermal diffusivities than pyrex one must decrease the calibration times below 4-5 milliseconds. Maximum calibration times of 100 microseconds were used in this investigation.

Heat-rate simulation

It has not been determined conclusively, to date, whether or not it is important to simulate a heat-transfer rate when calibrating a thin-film resistance thermometer. Although it is not evident from the calibration equations that heat-transfer rate simulation should be made, slightly different thermal products can be obtained by pulsing the gage at different energy levels. It has not been determined exactly if the difference in thermal product is due only to the increased average gage temperature as obtained from the higher energy level pulse. Some careful and intensive calibrations along this line are needed.

Variation of thermal product with temperature

To obtain the substrate thermal product as a function of temperature the gage is pulsed electrically in air (fluid #1) at room temperature then again in air (also fluid #2) in this case, at a known higher temperature. In both cases the thermal products of air (i.e., β_{f_1} and β_{f_2}) are negligible compared to the substrate thermal products (β_{b_1} and β_{b_2}). Equation B-5 then reduces to Equation B-8 below.

$$\frac{\beta_{b_1}}{\beta_{b_2}} = \frac{B}{A} \tag{B-8}$$

In equation B-8, β_{b_1} represents the room temperature substrate thermal product and β_{b_2} represents the elevated temperature substrate thermal product. The room temperature value of β_{b_1} (i.e., β_b) is obtained from Equation B-6 and the procedure leading to that equation. The elevated temperature value of β_{b_2} is obtained by combining Equations B-6 and B-8. However, in Equation B-8, B may not be equal to 1 because the gage resistance is different for different temperatures. The value of B can be obtained from Equation B-9 below

$$B = \frac{q_1}{q_2} \frac{(I_1)^2 R_1}{(I_2)^2 R_2} \tag{B-9}$$

By adjusting the capacitor discharge voltage to account for gage resistance change with temperature, one can make B = 1. The gage temperature response ratio A is obtained in a manner similar to that procedure previously indicated in using Equation B-6.

Somers (79) was the first to determine the variation of β with temperature

in Pyrex, however, such determinations were not required in this investigation.

Calibration Procedure

The following outline represents the steps necessary to obtain α and β calibrations using the circuit and apparatus shown in Figures 27, 28 and 29.

α calibration

1. Turn balance-calibrate switch to balance.
2. Attach to the calibration circuit a stable 50-Ohm Tektronix " termination resistor".
3. Adjust the current supply to the bridge circuit to the desired level. A typical value is 10 milliamps.
4. Proceed to balance the bridge by using in combination a decade box and the variable potentiometer in the bridge circuit for the adjustable balance resistor while using a precision voltmeter to monitor the bridge output voltage. When the bridge is balanced this voltage should be zero.
5. When the bridge is balanced turn the impedance bridge to measure the resistance of the balance resistor. Denote this resistance as R_{SB}.
6. Detach the 50-Ohm "termination resistor" from the calibration circuit and use the impedance bridge to measure precisely and directly this resistance. Denote this resistance as R_{SD}.
7. The resistance measurements obtained in items (5) and (6) above are used to determine the resistance correction for

lead wire and connections as follows:

True Bridge Resistance $\equiv R_{TB} = (49.97/49.99)(R_{SD}) = R_{SD}/1.004$

Correction Resistance $\equiv R_{CD} = R_{SD} - R_{TB}$

8. With the correction resistance now known one can proceed to use a thin-film gage in the calibration circuit following steps (3) through (5) above to obtain a resistance reading denoted as R_{GB}.
9. The true thin-film gage reading is then obtained by subtracting the correction resistance R_{CB} from R_{GB}. Thus,

   True Gage Resistance $\equiv R_{GT} = R_{GB} - R_{CB}$
10. By immersing the thin-film gage in a bottle of Freon 113 which in turn is immersed in a thermose to provide a constant temperature bath one can obtain a 3 point resistance variation with temperature plot. The temperatures used are the ice point (0°C), room temperature (20-25°C) and the Freon 113 boiling point (49°C).

β calibration

1. With a thin-film gage attached to the calibration circuit turn the balance-calibrate switch to balance, adjust the bridge current to 10 milliamps and proceed to balance the bridge as outlined in item (4) under α calibration.
2. After the bridge is balanced turn the capacitor switch to "on" and the balance-calibrate switch to calibrate.
3. The thin-film gage is now ready for the β calibration. To this end a Tektronix type 555 oscilloscope should be used to record the bridge output. The oscilloscope settings should

be as follows:

a) upper beam - 50 μsec/cm via time base B and 5 mv/cm.
lower beam- 50 μsec/cm via time base B and 10 v/cm.
delay time - 4.50 milliseconds = (9.00)(0.5)
delay setting - 9.00
time base A - 0.5 millisec/cm and on single sweep.
timing marks - 5 and 50 microseconds.

b) Time base A triggers (via the "gate") the relay that in turn controls the capacitor discharge time to the thin-film gage. It takes slightly more than 4.5 milliseconds for the relay contacts to close.

c) Time base A is triggered externally from the trigger output of a Tektronix 180A time mark generator.

d) Time base B is triggered by a delayed isgnal from time base B.

e) The gage output is observed on the upper beam sweeping according to time base B.

f) The timing pulses are observed on the lower beam sweeping according to time base B.

4. Pushing the reset button on time base A single sweep mode causes time base A to be triggered thus causing, in turn, the relay contacts to close and energy to be dissipated in the thin-film gage.

5. The amount of energy dissipated in the gage can be controlled by adjusting the 1 turn variable potentiometer (250 Ω) in the

capacitor discharge circuit. This potentiometer is adjusted to keep the oscilloscope trace of the bridge output below the upper graticule line on the oscilloscope face.

6. After the thin-film gage has been pulsed at room temperature in air the process is repeated while the gage is immersed in a bottle of Freon 113 to complete the calibration procedure.
7. The calibration traces should be analyzed according to Skinner's technique as presented previously.
8. Energy dissipation to the gage is approximately constant for 0.1% of the RC time constant of the calibration circuit. This RC time constant will vary with thin-film gage resistance (for the capacitor indicated) but is about .375 milliseconds for a 50 ohm gage. Thus, the calibration time of interest should be below 375 microseconds. A good nominal time is 300 microseconds.
9. Typical values of α/β in cgs units are between 0.01 and 0.07 with 0.02 being typical for a platinum gage on a pyrex substrate. Resulting values outside the range mentioned should be questioned.

Calibration Results

The result for α and β calibration are tabulated in Table 31 below. The values listed are for calibrations made before any experimental runs. After the experimental runs the gages were again calibrated and, except for gage 3, the results agreed with values listed in Table 31. Gage 3 developed an open circuit during final β calibrations and therefore could not be checked.

Table 31. Thin-film calibration results

Gage No.	α, 1/°C	β, cal/cm^2(°C)(sec)$^{1/2}$	β/α cal/cm^2(sec)$^{1/2}$
1	0.000909	0.0322	35.5
2	0.000650	0.0327	50.3
3	0.000652	0.0330	50.6
4	0.000791	0.0394	49.8

Figure 32. Plot to determine corrections for slight bridge unbalance in β calibration of gage 4

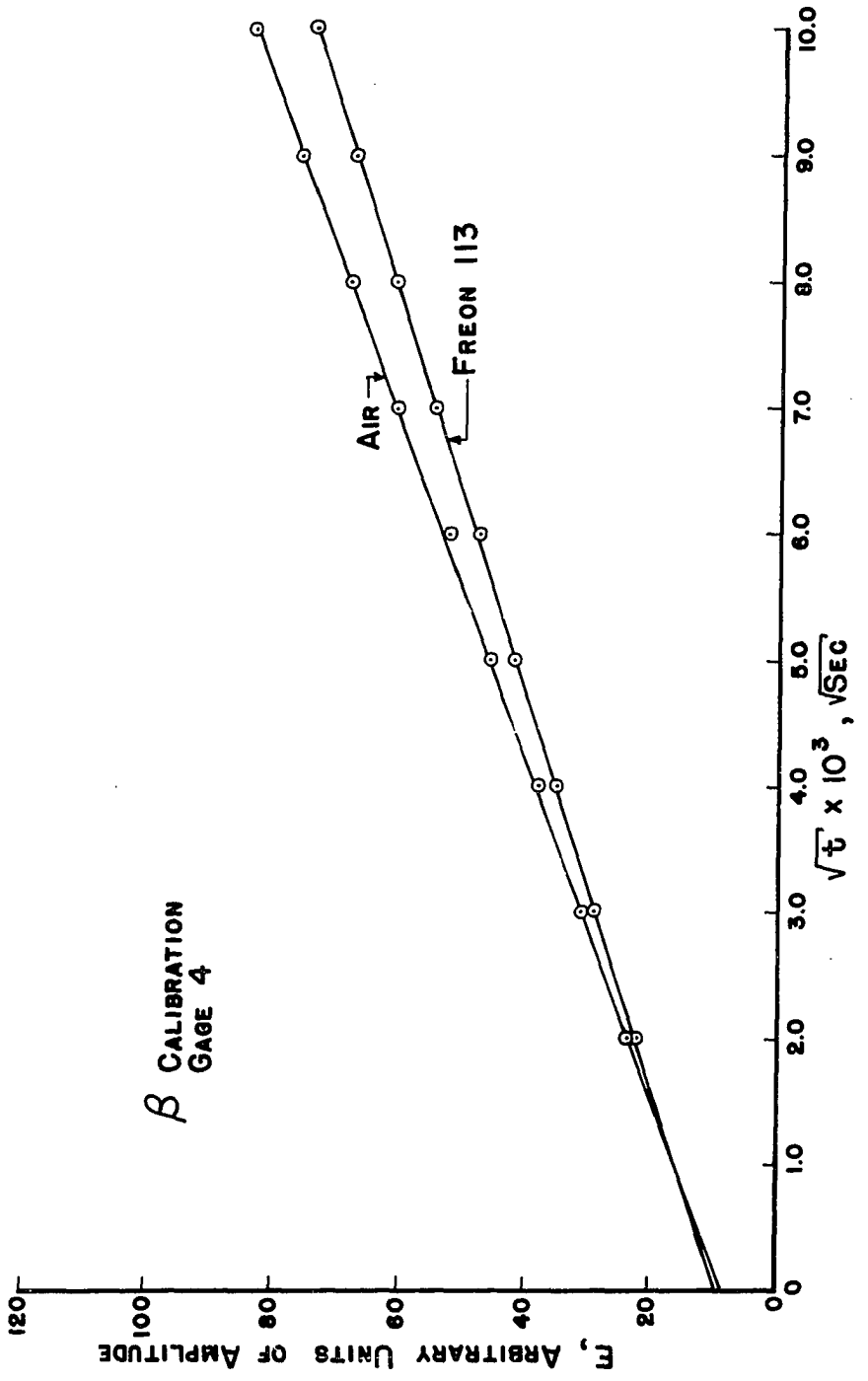
β CALIBRATION
GAGE 4
AIR
FREON 113
E, ARBITRARY UNITS OF AMPLITUDE
√t x 10³, √SEC
0
20
40
60
80
100
120
1.0
2.0
3.0
4.0
5.0
6.0
7.0
8.0
9.0
10.0

APPENDIX C: PRECISION OF RESULTS

Method of Calculation

The precision or measure of uncertainty of the results has been estimated using a procedure suggested by Kline and McClintock (73) and Beers (74) for single sample experiments. For an equation of the form

$$R = R(x_1, x_2, \ldots, x_n) \tag{C-1}$$

where R is a dependent variable calculated from independent variables $(x_1, x_2, \ldots, x_n)$, the uncertainty interval (W_R) of the result (R) is given (73,74) by the following "propagation" equation.

$$(W_R)^2 = \left(\frac{\partial R}{\partial x_1} W_{x_1}\right)^2 + \left(\frac{\partial R}{\partial x_2} W_{x_2}\right)^2 + \ldots + \left(\frac{\partial R}{\partial x_n} W_{x_n}\right)^2 \tag{C-2}$$

The restrictions on using the propagation equation are that the measured x variables must be completely independent of one another and that the same type of uncertainty interval is used consistently throughout the equation. For example, if the type of uncertainty interval desired on R is standard deviation, then standard deviations must be used for the uncertainty intervals on x variables.

The value of precision or uncertainty interval represents a range the experimenter believes the value of the variable to be within according to a specified probability level. Herein 20-to-1 odds are set (95% probability) that the value of the variable is within the range (uncertainty interval) given.

The uncertainty intervals $W_{x_1}, W_{x_2}, \ldots, W_{x_n}$ of the independent variables are estimated by the experimenter. They depend on the quality and accuracy of the measuring instruments and on the judgment of the

experimenter.

When R has the special form

$$R = (\text{constant})(x_1^{p_1} x_2^{p_2} \ldots x_n^{p_n}) \tag{C-3}$$

where p_1, p_2, ..., p_n are given numbers and may be positive, negative or zero, the propagation equation reduces to the following convenient form.

$$\left(\frac{W_R}{R}\right)^2 = \left(p_1 \frac{W_{x_1}}{x_1}\right)^2 + \left(p_2 \frac{W_{x_2}}{x_2}\right)^2 + \ldots + \left(p_n \frac{W_{x_n}}{x_n}\right)^2 \tag{C-4}$$

In this relation W_x/x represents the fractional uncertainty or the percent uncertainty.

Shock-Wave Mach Number

The shock-wave Mach number M_s was calculated by the following relation.

$$M_s = \frac{u_1}{a_1} = \frac{\Delta x/\Delta t}{\sqrt{\gamma g_c R T_1}} = \frac{\Delta x \sqrt{M}}{\sqrt{g_c R_u}\, \Delta t \sqrt{\gamma} \sqrt{T_1}} \tag{C-5}$$

Since R_u and g_c are universal contants assumed to have negligible uncertainty compared to other terms only the uncertainties of Δx, Δt, T_1, γ, and M need be considered and the propagation equation reduces to

$$\left(\frac{W_{M_s}}{M_s}\right)^2 = \left(\frac{W_{\Delta x}}{\Delta x}\right)^2 + \left(\frac{W_{\Delta t}}{\Delta t}\right)^2 + \frac{1}{4}\left[\left(\frac{W_M}{M}\right)^2 + \left(\frac{W\gamma}{\gamma}\right)^2 + \left(\frac{W_{T_1}}{T_1}\right)^2\right] \tag{C-6}$$

The percent uncertainty on Δx and Δt are estimated to be $\pm$ 2% while percent uncertainty on M, γ, and T are estimated to the $\pm$ 1%. Substitution of these values into Equation C-6, yields slightly less that $\pm$ 3% for the percent uncertainty on shock-wave Mach number. For example, this means that for a nominal M_s value of 4.5 (the midrange of these experiments) the uncertainty interval is $\pm$ 0.13. Thus, there is a 95% probability (20-to-1

odds) that M_s is actually within the range 4.50 ± 0.13. By dropping the hundreds digit shock-wave Mach numbers are then known to the nearest tenth (i.e., $M_s = 4.5 \pm 0.1$). Thus a tenth should be the smallest scale division used on the M_s scale of a plot so that the data would not be distorted by any peculiar plotting technique.

Heat-Transfer Rates

The heat-transfer rates in this investigations have been calculated by the following relation

$$q(t_n) = \frac{2}{\sqrt{\pi}\,\alpha E_f}\left[\sum_{i=1}^{n} \frac{E(t_i) - E(t_{i-1})}{\sqrt{t_n - t_i} + \sqrt{t_n - t_{n-1}}}\right] = \frac{2\beta}{\sqrt{\pi}\,\alpha E_f}\,\mathrm{SUM} \tag{C-7}$$

where α and β are experimentally determined calibration factors as explained in Appendix B, E_f is the nominal value of voltage supplied to the heat-flux gage, and SUM is found by performing the summation indicated on digital data as read from enlarged oscilloscope recordings. In view of Equation C-7, the propagation equation for heat-transfer rates becomes

$$\left(\frac{W_q}{q}\right)^2 = \left(\frac{W_\beta}{\beta}\right)^2 + \left(\frac{W_\alpha}{\alpha}\right)^2 + \left(\frac{W_{E_f}}{E_f}\right)^2 + \left(\frac{W_{SUM}}{SUM}\right)^2 \tag{C-8}$$

Since α and β are determined from plots of measured data their uncertainties are estimated to be $\pm$ 5%. The uncertainty on E_f as measured by a voltmeter was taken to be the manufacturerer's stated voltmeter precision of $\pm$ 2%. The uncertainty on SUM was taken as $\pm$ 5% although by checking a special case, where heat-transfer rate could be directly calculated for comparison, better than $\pm$ 3% was obtained. Substitution of these

uncertainty values into Equation C-8 yields an uncertainty of less than $\pm$ 9%. This uncertainty will be used in the next section for calculation of correlation parameter uncertainty.

Correlation Parameter

The correlation parameter CP can be written in terms of measured or calculated values as given below by using $x_\infty = u_1 t_\ell$, $\rho_1 u_1 = \rho_2 u_2$ and $p_1 = \rho_1 R_u T/M$ in Equations 76 and 77

$$CP = (St\sqrt{Re})_t = \frac{q_t \sqrt{T_1}\sqrt{t_\ell}\sqrt{R_u}}{(\Delta h)\sqrt{P_1}\sqrt{M}\sqrt{\mu_2}} \tag{C-9}$$

With R_u taken as a universal constant with negligible uncertainty compared to the other terms, the propagation equation becomes

$$\left(\frac{W_{CP}}{CP}\right)^2 = \left(\frac{W_q}{q}\right)^2 + \left(\frac{W_{\Delta h}}{\Delta h}\right)^2 + \frac{1}{4}\left[\left(\frac{W_M}{M}\right)^2 + \left(\frac{W_{t_\ell}}{t_\ell}\right)^2 + \left(\frac{W_{\mu_2}}{\mu_2}\right)^2 + \left(\frac{W_{p_1}}{p_1}\right)^2 + \left(\frac{W_{T_1}}{T_1}\right)^2\right] \tag{C-10}$$

Values of P_1, T_1, and M are measured or calculated with an uncertainty of $\pm$ 1% or better. Laboratory time increment t_ℓ has the same uncertainty of $\pm$ 2% as previously used Δt in the shock-wave Mach number uncertainty calculation. Values of Δh and μ_2 depend on calculations of free-stream flow properties for a given M_s and are therefore assumed to have the same uncertainty as M_s at $\pm$ 3%. Substitution of these estimated uncertainties, and that previously calculated for q, in Equation C-10 yields an uncertainty of less than $\pm$ 10% for the correlation parameter. The largest portion of this uncertainty is due to the uncertainty in heat-transfer rate as can be surmised from Equation C-10. At a nominal value of 1.00

(the approximate midrange of these experiments) the uncertainty interval becomes $\pm$ 0.10 and by dropping the hundredths digit this nominal value becomes 1.0 $\pm$ 0.1 with 95% probability. Thus, to prevent distortion of the correlation parameter when plotting such data, a least scale division of 0.1 should probably be used.

APPENDIX D: SPECIAL DERIVATIONS

Heat-Flux Equation for Computer Reduction

Equation 46 can be reduced to an expression convenient for computer solution by first noting that for a continuous function E(t) one may write

$$I(t_m) = \frac{1}{2}\int_0^{t_m} \frac{E(t_m) - E(t)}{(t_m - t)^{3/2}} = \frac{1}{2}\sum_{i=1}^{m}\int_{t_{i-1}}^{t_i} \frac{E(t_m) - E(t)}{(t_m - t)^{3/2}}\,dt \qquad \text{(D-1)}$$

where $0 \leq t \leq t_m$. Using the concept of the Mean Value theorem (80) one may replace the continuous function E(t) by the piecewise linear approximation

$$E(t) \simeq E(t_{i-1}) + \left[\frac{E(t_i) - E(t_{i-1})}{(t_i - t_{i-1})}\right](t - t_{i-1}) \qquad \text{(D-2)}$$

where i takes on integer values from 1 to m and the increments of time are unequally chosen to allow versatility in approximating the continuous function by the piecewise linear function. Substitution of Equation D-2 into Equation D-1 yields

$$I(t_m) = \frac{1}{2}\sum_{i=1}^{m}\int_{t_{i-1}}^{t_i} \frac{1}{(t_m - t)^{3/2}}\left\{E(t_m) - E(t_{i-1}) - \left[\frac{E(t_i) - E(t_{i-1})}{(t_i - t_{i-1})}\right](t - t_{i-1})\right\}dt$$

$$= \frac{1}{2}\sum_{i=1}^{m}\left\{\left[E(t_m) - E(t_{i-1})\right]\int_{t_{i-1}}^{t_i} \frac{dt}{(t_m - t)^{3/2}}\right\}$$

$$- \frac{1}{2}\sum_{i=1}^{m}\left[\frac{E(t_i) - E(t_{i-1})}{(t_i - t_{i-1})}\right]\int_{t_{i-1}}^{t_i} \frac{(t - t_{i-1})dt}{(t_m - t)^{3/2}} \qquad \text{(D-3)}$$

The first integral in Equation D-3 may be directly integrated to yield

$$\int_{t_{i-1}}^{t_i} \frac{dt}{(t_m-t)^{3/2}} = 2(t_m-t)^{-\frac{1}{2}} \Big|_{t_{i-1}}^{t_i} = 2\{\frac{1}{\sqrt{t_m-t_i}} - \frac{1}{\sqrt{t_m-t_{i-1}}}\} \qquad \text{(D-4)}$$

The second integral in Equation D-3 may be integrated by parts to yield

$$\int_{t_{i-1}}^{t_i} \frac{(t-t_{i-1})dt}{(t_m-t)^{3/2}} = \frac{2(t-t_{i-1})}{(t_m-t)^{1/2}} \Big|_{t_{i-1}}^{t_i} - 2\left(-2(t_m-t)^{1/2}\Big|_{t_{i-1}}^{t_i}\right)$$

$$= 2\{\frac{(t_i-t_{i-1})}{\sqrt{t_m-t_i}} + 2(\sqrt{t_m-t_i} - \sqrt{t_m-t_{i-1}})\} \qquad \text{(D-5)}$$

By noting $A-B = (A^2-B^2)/(A+B)$ one obtains

$$\sqrt{t_m-t_i} - \sqrt{t_m-t_{i-1}} = \frac{(t_i - t_{i-1})}{\sqrt{t_m-t_i} + \sqrt{t_m-t_{i-1}}} \qquad \text{(D-6)}$$

Substitution of Equation D-6 into Equation D-5 and subsequent substitution of Equations D-5 and D-4 into Equation D-3 yields

$$I(t_m) = \sum_{i=1}^{m} \{[\frac{E(t_m)-E(t_{i-1})}{\sqrt{t_m-t_i}} - \frac{E(t_m) - E(t_{i-1})}{\sqrt{t_m-t_{i-1}}}]$$

$$- [\frac{E(t_i) - E(t_{i-1})}{(t_i-t_{i-1})}][\frac{t_i-t_{i-1}}{\sqrt{t_m-t_i}} - \frac{2(t_i-t_{i-1})}{\sqrt{t_m-t_i} + \sqrt{t_m-t_{i-1}}}]\} \qquad \text{(D-7)}$$

Appropriate cancellation and regrouping of terms yields

$$I(t_m) = \sum_{i=1}^{m} \left\{\frac{E(t_m)-E(t_i)}{\sqrt{t_m-t_i}}\right\} - \sum_{i=1}^{m} \frac{E(t_m)-E(t_{i-1})}{\sqrt{t_m-t_{i-1}}}$$

$$+ 2 \sum_{i=1}^{m} \left\{\frac{E(t_i) - E(t_{i-1})}{\sqrt{t_m-t_i} + \sqrt{t_m-t_{i-1}}}\right\} \qquad \text{(D-8)}$$

The first summation in Equation D-8 has a term that is indeterminate when i=m, however, use of L'Hospital's rule indicates it is zero as follows

$$\lim_{t_i \to t_m} \frac{E(t_m)-E(t_i)}{\sqrt{t_m-t_i}} = \lim_{t_i \to t_m} \left(- 2E'(t_i) \sqrt{t_m-t_i} \right) = 0 \qquad \text{(D-9)}$$

Using the result of Equation D-9 it may be noted that the first two summations in Equation D-8 cancel except for a single term to yield the following result

$$I(t_m) = \left[\sum_{i=1}^{m} \left\{\frac{E(t_i) - E(t_{i-1})}{\sqrt{t_m-t_i} + \sqrt{t_m-t_{i-1}}}\right\}\right] - \left[\frac{E(t_m) - E(t_o)}{\sqrt{t_m-t_o}}\right] \qquad \text{(D-10)}$$

In this investigation $t_o=0$ and $E(t_o)=0$ so that substitution into Equation D-10 as shown yields the following equation used for digital-computer calculation of heat-transfer rates in this investigation

$$q(o,t) = q(t_m) = \frac{2\beta}{\sqrt{\pi}\, I\alpha R_o} \left[\sum_{i=1}^{m} \left\{\frac{E(t_i) - E(t_{i-1})}{\sqrt{t_m-t_i} + \sqrt{t_m-t_{i-1}}}\right\}\right] \qquad \text{(D-11)}$$

An approach somewhat similar to that above was used by Cook and Felderman (55) to obtain a result for the special case of equal time increments.

Boundary-Layer Thickness

To determine boundary-layer thickness δ as a function of distance from the shock wave one may use Von Karman's integral technique as illustrated in Reference 70. With this technique one considers a two-dimensional region of fluid including the boundary layer and having differential length dx. Newton's second law is applied to the region so that forces acting on the region boundaries may be related to the rate of momentum change within the region. This results in the following integral momentum equation for zero pressure gradient where fluid properties are assumed to be appropriate averages and treated as constants throughout this equation.

$$\frac{\partial}{\partial x}\int_{o}^{\delta} u(u-u_e)dy = -\nu\left(\frac{\partial u}{\partial y}\right)_w = -\frac{\tau_w}{\rho} \qquad \text{(D-12)}$$

The Pohlhausen approach (70) is now taken by assuming the following polynomial for the boundary-layer velocity profile

$$u = c_o + c_1 y + c_2 y^2 + c_3 y^3 \qquad \text{(D-13)}$$

where c_o, c_1, c_2 and c_3 are constants to be determined from the following boundary conditions.

$$\begin{aligned} &\text{i)}\ u = u_w \text{ at } y = 0 \\ &\text{ii)}\ u = u_e \text{ at } y = \delta \\ &\text{iii)}\ \frac{\partial u}{\partial y} = 0 \text{ at } y = \delta \\ &\text{iv)}\ \frac{\partial^2 u}{\partial y^2} = 0 \text{ at } y = 0 \end{aligned} \qquad \text{(D-14)}$$

The boundary conditions given in Equation D-14 apply to shock-tube

boundary layers and allow Equation D-13 to become

$$\frac{u-u_w}{u_e-u_w} = \frac{3}{2}\left(\frac{y}{\delta}\right) - \frac{1}{2}\left(\frac{y}{\delta}\right)^3 \qquad \text{(D-15)}$$

Equation D-12 is now manipulated so Equation D-15 may be conveniently substituted as follows

$$\frac{\partial}{\partial x}\int_o^\delta u(u-u_e)dy = \frac{\partial}{\partial x}\int u\{(u-u_w) - (u_e-u_w)\}dy = -\frac{\tau_w}{\rho}$$

$$= \frac{\partial}{\partial x}\int_o^\delta \frac{(u-u_w)}{(u_e-u_w)}\left\{\frac{(u-u_w)}{u_e-u_w} - 1\right\}\ (u_e-u_w)^2\ dy$$

$$+ \frac{\partial}{\partial x}\int_o^\delta u_w\left\{\frac{(u-u_w)}{(u_e-u_w)} - 1\right\}\ (u_e-u_w)\ dy$$

$$= \frac{\partial}{\partial x}\left[(u_e-u_w)^2\int_o^\delta \left\{\frac{3}{2}\left(\frac{y}{\delta}\right) - \frac{1}{2}\left(\frac{y}{\delta}\right)^3\right\}\left\{\frac{3}{2}\left(\frac{y}{\delta}\right) - \frac{1}{2}\left(\frac{y}{\delta}\right)^3 - 1\right\}dy\right.$$

$$\left. + \{(u_w)(u_e-u_w)\}\int_o^\delta \left\{\frac{3}{2}\left(\frac{y}{\delta}\right) - \frac{1}{2}\left(\frac{y}{\delta}\right)^3 - 1\right\}dy\right] \qquad \text{(D-16)}$$

Performing the indicated integration in Equation D-16 yields

$$-\frac{\tau_w}{\rho} = \frac{\partial}{\partial x}\left[(u_e-u_w)^2\left\{\frac{9\,y^3}{12\,\delta^2} - \frac{3\,y^5}{10\,\delta^4} + \frac{y^7}{28\,\delta^6} - \frac{3y^2}{4\,\delta} + \frac{y^4}{8\,\delta^3}\right\}\Bigg|_0^\delta\right.$$

$$\left. + (u_w)(u_e-u_w)\left\{\frac{3\,y^2}{4\,\delta} - \frac{y^4}{8\,\delta^3} - y\right\}\Bigg|_0^\delta\right]$$

$$= \frac{\partial}{\partial x}\left[(u_e-u_w)^2\left(-\frac{39}{280}\,\delta\right) + (u_w)(u_e-u_w)\left(-\frac{3}{8}\,\delta\right)\right]$$

$$= \frac{\partial}{\partial x}\left[(u_e-u_w)\left(\frac{\delta}{280}\right)(-39\,u_e - 66\,u_w)\right]$$

$$= -\frac{(u_e-u_w)\,(39\,u_e + 66\,u_w)}{280}\,\frac{d\delta}{dx} \qquad \text{(D-17)}$$

Combination of Equation D-15 with the right-hand side of Equation D-12 yields

$$-\frac{\tau_w}{\rho} = -\nu\left(\frac{\partial u}{\partial y}\right)_w = -\frac{3(u_e-u_w)\nu}{2\delta} \qquad \text{(D-18)}$$

so that Equation D-17 becomes

$$\frac{3}{2}\,\frac{\nu}{\delta} = \frac{(39\,u_e + 66\,u_w)}{280}\,\frac{d\delta}{dx}$$

or

$$\delta\frac{d\delta}{dx} = \frac{140\,\nu}{(13\,u_e + 22\,u_w)} = \frac{140\,\nu}{13\,u_e\left\{1 + \dfrac{22\,u_w}{13\,u_e}\right\}} \qquad \text{(D-19)}$$

Equation D-19 may be integrated directly to yield

$$\frac{\delta^2}{2} = \frac{140\ \nu x}{13\ u_e \left\{1 + \frac{22\ u_w}{13\ u_e}\right\}} + c \qquad \text{(D-20)}$$

The boundary-layer thickness is zero at an x of zero and the integration constant c is therefore zero. Using the definition of Reynolds number Re and dimensionless velocity U in Equation D-20 yields

$$\frac{\delta}{x} = \frac{\sqrt{280/13}}{\sqrt{Re_x}\sqrt{1 + (22/13)U}} = \frac{a}{\sqrt{Re_x}\sqrt{1 + b\ U}} \qquad \text{(D-21)}$$

The form of Equation D-21 is important in that it is consistent regardless of the degree of polynomial chosen in Equation D-13. Only the values of constants a and b change with polynomial degree. For example, when a first degree (linear) polynomial is chosen the constants a and b become $\sqrt{12}$ and 2 respectively while for the third degree polynomial used herein they become 4.64 and 1.693 respectively in Equation D-21. The value of a turns out to be the same as for conventional flat-plate flow. The denominator factor $\sqrt{1 + bU}$ is always larger than one, therefore, Equation D-21 indicates a shock-tube boundary layer will always be thinner than the corresponding conventional flat-plate flow since, except for this factor, Equation D-21 is the result for such conventional flat-plate flow (70).

A similar approach to that indicated above was attempted on the integral-energy equation to determine the thickness Δ of the thermal boundary layer. The integral-energy equation and assumed third degree temperature profile are, respectively,

$$\frac{\partial}{\partial x}\int_0^{\Delta}(T_e-T)u\,dy + \frac{\nu}{c_p}\int_0^{\Delta}\left(\frac{\partial u}{\partial y}\right)^2 dy = K\left(\frac{\partial T}{\partial y}\right)_w \qquad \text{(D-22)}$$

$$\frac{T-T_w}{T_e-T_w} = \frac{3}{2}\left(\frac{y}{\Delta}\right) - \frac{1}{2}\left(\frac{y}{\delta}\right)^3 \qquad \text{(D-23)}$$

Proceeding in a manner similar to that used to find δ from the integral momentum equation yielded the following non-linear differential equation

$$\left[C_1\Delta + \frac{C_2\Delta^2}{\sqrt{x}} + \frac{C_3\Delta^2}{x} + \frac{C_4\Delta^4}{x\sqrt{x}} + \frac{C_5\Delta^4}{x^2} + \frac{C_6\Delta^6}{x^3}\right]\frac{d\Delta}{dx} = C_7 \qquad \text{(D-24)}$$

where C_1 through C_7 are appropriate constants with respect to x. No attempts were made to solve this equation for Δ because of its nature. Instead, δ was used for a characteristic boundary-layer thickness in this investigation. However, further work might include solving Equation D-24 numerically or finding a valid simplifying assumption so that it may be solved analytically.

APPENDIX E: FLOW DIAGRAMS AND COMPUTER PROGRAMS

Figure 33. Block diagram for computer calculation of heat-transfer rates

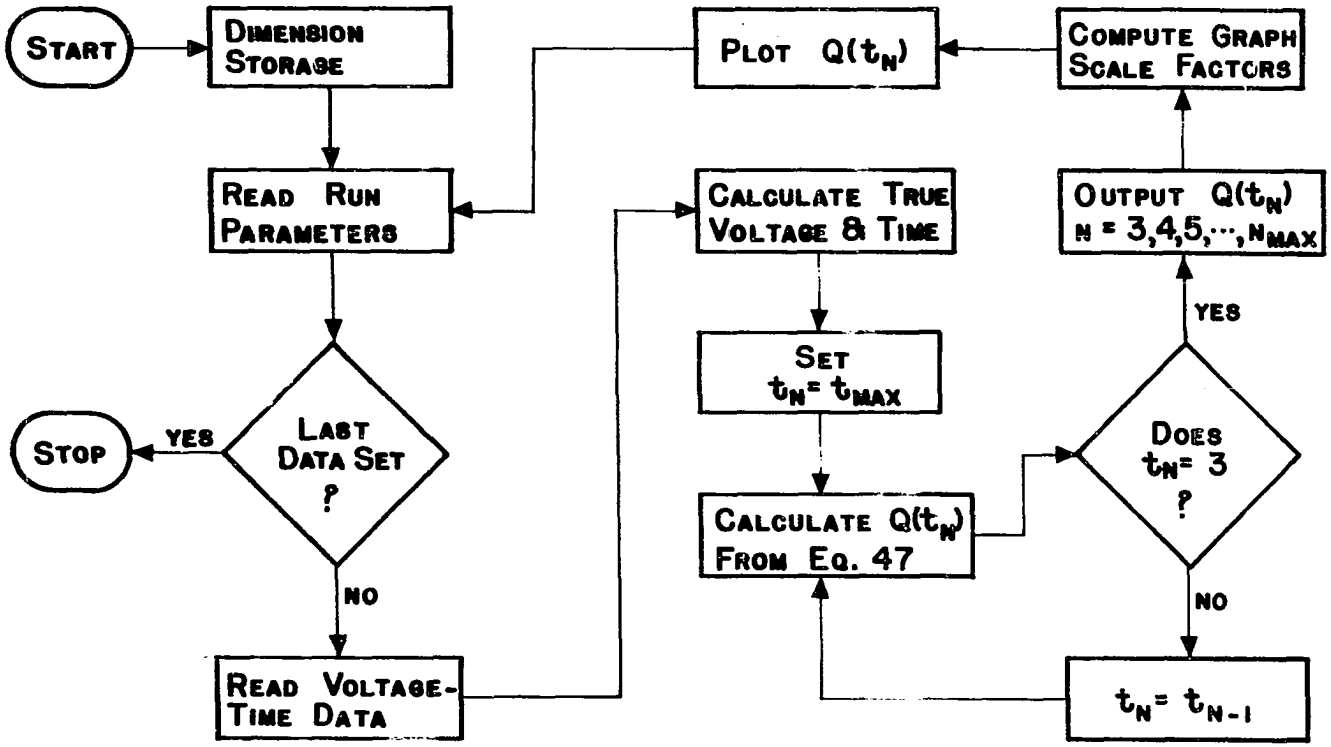
START
DIMENSION STORAGE
READ RUN PARAMETERS
READ VOLTAGE-TIME DATA
LAST DATA SET ?
YES
STOP
NO
CALCULATE TRUE VOLTAGE & TIME
SET $t_N = t_{MAX}$
CALCULATE $Q(t_N)$ FROM EQ. 47
DOES $t_N = 3$?
YES
NO
$t_N = t_{N-1}$
OUTPUT $Q(t_N)$ $N = 3,4,5,\cdots,N_{MAX}$
COMPUTE GRAPH SCALE FACTORS
PLOT $Q(t_N)$

```
BEGIN COMPILATION
      C     HEAT TRANSFER RATES
S.0001        DIMENSION TA(99),VA(99),T(99),V(99),RT(99),CN(5),
             1RTY(99),QC(99),QCSQ(99),QA(99),QB(99),AXTEMP(99),
             2AXISX(5),AXISY(5),AXISZ(5),X(99),Y(99),Z(99)
S.0002        READ(1,105)(AXISX(I),I=1,5),(AXISY(I),I=1,5),(AXISZ(I),I=1,5)
S.0003      105 FORMAT(15A4)
S.0004       11 READ(1,100)(CN(J),J=1,5),BOA,REF,VS,VSF,HSF,TN
S.0005      100 FORMAT(5A4,6F10.4)
S.0006        WRITE (3,300)
S.0007      300 FORMAT (1H1)
S.0008        IF(TN)13,13,1
S.0009        1 WRITE(3,301)(CN(J),J=1,5),BOA,REF,VS,VSF,HSF,TN
S.0010      301 FORMAT(3X,'RUNCODE',2X,'TRACE',4X,'BETA/ALPHA',3X,'RECIPEF',2X,
             1'VERTSENS',1X,'V SCALE F',2X,'H SCALE F',2X,'POINTS'/5A4,6F10.4//)
S.0011        N=TN
S.0012        READ(1,102)(TA(I),VA(I),I=1,N)
S.0013      102 FORMAT(8F10.4)
S.0014        DO 2 I=1,N
S.0015        T(I)=TA(I)/HSF
S.0016        V(I)=VA(I)*VS/VSF
S.0017        2 AXTEMP(I)=V(I)*REF
S.0018        WRITE(3,303)
S.0019      303 FORMAT(4X,'V(MV)',4X,'T(USEC)',3X,'SQRT T',11X,'QC',13X,'QB',13X,
             1'QA',9X,'QCSQ',9X,'VA',8X,'TA',9X,'A*TEMP')
S.0020       10 TT=T(N)
```

Figure 34. Computer program for heat-transfer rates

```
S.0021          RTZ=SQRT(TT)
S.0022          RTY(N)=RTZ
S.0023          DO 3 I=2,N
S.0024          IF(TT-T(I-1)) 11,11,3
S.0025        3 RT(I-1)=SQRT(TT-T(I-1))
S.0026          S=0
S.0027          MM=N-1
S.0028          DO 4 I=2,MM
S.0029        4 S=(V(I)-V(I-1))/(RT(I)+RT(I-1))+S
S.0030          BRCKT=S+(V(1)/(RT(1)+RTZ))+((V(N)-V(N-1))/RT(N-1))
S.0031          QC(N)=1.12838*REF*RCA*BRCKT
S.0032          QCSQ(N)=QC(N)*QC(N)
S.0033          QW(N)=4.18600*QC(N)
S.0034          QB(N)=0.88056*QW(N)
S.0035          WRITE(3,304)V(N),T(N),RTY(N),QC(N),QB(N),QW(N),QCSQ(N),VA(N),
               1TA(N),AXTEMP(N)
S.0036      304 FORMAT(3F10.4,3F15.4,E15.7,3F10.4)
S.0037          N=N-1
S.0038          IF(N-2) 12,12,10
S.0039       12 NPTS=TN-2
S.0040          DO 85 N=1,NPTS
S.0041          X(N)=T(N+2)
S.0042          Y(N)=QC(N+2)
S.0043       85 Z(N)=RTY(N+2)
S.0044          NPTS=NPTS-5
S.0045          LRX=X(NPTS)/10.0
S.0046          XSCL=LRX+1.0
S.0047          XSCLP1=XSCL+1.0
S.0048          LRY=Y(3)/10.0
```

Figure 34. (Continued)

```
S.0049          YSCL=LBY+1.0
S.0050          IF(YSCL-10.0)23,23,33
S.0051       33 YSCL=10.0
S.0052          GO TO 53
S.0053       23 IF(YSCL-5.0)43,43,53
S.0054       43 YSCL=2.0*YSCL
S.0055          DY=5.0
S.0056          GO TO 63
S.0057       53 DY=10.0
S.0058       63 DX=10.0
S.0059          XOR=0.0
S.0060          YOR=0.0
S.0061          KS=12
S.0062          MODE=11
S.0063          CALL GRAPH(NPTS,X,Y,KS,MODE,XSCL,YSCL,DX,XOR,DY,YOR,
                1AXISX,AXISY,AXISZ,CN)
S.0064          GO TO 11
S.0065       13 STOP
S.0066          END
                   SIZE OF COMMON  00000     PROGRAM  07926
END OF COMPILATION  MAIN
        COMPILATION TIME WAS    0002.58  SECONDS
```

Figure 34. (Continued)

Figure 35. Block diagram for computer calculation of flow properties, induction times and dimensionless variables

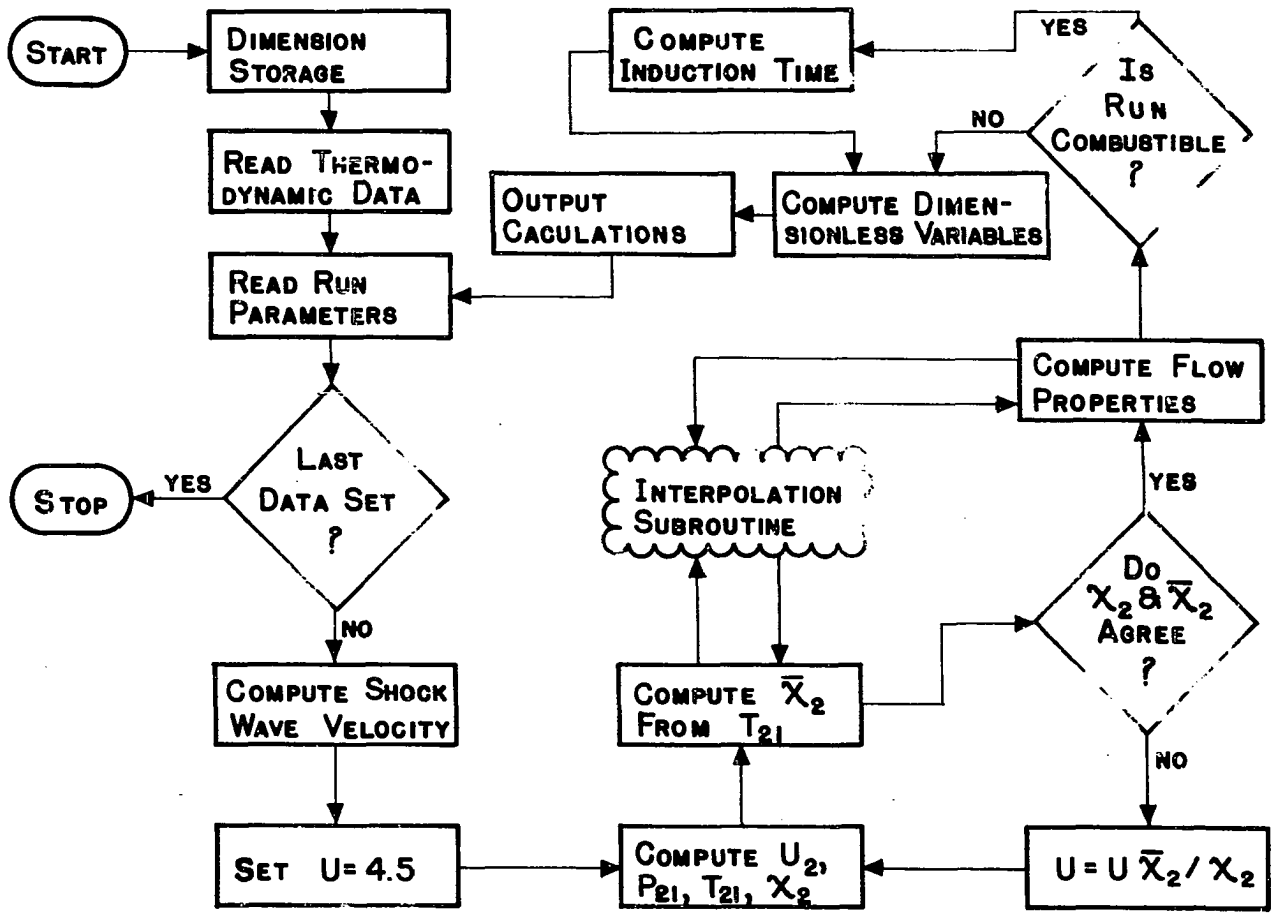
START
DIMENSION STORAGE
READ THERMO-DYNAMIC DATA
READ RUN PARAMETERS
LAST DATA SET ?
YES
STOP
NO
COMPUTE SHOCK WAVE VELOCITY
SET U= 4.5
COMPUTE U_2, P_{21}, T_{21}, χ_2
COMPUTE $\bar{\chi}_2$ FROM T_{21}
INTERPOLATION SUBROUTINE
$U = U\,\bar{\chi}_2 / \chi_2$
DO χ_2 & $\bar{\chi}_2$ AGREE ?
YES
NO
COMPUTE FLOW PROPERTIES
IS RUN COMBUSTIBLE ?
YES
NO
COMPUTE INDUCTION TIME
COMPUTE DIMEN-SIONLESS VARIABLES
OUTPUT CACULATIONS

```
BEGIN COMPILATION
S.0001      DIMENSION TA(4),HSF(4),T(4),VS(4),CN(6),H(10),VIS(10),THC(10),
           1DPR(10),DLE(10),DH(10),DCHI(10),QT(4),TT(4),DRE2S(4),DRESS(4),
           2DRE2U(4),DRESU(4),DST2S(4),DST2U(4),RTRE2S(4),RTRESS(4),RTRE2U(4),
           3RTRESU(4),COR2S(4),CORSS(4),COR2U(4),CORSU(4),XX(4),RTXX(4),QW(4),
           4TW(4),X(40),XL(40),IG(2,40),DIST(4),IRRAY(20),TIR(4),IX(40),
           5DSTSS(4),DSTSU(4),DELQX(4),DRE2D(4),COR2D(4),RTRE2D(4)
S.0002      READ(1,109) (IRRAY(I),I=1,20)
S.0003    109 FORMAT(20A1)
S.0004      1 READ(1,100) (H(I),I=1,10),(VIS(I),I=1,10),(THC(I),I=1,10)
S.0005    100 FORMAT(10F8.2)
S.0006      READ(1,110) VELH2,PD1,ICK
S.0007    110 FORMAT(F8.4,I1,I1)
S.0008      IQ2=0
S.0009      READ(1,101) (DPR(I),I=1,10),(DLE(I),I=1,10)
S.0010    101 FORMAT(10F8.4)
S.0011      IF(DPR(1))2,99,2
S.0012      2 READ(1,103) (CN(I),I=1,6),DT,T1,GRS,WMRS,G,WM
S.0013    103 FORMAT(A1,A4,A3,F4.1,2A4,6F10.4)
S.0014      WRITE(3,300)
S.0015    300 FORMAT(1H1)
S.0016      WRITE(3,301) (CN(I),I=1,5),DT,T1,GRS,WMRS,G,WM
S.0017    301 FORMAT(4X,'CODE NUMBER',9X,'DT',8X,'T1',8X,'GRS',6X,'WMRS',8X,
           2'G',9X,'M'/A1,A4,A3,2X,F4.1,2X,A4,6F10.4)
S.0018      IF(DT) 1,1,3
S.0019      3 READ(1,104) (TA(I),HSF(I),I=1,4),(QT(I),TT(I),I=1,4)
S.0020    104 FORMAT(8F10.4)
S.0021      WRITE(3,302) (QT(I),TT(I),I=1,4)
S.0022    302 FORMAT(1HO,4X,'QT1',7X,'TT1',7X,'QT2',7X,'TT2',7X,'QT3',7X,'TT3',
           27X,'QT4',7X,'TT4'/8F10.4)
```

Figure 36. Computer program for flow property calculations

```
S.0023          DO  4  I=1,4
S.0024        4 T(I)=((TA(I)/HSF(I))+DT)
S.0025          DO  5  I=1,10
S.0026          DH(I)=((B(I)*WM)/(1.98726*T1))
S.0027        5 DCHI(I)=DH(I)-DH(I)
S.0028          DH1=DH(1)
S.0029          DT21=T(2)-T(1)
S.0030          DT43=T(4)-T(3)
S.0031          VS(4)=43.C/DT43
S.0032          VS(2)=44.5/DT21
S.0033          AVS=(VS(2)+VS(4))/2.0
S.0034          ASQ=(0.00831877*G*T1/WM)
S.0035          A=SQRT(ASQ)
S.0036          B=SQRT(G)
S.0037          SM=AVS/A
S.0038          U1=SM*3
S.0039          RHO21=4.5
S.0040        9 U=RHO21
S.0041          U2=U1/U
S.0042          P21=(1.0+(U1*U1)-(U*U2*U2))
S.0043          T21=P21/U
S.0044          DCHI2=0.5*(U1*U1-U2*U2)
S.0045          CALL  DIFIT(DCHI,T21,DCHIC)
S.0046          DCHIR=DCHIC/DCHI2
S.0047          IF(ABS(DCHIR-1.C)-C.CCC5)11,11,10
S.0048       10 RHO21=DCHIR*RHO21
S.0049          GO  TO  9
```

Figure 36. (Continued)

```
S.0050        11 P1=CN(4)
S.0051           P2=P21*P1
S.0052           T2=T21*T1
S.0053           RHO1=0.0CCC1602267*P1*WM/T1
S.0054           RHO2=RHO21*RHO1
S.0055           RHOW=RHO2*T21
S.0056           WRITE(3,303) VS(2),VS(4),AVS,SM,U1,U2,A,B
S.0057       303 FORMAT(1HC,4X,'VS2',7X,'VS4',7X,'AVS',7X,'SM',8X,'U1',8X,'U2',9X,
                2'A',6X,'SQRT G'/8F10.4)
S.0058           WRITE(3,304) P21,P2,T21,T2,RHO21,RHO2,RHOW
S.0059       304 FORMAT(1HC,4X,'P21',7X,'P2',8X,'T21',7X,'T2',7X,'RHO21',10X,
                2'RHO2',12X,'RHOW '/5F10.4,2E15.8)
S.0060           DH2=DCH12+DH1
S.0061           DHC=DH2+U2*U2/2.0
S.0062           CALL DIFIT(VIS,T21,VIS2)
S.0063           CALL DIFIT(THC,T21,THC2)
S.0064           CALL DIFIT(DPR,T21,DPR2)
S.0065           CALL DIFIT(DLE,T21,DLE2)
S.0066           CE=VIS2/(VIS(1)*T21)
S.0067           DHRM=DH2+((U-1.0)**2.3)*(U2*U2/2.0)*(DPR2**(0.39-0.023*U))
S.0068           QL=.307301*SQRT(AVS*RHOW*VIS(1)/(2.0*U))*(DHRM-DH1)*(DPR2**(0.43+
                20.022*U))*SQRT(1.0+1.665*U)*(CE**0.29)*(T1/WM)/DPR(1)
S.0069           RF=SQRT(DPR2)
S.0070           RH2=RF
S.0071           WRITE(3,305) DCH12,DHC,DH2,VIS2,THC2,DPR2,DLE2,RF2
S.0072       305 FORMAT(1HC,3X,'DCH12',6X,'DHC',7X,'DH2',6X,'VIS2',6X,'THC2',6X,
                2'DPR2',6X,'DLE2',8X,'RF2'/8F10.4)
S.0073           DHR=DH2+RF*U2*U2/2.0
S.0074           DCHIK=DHR-DH1
S.0075           IF(T21-3.0)12,12,12
```

Figure 36. (Continued)

```
S.0076        12 IF(T21-8.0)13,13,2
S.0077        13 TS1=(T21+1.0)/2.0
S.0078        14 CALL DIFIT(DPR,TS1,DPRS)
S.0079           RFS=SQRT(DPRS)
S.0080           DHS=0.5*(DH2+DH1)+(0.22*RFS*U2*U2/2.0)
S.0081           DCHIS=DHS-DH1
S.0082           CALL DIFIT(DCHI,TS1,DCHISC)
S.0083           DCHISR=DCHIS/DCHISC
S.0084           IF(ABS(DCHISR-1.0)-0.0005)16,16,15
S.0085        15 TS1=TS1*DCHISR
S.0086           IF(TS1-2.0)70,17,17
S.0087        17 GO TO 14
S.0088        16 CALL DIFIT(VIS,TS1,VISS)
S.0089           CALL DIFIT(THC,TS1,THCS)
S.0090           CALL DIFIT(DLE,TS1,DLES)
S.0091           WRITE(3,306) TS1,DHR,DHS,VISS,THCS,DPRS,DLES,RFS
S.0092     306 FORMAT(1HC,4X,'TS1',7X,'DHR',7X,'DHS',6X,'VISS',6X,'THCS',6X,
               2'DPRS',6X,'DLES',7X,'RFS'/8F10.4)
S.0093           IF(ICK)25,25,30
S.0094        30 CALL DTIME(T2,P2,VOLH2,TI2)
S.0095           GO TO 27
S.0096        25 TI2=RHO21*10.0
S.0097        27 TIL=TI2/RHO21
S.0098           DMA2=U1/SQRT(G*U*P21)
S.0099           DCOMB=68315./(1.98726*T1*DHR)
S.0100           DELFAC=SQRT(1.0+1.693*U)
S.0101           QT(3)=QT(4)
S.0102           TT(3)=TT(4)
S.0103           X(13)=TIL
S.0104           X(14)=DELFAC
S.0105           X(15)=(U-1.0)**2.0
```

Figure 36. (Continued)

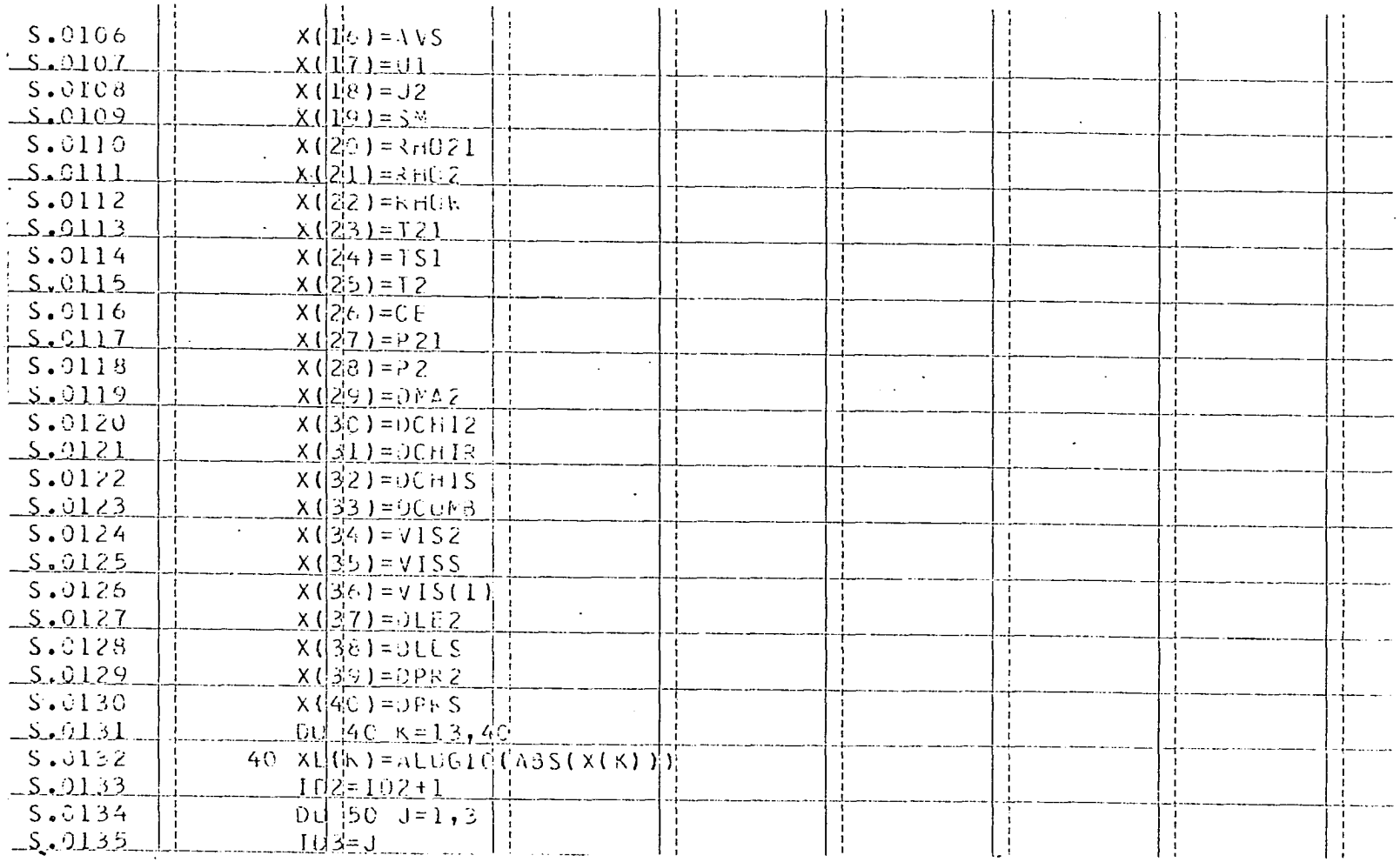

```
S.0106          X(16)=AVS
S.0107          X(17)=U1
S.0108          X(18)=U2
S.0109          X(19)=SM
S.0110          X(20)=RHO21
S.0111          X(21)=RHO2
S.0112          X(22)=RHOK
S.0113          X(23)=T21
S.0114          X(24)=TS1
S.0115          X(25)=T2
S.0116          X(26)=CE
S.0117          X(27)=P21
S.0118          X(28)=P2
S.0119          X(29)=DMA2
S.0120          X(30)=DCH12
S.0121          X(31)=DCH1R
S.0122          X(32)=DCH1S
S.0123          X(33)=DCOMB
S.0124          X(34)=VIS2
S.0125          X(35)=VISS
S.0126          X(36)=VIS(1)
S.0127          X(37)=DLE2
S.0128          X(38)=DLES
S.0129          X(39)=DPR2
S.0130          X(40)=DPRS
S.0131          DO 40 K=13,40
S.0132       40 XL(K)=ALOG10(ABS(X(K)))
S.0133          ID2=ID2+1
S.0134          DO 50 J=1,3
S.0135          ID3=J
```

Figure 36. (Continued)

```
S.0136          DIST(1)=3.30
S.0137          DIST(2)=7.75
S.0138          DIST(3)=18.40
S.0139          TIR(J)=TT(J)/TIL
S.0140          DRE2S(J)=1333.2237*U1*U1*P1*TT(J)/VIS2
S.0141          DRESS(J)=DRE2S(J)*(VIS2/VISS)*(T21/TS1)
S.0142          DRE2U(J)=DRE2S(J)*(U-1.C)**2.C
S.0143          DRESU(J)=DRESS(J)*(U-1.C)**2.0
S.0144          DST2S(J)=C.31397967*QT(J)/((DHF-DH1)*AVS*P1)
S.0145          DST2U(J)=DST2S(J)/(U-1.C)
S.0146          DSTSS(J)=DST2S(J)*TS1/T21
S.0147          DSTSU(J)=DSTSS(J)/(U-1.C)
S.0148          RTRE2S(J)=SQRT(DRE2S(J))
S.0149          RTRESS(J)=SQRT(DRESS(J))
S.0150          RTRE2U(J)=SQRT(DRE2U(J))
S.0151          RTRESU(J)=SQRT(DRESU(J))
S.0152          DELCX(J)=4.64/RTRE2S(J)*DELFAC
S.0153          DRE2D(J)=DRE2S(J)*DELCX(J)
S.0154          RTRE2D(J)=SQRT(DRE2D(J))
S.0155          EXPF2=DPR2**C.6667
S.0156          EXPRS=DPRS**C.6667
S.0157          CDR2S(J)=DST2S(J)*RTRE2S(J)
S.0158          CDRSS(J)=DSTSS(J)*RTRESS(J)*EXPRS
S.0159          CDR2U(J)=DST2U(J)*RTRE2U(J)*EXPR2
S.0160          CDRSU(J)=DSTSU(J)*RTRESU(J)*EXPRS
S.0161          CDR2D(J)=CDR2S(J)*SQRT(DELCX(J))
S.0162          XX(J)=AVS*TT(J)
S.0163          RTXX(J)=SQRT(XX(J))
S.0164          QS(J)=VL/RTXX(J)
S.0165          X(1)=DELCX(J)
S.0166          X(2)=TT(J)
```

Figure 36. (Continued)

```
S.0167          X(3)=TIR(J)
S.0168          X(4)=DRE2L(J)
S.0169          X(5)=DRE2S(J)
S.0170          X(6)=DRESS(J)
S.0171          X(7)=DRE2U(J)
S.0172          X(8)=DRESU(J)
S.0173          X(9)=DST2S(J)
S.0174          X(10)=DSTSS(J)
S.0175          X(11)=DST2U(J)
S.0176          X(12)=DSTSU(J)
S.0177          DO 35 K=1,12
S.0178       35 XL(K)=ALOG10(ABS(X(K)))
S.0179          WRITE(2,201) ID1,ID2,ID3,(XL(M),M=1,10),
                2(ID1,ID2,ID3,(XL(M),M=11,20),
                3(ID1,ID2,ID3,(XL(M),M=21,30),
                4(ID1,ID2,ID3,(XL(M),M=31,40)
S.0180          WRITE(3,201) ID1,ID2,ID3,(XL(M),M=1,10),
                2(ID1,ID2,ID3,(XL(M),M=11,20),
                3(ID1,ID2,ID3,(XL(M),M=21,30),
                4(ID1,ID2,ID3,(XL(M),M=31,40)
S.0181       201 FORMAT('C22801',I1,I2,I1,10(F7.4)/
                2'C22802',I1,I2,I1,10(F7.4)/
                3'C22803',I1,I2,I1,10(F7.4)/
                4'C22804',I1,I2,I1,10(F7.4))
S.0182          WRITE(3,320)(X(I),I=1,40)
S.0183       320 FORMAT(1HC,10E12.5)
S.0184        50 CONTINUE
S.0185          QSOLV=SQRT(3.41593/AVS)*QL
S.0186          TV(1)=T1+QSOLV/32.029
S.0187          TV(2)=T1+QSOLV/32.708
```

Figure 36. (Continued)

```
S.0188          TW(3)=T1+QSQRTV/33.007
S.0189          TW(4)=T1+QSQRTV/39.415
S.0190          ATW=(TW(1)+TW(2)+TW(4))/3.0
S.0191          AQW=(QW(1)+QW(2)+QW(3))/3.0
S.0192          ACOR2S=COR2S(1)+COR2S(2)+COR2S(3)
S.0193          ACOR2S=ACOR2S/3.0
S.0194          ADRE2S=DRE2S(1)+DRE2S(2)+DRE2S(3)
S.0195          ADRE2S=ADRE2S/3.0
S.0196          ADRE2S=SQRT(ADRE2S)
S.0197          WRITE(3,307)(DRE2S(J),DRESS(J),DRE2U(J),DRESU(J),DRE2D(J),
                2DELOX(J),DST2S(J),DSTSS(J),DST2U(J),DSTSU(J),J=1,3)
S.0198        307 FORMAT(1HC,4X,'DRE2S',7X,'DRESS',7X,'DRE2U',7X,'DRESU',7X,
                2'DRE2D',7X,'DELOX',7X,'DST2S',7X,'DSTSS',7X,'DST2U',7X
                3'DSTSU'/(10E12.5))
S.0199          WRITE(3,308)(RTRE2S(J),RTRESS(J),RTRE2U(J),RTRESU(J),
                2RTRE2D(J),J=1,3),EXPR2,EXPRS,DELFAC
S.0200        308 FORMAT(1HC,4X,'RTRE2S',6X,'RTRESS',6X,'RTRE2U',6X,'RTRESU',6X,
                2'RTRE2D',7X,'EXPR2',7X,'EXPRS',7X,'DELFAC'/5E12.5/5E12.5/5E12.5,
                33F12.5)
S.0201          WRITE(3,309)(COR2S(J),CORSS(J),COR2U(J),CORSU(J),COR2D(J),J=1,3)
S.0202        309 FORMAT(1HC,4X,'COR2S',7X,'CORSS',7X,'COR2U',7X,'CORSU',7X,
                2'COR2D'/(5E12.5))
S.0203          WRITE(3,310)(XX(J),RTXX(J),QW(J),TW(J),TIR(J),J=1,3)
S.0204        310 FORMAT(1HC,4X,'XX',8X,'RTXX',6X,'QW',13X,'TW',8X,'TIR'/
                2(2F10.4,F15.7,2F10.4))
S.0205          WRITE(3,311) QL,DHRM,ATW,AQW,ACOR2S,ADRE2S,TIL,CE,DHA2,DCOMB
S.0206        311 FORMAT(1HC,9X,'QL',8X,'DHRM',7X,'ATW',7X,'AQW',9X,'ACOR2S',9X,
                2'ADRE2S',9X,'TIL'/E15.7,2F10.4,7E12.5)
S.0207          GO TO 2
S.0208         70 TSI=(T2)+1.0)/2.0
S.0209          CALL SPLIT(DPR,TSI,DPRS)
```

Figure 36. (Continued)

```
S.0210          RES=SQRT(DRS)
S.0211          DHS=0.5*(DH2+DH1)+(0.22*RES*U2*U2/2.0)
S.0212          DCHIS=DHS-DHI
S.0213          GO TO 16
S.0214       99 STOP
S.0215          END
                      SIZE OF COMMON  00000     PROGRAM  09076
END OF COMPILATION  MAIN
        COMPILATION TIME WAS    0000.10  SECONDS

BEGIN COMPILATION
            C     STIRLING'S INTERPOLATION FORMULA
S.0001          SUBROUTINE DIFIT(ARRAY,ARGUMT,FUNCTN)
S.0002          DIMENSION ARRAY(10)
S.0003          DO 1000 JJ=1,19
S.0004          HOLNUM=JJ
S.0005          IF(ARGUMT-HOLNUM)3000,3000,1000
S.0006       1000 CONTINUE
S.0007       3000 DDX=ARGUMT-HOLNUM+1.0
S.0008          YIM1=ARRAY(JJ-2)
S.0009          YI=ARRAY(JJ-1)
S.0010          YIP1=ARRAY(JJ)
S.0011          YIP2=ARRAY(JJ+1)
S.0012          FUNCTN=YI+(DDX*(YIP1-YIM1)/2.0)+(DDX*DDX*(YIP1-2.0*YI+YIM1)/2.0)
S.0013          RETURN
S.0014          END
                      SIZE OF COMMON  00000     PROGRAM  00436
END OF COMPILATION  DIFIT
        COMPILATION TIME WAS    0000.83  SECONDS
```

Figure 36. (Continued)

```
BEGIN COMPILATION
      C     INDUCTION TIME FOR HYDROGEN-AIR MIXTURES
S.0001      SUBROUTINE UTIME(TEMP,PRESS,VOLH2,TIME)
S.0002      CONCH2=PRESS*VOLH2/(62.358*TEMP)
S.0003      CONCO2=PRESS*(0.2095)*(1.0-VOLH2)/(62.358*TEMP)
S.0004      RK1=(6.30E+10)*EXP(-5.9CE+03/(1.98726*TEMP))
S.0005      RK2=(4.00E+11)*EXP(-1.7CE+04/(1.98726*TEMP))
S.0006      RK3=(1.20E+10)*EXP(-3.95E+03/(1.98726*TEMP))
S.0007      RK1=(2.50E+09)*EXP(-3.9CE+04/(1.98726*TEMP))
S.0008      PAN=SQRT(1.0+((8.0*RK2*CONCO2)/(RK3*CONCH2)))
S.0009      PRN=(2.0+(1.0+((RK1*CONCH2)/(RK2*CONCO2)))*(PAN+1.0))
S.0010      PCO=(2.0*RK1*RK3*(PAN-1.0))
S.0011      PDC=(SQRT(PRN/PCO))/CONCH2
S.0012      PEL=ALOG((RK1*1.00E-06)/(2.0*RK1*CONCO2))
S.0013      TIME=PDC*PEL*1.00E+06
S.0014      RETURN
S.0015      END
          SIZE OF COMMON  00000     PROGRAM  00874
END OF COMPILATION  UTIME
          COMPILATION TIME WAS   0001.01  SECONDS
```

Figure 36. (Continued)